SECTION IV: TABLE OF CONTENTS

4.   EXPERIMENTAL WORK AND VERIFICATION OF CFD METHODOLOGY

4.1   Experimental Work

4.1.1   Cage Condition

4.1.1.1   Objective

Several series of experimental scenarios were defined to consider a known mouse cage placed in a wind tunnel. The primary objective of the experimental measurements was to create and measure various airflow s within the mouse cage in such a manner as to lay the ground work for determining the boundary conditions for the computational fluid dynamics (CFD) analysis of the cage. In particular, a series of CFD models were constructed to simulate the cage wind tunnel experiments. The primary reason for the validation of the CFD model of the cage against experimental data were to obtain an appropriate set of boundary conditions to represent the cage in the whole room simulations. The two sets of boundary conditions that are of most concern are those associated with the transfer mechanisms into and out of the cage, namely the side cracks and the top of the cage, that includes the filter media.

4.1.1.2   Experimental Apparatus

The apparatus used in this series of experimental scenarios was kept relatively constant throughout, with the main difference being the representation of the mice within the cage.

The wind tunnel cross section was 0.40 m x 0.50 m (15.75" wide x 20" deep). It was 1.72m (68") long with a 0.80m (32") long test section in the center. Room air entered the wind tunnel through a furnace filter (0.41m x 0.50m x 2.5e-2m (16" x 20" x 1")); American Air Filter, Louisville, KY) then passed through three perforated metal screens (60 percent, 40 percent, then 33 percent open area) that acted as a settling means so airflow approaching the test section was uniform. The inlet filter was placed 0.10 m (4") from the end of the wind tunnel and the outlet filter was 0.43 m (17") from the other end. The first metal screen was 0.10m (4") from the inlet filter and the screens were spaced 0.10 m (4") apart. Detailed drawings of the wind tunnel are presented in the figures 4.01 to 4.03, while a picture of the wind tunnel with the cage in the parallel orientation is shown in figure 4.04.

The instrumented mouse cage was made from a standard Lab Products, Inc., shoebox mouse cage with approximate top dimensions of 0.18m x 0.28m x 0.13 m (7" wide x 11" long x 5" high) (see figures 4.05 to 4.11). The filter top was the high profile type and the filter was a Reemay #2024, 2.1 oz/yd^2, 12 mils thick. The cage had approximately 1.25e-2m (0.5") of hardwood shavings bedding on the floor, a wire rack, water bottle, and simulated feed.

The cage also contained one of two mouse heater representations: a simple, small electric heater, that will be known hereafter as the default mouse heater (DMH) (shown in figure 4.12); and a more realistic representation of the physical presence and heat transfer characteristics of the mice huddle, that will be know hereafter as the simulated mouse object (SMO) (shown in figure 4.13). In the cases that included the DMH, the cage had an electric heater placed on the bedding towards the front of the cage that produced heat equivalent to the total heat production of five mice weighing 2.0e-2 kg (4.4e-1 lb) each, 2.3 W. Heat production simulated was based on the ASHRAE (1993) equation:

$$ATHG = 2.5\ M \qquad\qquad\qquad\qquad (4.1)$$
$$M = 3.5\ W^{0.75}$$

Where:

   ATHG = average total heat production from laboratory animal, W/animal
   M = metabolic rate of animal, W/animal
   W = mass of animals, kg

The DMH was a 200 ohm precision resistor with approximately 21.5 V of direct current from a regulated, filtered D.C. power supply.

In the cases that included the SMO, the cages included a more accurate mice huddle representation, that was placed within the cage at a location centered width-wise and towards the front one-third in the same location as the resistor heater (see figures 4.08 to 4.10). The SMO was designed to simulate five mice for volume obstruction, sensible heat production, and surface temperature. The mice were simulated using 2.20e-1m (7/8") outside diameter PVC pipe. The pipe had a wall thickness of 2.4e-3m (3/32") and was cut to 4.3e-2m (1-11/16") lengths. The ends of the pipe were covered with duct tape and plastic caps (see figures 4.13 and 4.14). Sensible heat was simulated using one 200 ohm precision resistor powered at 9 volts per pipe. Before starting the experiment the surface temperature of the SMO was measured several times at various locations, using a Cole Palmer infrared thermometer (see figure 4.14), and shown to closely correspond to those found on the fur of the dorsal surface of mice by Chris Gordon (about 26.7 °C (80.0 °F)). Justification for the physical sizing of the SMO is given in appendix I: section 2.3.

In both mouse heater representations, a voltage regulator (Epsco model EFB) was used to produce the voltage. The voltage was constantly monitored using a Fluke 75 multi-meter. Resistance was checked at the beginning of each experiment with the Fluke to guarantee the resistor was in working order.

The cage was instrumented to measure air velocities approaching or moving past the cage on all four sides, at approximately the top edge of the cage, or the lip of the top. An air velocity sensor was placed on each of the four sides at approximately 2.0e-2m (0.75") distance out from the cage at the midlength of each side. Air velocities, temperatures, and air exchange rates were measured

inside the cage. Air velocities and temperatures were measured with thermistor based BESS Lab air velocity sensors and type T thermocouples, respectively. Six air velocity sensors were placed approximately 2.5e-2m (1") above the bedding and uniformly spaced around the cage at this level. Six thermocouples were placed approximately 2.5e-2m (1") from each air velocity sensor at the same height. A Campbell 21X data logger with an AM416 Multiplexer collected cage sensor outputs.

Exact sensor locations, cage dimensions, and cage locations within the wind tunnel are available from the drawings in the figures 4.01 to 4.13.

4.1.1.3   *Experimental Data Sets Considered*

There were nine series of experimental scenarios considered in this project:

Series Set Base

In this series of experiments, the tracer gas used to determine the ventilation rate was exclusively 99.8 percent purity CO_2, that was injected (and sampled) at a rate of 1 L/min into the cage. The approaching air impacted the cage in three different orientations: the parallel orientation, in that the tunnel air moved horizontally towards the front edge of the cage; the perpendicular orientation, in that the tunnel air moved horizontally towards the side of the cage; and the vertical orientation, in that the tunnel air moved vertically downwards towards the top of the cage. These three orientations are summarized in figures 4.01 to 4.03. In each orientation, the air velocities approaching the cage were 15, 20, 30, 40, 50, 60, 70, 80, 90 and 100 fpm (0.075, 0.10, 0.15, 0.20, 0.25, 0.3, 0.35, 0.40, 0.45 and 0.5 m/s respectively).

Series Sets One and Two

It was decided that the injection rate of CO_2 utilized in series set base was too large in comparison with the likely gaseous generation rates from the mice in the actual physical case, and that the magnitude of the injection could affect the flow field conditions within the cage, i.e., the gas would no longer act as a tracer gas. Also, it was decided that the higher end of the velocity range chosen, i.e., 0.3 m/s (60 fpm) and above, was unlikely to be present in the animal room facility close to the cages.

In series sets one and two therefore, the injection rate was reduced to more realistic levels, and the tunnel approach velocity range was clipped at 0.25 m/s (50 fpm). In both series set one and two, the injection (and sampling) rate was set at 100 mL/min: in series set one, the tracer gas used was 99.8 percent purity CO_2; in series set two, the tracer gas used was 4.99 ppm SF_6. The tests ran at 15, 20, 30, 40 and 50 fpm (0.075, 0.10, 0.15, 0.20 and 0.25 m/s respectively). The parallel and perpendicular orientations were both considered.

Series Set Three

In the third series set, the parallel cage orientation with CO_2 tracer gas was repeated with the heater on and the heater off for only the 20 and 40 fpm (0.10 and 0.20 m/s) air velocities to determine if the heater had a significant effect.

Series Sets Four and Five

Series sets four and five compared two tracer gas methods: the decay method and the constant injection method. In both methods, CO_2 was injected at 100 mL/min (3.53e-3 ft^3/min) in the same locations as in series set one. A simulated mice obstruction (SMO) occupied approximately the same volume, produced the same sensible heat, and had approximately the same surface temperature as five mice in a tight group. The tests were run at three approach air velocities: 20, 30 and 40 fpm (0.10, 0.15 and 0.20 m/s respectively), and three cage orientations to airflow (parallel, perpendicular and vertical).

It should be noted that the primary reason for the series set four experimental tests was to replicate and expand the work performed by Keller, White, Snyder, and Lang (1989). In particular, in that paper, the authors measured decay data for a cage that was orientated in the parallel direction, and was subject to an approach velocity of 16 fpm (0.08m/s). The cage used in the Keller, White, Snyder, and Lang (1989) paper was very similar to that used in this present study. The emphasis of this experimental data set is to demonstrate that the experimental procedure being utilized in the current study was technically correct, and that the cage considered was representative of a typical mouse cage.

Series Sets Six and Seven

Series sets six and seven were conducted with the filter lid on but with a seal around the lip edges so all airflow through the cage passed through the filter, or with the filter lid sealed and the lip edge open. These results were compared to the results from series set three. The tests were similar to series set three except for the sealed edge and top, only the constant injection method was used, and only the 20 and 40 fpm (0.10 and 0.20 m/s) air velocities were used with only parallel and perpendicular airflow orientations. Also, during part of this series set, the SMO was introduced into the cage in place of the resistor, as a heat source. Data were collected using a randomized complete block design with the lid condition being blocked. The SMO was always allowed to produce heat. The heater state and air velocity levels were randomized within each lid condition block.

Series Set Eight

Series set eight was conducted with pairs of cages together, as shown in figures 4.15 and 4.16. In these tests, two cages were considered side by side for both the parallel and perpendicular cage orientations with the spacing between the cages set to that that the cages would experience in an animal facility room. In particular, the spacing between the cages in both cases was set to 2.81e-

2m (1.11"). Only one tunnel velocity, 30 fpm (0.15 m/s) was considered for each orientation. Instrumentation was included in one cage only. The other cage was left basically empty.

These sets are summarized in table 4.1.01 below:

Table 4.1.01 Table of Cage Condition Experimental Series

Series Set	Tracer Gas	Injection Rate (L/ min)	Sampling Method	Mouse Heater Type	Cage Orientation	Tunnel Air Velocity Range (fpm)
Base	CO_2	1.0	Steady	DMH (On/ Off)	Par, Perp, Vert	15 – 100
One	CO_2	0.1	Steady	DMH (On only)	Par, Perp	15 – 50
Two	SF_6	0.1	Steady	DMH (On only)	Par, Perp	15 – 50
Three	CO_2	0.1	Steady	DMH (On/ Off)	Par, Perp, Vert	20, 40
Four	CO_2	0.1	Steady	SMO (On only)	Par, Perp, Vert	20, 30, 40
Five	CO_2	0.1	Decay	SMO (On only)	Par, Perp, Vert	20, 30, 40
Six	CO_2	0.1	Steady	DMH (On/ Off); SMO (On Only)	Par, Perp	20,40
Seven	CO_2	0.1	Steady	DMH (On/ Off); SMO (On Only)	Par, Perp	20, 40
Eight	CO_2	0.1	Steady	SMO (On Only)	Par, Perp	30

4.1.1.4   Experimental Procedure

4.1.1.4.1   Common Calibration Procedures

The following calibration procedures were performed before all experimental test series.

Thermocouple Calibration

During all of the results sets, the cage housed the same six T-type thermocouples. The thermocouples were calibrated at five temperatures using a water bath. Water bath temperatures were determined using a SAMA thermometer. Regressions were formed by comparing thermocouple readings to the thermometer readings. The thermocouples were connected to a Campbell 21x data logger when readings were taken. The regression equations were used to obtain predicted temperature readings. The standard error of the predicted readings vs. the thermometer readings was computed for each thermocouple. No standard error reading exceeded 9.0e-2 ^{o}C (1.6e-1 ^{o}F). Calibration results are presented in appendix I: section 2.1.1.

Cage Anemometer Calibration

BESS Lab thermal anemometer probes surrounded the cage for each result set. The sensors were calibrated using a TSI model 8390 Bench Top Wind Tunnel with a TSI model 8910 pressure transducer. Because of the relationship between anemometer performance and temperature, the calibration air was recycled in a closed loop to prevent temperature fluctuations. This was done by having the intake air of the calibrator come from an 2.44 m (8') x 1.22m (4') x 1.22 m (4') x 5.08e-2m (2") thick insulated box and directing the exhaust air back into the box (see figure 4.17). The insulated box was cooled for at least ten minutes using air from a chiller to about 20.0 ^{o}C (68.0 ^{o}F) at that time the box was sealed and the calibration started. The temperature was allowed to rise by conduction until a temperature near room temperature was reached. At this time a low power electric heater was turned on to obtain temperatures greater than room temperature. Each probe was subjected to velocities of 15, 20, 30, 40 and 50 fpm (0.076, 0.10, 0.15, 0.20, 0.25 m/s) and temperatures ranged from 20.0 ^{o}C to 29.3 ^{o}C (68.0 to 84.7 ^{o}F). Velocities within the calibrator were precisely calculated by the manufacturer and presented in a table that relates pressure differences to chamber velocities. Temperature and velocity sensor output voltage were taken every second and averaged over one minute using a Campbell 21x Data Logger.

Temperature and voltage data were analyzed to form trend lines for each velocity. The trend lines were used to generate predicted voltage values. The velocity data, temperature data, and predicted voltage values were then combined and plotted to form a contour map that had axes of velocity, temperature, and contours of voltage. The map was made using a third order polynomial regression. A third order polynomial regression was chosen because it provided an equation that could easily be used to determine velocity values within a spreadsheet and because it displayed contour lines that closely followed those lines displayed by other curve-fit methods. The contour map was made as a visual means of finding if values were not outside the calibration range, i.e. greater than 0.25 m/s (50 fpm) or less than 0.10 m/s (20 fpm). Calibration results are presented in appendix I: section 2.1.2.

Procedure to Set an Approach Velocity

The wind tunnel air velocity was determined by a calibrated thermal anemometer (IAT model AVS-94A-10X). The anemometer was placed in front of the cage, centered on the cage. Air velocity within the cage wind tunnel was adjusted using a voltage regulator (Variac Auto Transformer) to adjust fan speed, a bypass door, and for lower velocities, a pressure restriction. Velocities were adjusted until the desired approach air velocities (15, 20, 30, 40, 50, 60, 70 or 80 fpm 0.076, 0.10, 0.15, 0.20, 0.25, 0.30, 0.35 or 0.40 m/s respectively)) were read from the anemometer, in the form of a corresponding voltage. Air velocities were controlled by a centrifugal fan (0.15m (approx. 6") diameter inlet) and exhaust was vented through a flexible conduit (0.20m (approx. 8" diameter)) to the outside.

Anemometer Calibration

The IAT AVS-94A was calibrated prior to each test in a wind tunnel calibrator (TSI model 8390). Velocities within the calibrator were precisely calculated by the manufacturer and presented in a table that related pressure differences to chamber velocities. To sense pressure differences within the chamber, a Dwyer Micro Detector micromanometer was used. As a safety check the micromanometer values were compared to pressure readings displayed by a digital pressure transducer (TSI model 8910). Calibrating the anemometer used to determine the approach air velocities required taking data at the desired approach air velocity (15, 20, 30, 40, 50, 60, 70 or 80 fpm (0.076, 0.10, 0.15, 0.20, 0.25, 0.30, 0.35 or 0.40 m/s respectively). For each calibration temperature, sensor voltage, transducer reading, and micromanometer data were taken for the desired approach air velocity. Temperatures were taken near the calibrator using a SAMA mercury thermometer. The date and time of calibration was recorded. Calibrator pressures were regulated by adjusting the wind tunnel fan speed with a voltage regulator (Dart 250). Pressures were adjusted until they matched the pressures corresponding to the desired approach velocity. When the desired pressure was reached the sensor voltage was noted and the sensor was placed into the wind tunnel.

4.1.1.4.2   Specific Series Procedures

Siting of Sampling Tubes

The question of locating the sampling tubes was considered prior to the series set base experimental measurements. The cage air exchange rates were measured with the tracer gas method using CO_2 as the tracer gas. When tunnel air approaches a cage, air is drawn from one part of the cage and fresh air enters the cage at another location. Therefore, air has to be sampled at both the entering and exiting locations of the cage. Smoke sticks (titanium tetrachloride) were placed into the cage to visually determine the locations where air entered and exited the cage in order to determine the locations for the sampling locations. Refer to figures 4.05 through 4.10 for the placement of the air sampling tubes.

Series Set Base

Carbon dioxide (at least 99.8 percent pure, bone dry) was injected into the cage near the bedding at a rate of 1 L/min through two diffuser stones spaced 0.08m (3.15") apart. The injection rates were calibrated using a digital flow meter (Humonics 650 Digital Flowmeter). The injection rate was monitored continuously with a Gilmont (model 1260) calibrated flowmeter with an accuracy of +/- 2 percent. The CO_2 was injected at locations that allowed enough distance to mix well with the cage air before it was sampled at the cage exhaust area. The injection locations were also determined with smoke tests and are presented in figures 4.05 to 4.07.

Air was sampled from two sampling tubes at different locations in the cage to determine CO_2 content of air exhausting from and air entering into the cage as discussed above. The cage airflow was allowed to stabilize for ten minutes before samples were drawn. Sampling rate was 1 L/min at each location but samples were not drawn from both locations at the same time: a two minute minimum stabilization time was allowed between sampling the front and back locations of the cage. Consequently, at all sampling times, 1 L/min of CO_2 was injected into the cage and 1 L/min of air/ CO_2 mixture was removed from the cage by the sampling system. Sampling air was drawn from the cage with a SKC Airchek Sampler pump and the flow rate was checked against the Gilmont (model 1260) flowmeter prior to and during the experiment. Sampling was taken through tubes with five uniformly distributed holes to obtain an average CO_2 concentration over a distance since the concentration varies with location, figure 4.18. CO_2 concentration also varied slightly over time so the samples were drawn for five minutes into a gas sampling bag (Tedlar, polyvinyl fluoride), then the concentration in the bag was measured to determine the average concentration over the five sampling locations and over the five minute period. Three bags of gas samples were taken at the air exiting location and one at the entering air conditions. The same sampling procedure was used as for the exhaust air. CO_2 levels in the gas sampling bags were measured with a Beckman LB2 carbon dioxide infrared gas analyzer (Beckman Instruments, Inc.). The analyzer calibration was compared to two certified gases (0.55 percent and 1.58 percent CO_2) prior to each use. Before the bags were used again they were emptied using a vacuum pump to remove any accumulated CO_2. The tubing system going into the analyzer was checked for leaks before any concentration readings were taken. The analyzer was calibrated by first adjusting the instrument zero dial to match the lower concentration and then by adjusting the gain to match the higher concentration.

To monitor the possibility of CO_2 buildup in the test room, a CO_2 analyzer (Fuji Electric model ZFP5YA31) was periodically turned on and background CO_2 concentrations were taken.

Series Sets One and Two

The same injection/sampling procedures as followed in series set base were maintained for series set one, but for series set two, that considered SF_6 as the tracer gas, the procedures were somewhat different.

The SF_6 was injected through Teflon tubing. Teflon was used to prevent SF_6 absorption/ readmission problems that are characteristic of that class of gas.

Three SF_6 samples were removed from both the front and back locations of the cage using syringes (GASTIGHT #1750). The syringes pierced a rubber septum in the tubing that ran to the billows pump and was connected to the tubing by a T joint. After piercing the septum, each syringe was repeatedly filled and emptied into the tube three times before an approximately 0.5mL ($3.05e\text{-}2in^3$) sample was withdrawn.

The SF_6 concentrations were measured with a Varian 3700 Gas Chromatograph (GC) with an Electron Capture Detector. The 0.25mL ($1.53e\text{-}2in^3$) samples of standard gas mentioned above were injected from precision syringes into the Varian through a frequently changed septum. The Varian was attached to a printer that produced a concentration peak graph and gave the SF_6 concentration. Syringe labels were recorded on the graph and the process repeated. After every syringe concentration had been recorded, each syringe was dismantled and cleaned by blowing compressed air through it and onto its pull.

The GC was calibrated using a one-point calibration with a 500 ppb standard gas. 0.25ml ($1.53e\text{-}2in^3$) samples of standard gas were injected into the GC repeatedly until consistent, sharp peaks were obtained on the output chart. The calibration was checked with the standard gas after every three sets of injections. The GC was recalibrated when the expected sharp, consistent peaks were not seen on the output chart.

To monitor the possibility of SF_6 buildup in the test room, wind tunnel entrance samples were taken to measure the background SF_6 concentration. To further safeguard against SF_6 buildup, all air exiting the billows pump was bagged. Along with these measures all exhaust air from the wind tunnel was ducted outside of the room.

In both series, data were collected using a randomized complete block design with the tracer gas and air velocity level being randomized.

Series Set Three

The same injection/sampling procedure was followed as for series set base. Data were collected using a randomized complete block design with the heater state and air velocity level being randomized.

Series Sets Four and Five

A standard concentration of CO_2 [99.8 percent] was used as the tracer gas. Injection rate was set at 100 mL/min ($3.53e\text{-}3 \text{ ft}^3$/min). The injection rates were calibrated using a digital flow meter (Humonics 650 Digital Flowmeter). Digital flowmeter measurement, time, and date were recorded for each calibration. The injection rate was measured continuously with a correlated flowmeter (Gilmont, tube size 1, accuracy +/-2 percent of reading). Tracer gas was injected

through two diffuser stones that were spaced 0.08m (3.15") apart. CO_2 injector location varied with cage orientation (see figure 4.05 to 4.10 and 4.19). Two tracer gas methods were conducted simultaneously: the decay method and the constant injection method.

All sample concentrations were measured using a Beckman CO_2 Analyzer. CO_2 samples were pulled into the Beckman Analyzer using the analyzer pump. Flow through the analyzer was monitored and controlled using a flow controller/monitor. The flow was held constant at 469 mL/min (1.66e-2 ft^3/min). Flow rate readings were checked using a digital flow meter (Humonics 650 Digital Flowmeter) once daily. To produce an effective average flow rate of 100 mL/min (3.53e-3 ft^3/min), at 469 mL/min (1.66e-2 ft^3/min) of air was pumped out of the cage for 20 seconds with a 73.8 second waiting period during that background CO_2 concentration was measured. All wind tunnel exhaust air was ducted outside of the room.

The analyzer was calibrated using 1.58 percent and 0.55 percent standard concentrations of CO_2. The analyzer was calibrated by first adjusting the zero dial to match the lower concentration and then by adjusting the gain to match the higher concentration. This was done at the beginning of each experiment.

Samples from a bag of standard gas were drawn at the beginning of each day from each of three points that corresponded to those used during the decay method (see figure 4.20) and analyzed as a means of detecting leaks within the system. A leak was present if the concentration pulled through the sampling lines did not correspond to the known concentration within the bag. These values were recorded on the strip chart.

Cage CO_2 concentration was monitored at each cage decay location. Solenoid valves and Viewdac computer software were used to control from that cage location each sample was drawn. Concentrations were monitored from the beginning of injection until stabilization had been reached. Stabilization was defined as the point when two consecutive readings at all three decay sampling points were constant. Once stabilization had been reached, data collection from the decay sampling points were stopped. At this time constant injection sampling began. Constant injection data were recorded for 20 seconds at both the front and back locations of the cage with a 73.8 second pause between readings. The constant injection method samples were taken at various locations depending on cage orientation (see figures 4.05 to 4.07).

Once constant injection data had been taken, the decay method began. Soon after starting the decay method, the tracer gas flow was stopped. All decay samples were taken sequentially from one of three zones. Sequential data collection sequences for the decay method were randomly chosen from one of the six possible sequences that could be formed with three numbers.

Series Set Six and Seven

In results sets six and seven, tests was conducted with the filter lid on but it was sealed with putty around the lip edges so all airflow through the cage had to pass through the filter in the top, or it

was sealed on the filter top with plastic so all the airflow had to pass through the lip edge. The basic injection/sampling procedure as used in series set base was used in these series.

Each airflow orientation and lid condition was randomized separately. Data collection was randomized using randomized complete block design with the airflow orientation and the lid condition being blocked. The tracer gas method and air velocity levels were randomized within each block. The heater state and air velocity levels were randomized within each lid condition block.

Series Set Eight

As noted above, only one of the cages was instrumented in these tests. The basic injection/ sampling procedure as used in series set base was used in these series.

4.1.1.5   Methodology for Calculation of Cage ACH

The cage ventilation rate for all steady state injection cases was calculated from (Bennett and Myers (1982)):

$$Q \quad = \quad (C_S Q_S - C_O Q_S)/(C_O - C_I) \tag{4.2}$$

Where:

Q	=	cage ventilation rate, ft^3/min
C_S	=	CO_2 or SF_6 concentration of tracer gas:
		99.8 percent for CO_2;
		4.998ppm for SF_6
Q_S	=	rate of tracer gas injection and air sampling from cage:
		3.53e-2 ft^3/ min for 1 L/min cases;
		3.53e-3 ft^3/min for 100 mL /min cases;
C_O	=	CO_2 or SF_6 concentration of air exiting cage, percent
C_I	=	CO_2 or SF_6 concentration of air entering cage, percent

The cage ventilation rates were adjusted to standard air density conditions at sea level (Barometric pressure = 29.92" of Hg) and 70 F by multiplying by a factor K.

$$K \quad = \quad (29.92/\text{Barometric Pressure, in. Hg}) \text{ x } ((490 + \text{air temp. F})/(460+70))$$
$$\tag{4.3}$$

This procedure was followed for both the experimental and CFD results.

4.1.1.6   Graphical Representation of Experimental Data

The graphical representations of the experimental data sets are shown in figures 4.21 to 4.31. The obvious trend to be seen in all the steady state plots is that the cage ventilation rate increases with an increase in approach velocity. The principal conclusion here is that the environment external

to the cage will therefore have an impact on the ventilation within the cage; higher external flow velocities will result in better cage ventilation. The tabulated and the graphical representation of all the data is presented in appendix I: section 2.2, while the comparison between the CFD and experimental data, intended as a means of validating the CFD cage model, is given in section 4.2.1.2.2.

The decay data is interesting in that it can be compared against previous work. In the case of a decaying concentration within a volume, the level of concentration remaining can be calculated from:

$$C = Co \ e^{-\lambda t} \hspace{8cm} (4.4)$$

Where:

C	-	percent concentration, at time t
Co	-	percent initial concentration, at t = 0
λ	-	Decay constant

As the level of initial concentration varies from case to case, it is more convenient to normalize the decay such that the initial concentration is considered as 100 percent. The time taken to decay by a certain amount can then be tabulated. Table 4.1.02 below compares the time taken to decay the concentration by 90, 95 and 99 percent for the cage considered in Keller, White, Snyder and Lang (1989), and the parallel orientation cases considered in series set five.

Table 4.1.02 Time taken to decay concentration by 90, 95 and 99 percent for Keller, White, Snyder and Lang (1989) cage, and series set five: parallel orientation results.

Tunnel Velocity	Time to Decay (min)		
(fpm)	90 percent	95 percent	99 percent
Keller, White, Snyder and Lang Paper @ 16 fpm (May 1989)	18.27	23.77	36.54
20	16.69	21.27	33.37
30	12.38	16.11	24.76
40	11.29	14.68	22.57

Further, figure 4.31 displays the comparison between the series set five: parallel orientation results and the results presented in Keller, White, Snyder and Lang (1989) with the concentration levels normalized such that the initial concentration is considered as 100 percent.

The plot and table 4.1.02 clearly shows that the current data are entirely consistent with those data presented in the previous study. There are two conclusions to be drawn from this comparison:

The experimental procedure followed in this section of the study, as well as the method for determining the decay characteristics of the cage, were consistent with other experimental studies.

The cage used in this section of the study is a typical microisolator type cage, not a cage fabricated to exhibit certain characteristics.

Top View

Side View
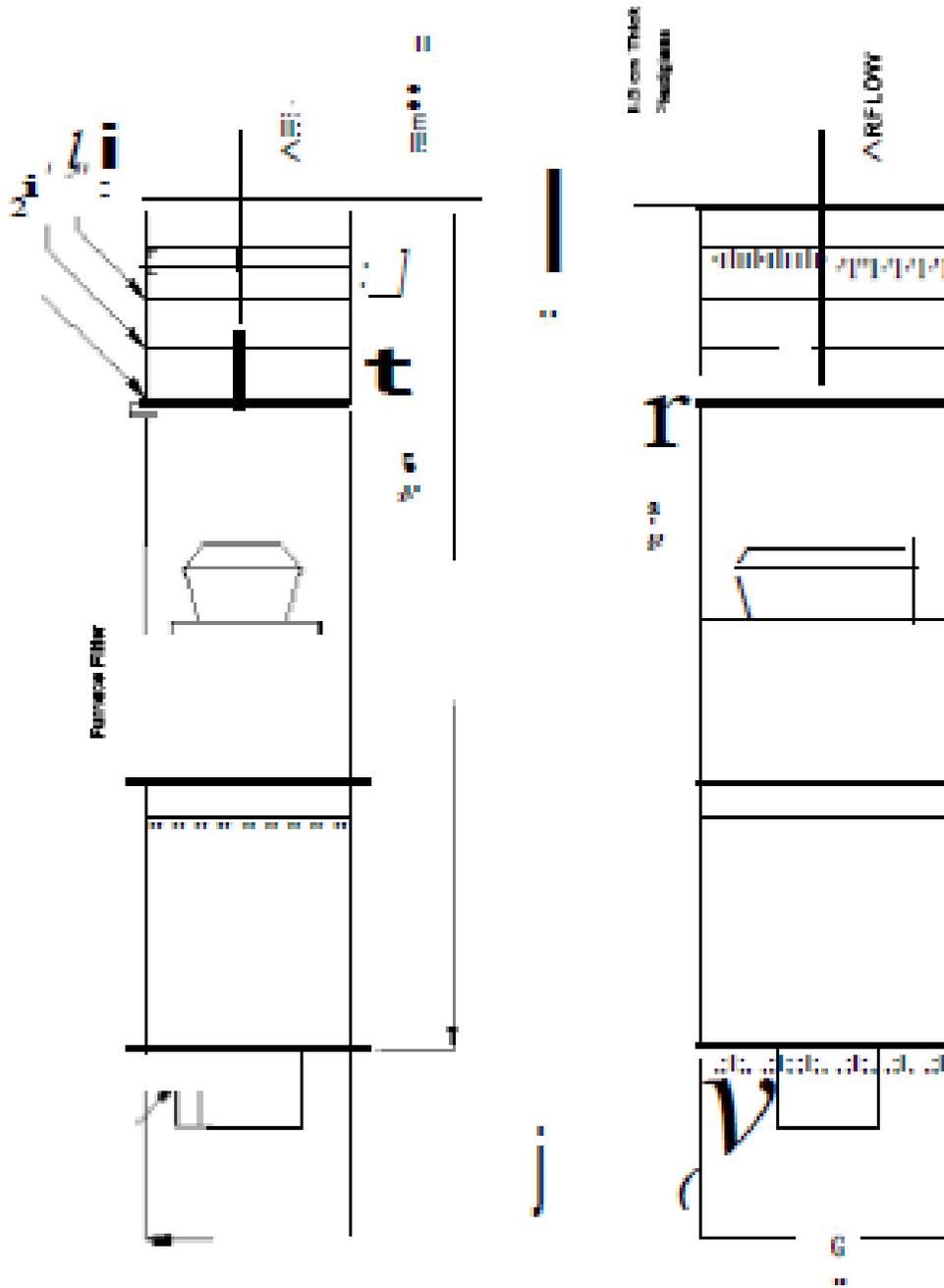
Top View

Figure 4.03 Vertical Cage Orientation Layout.
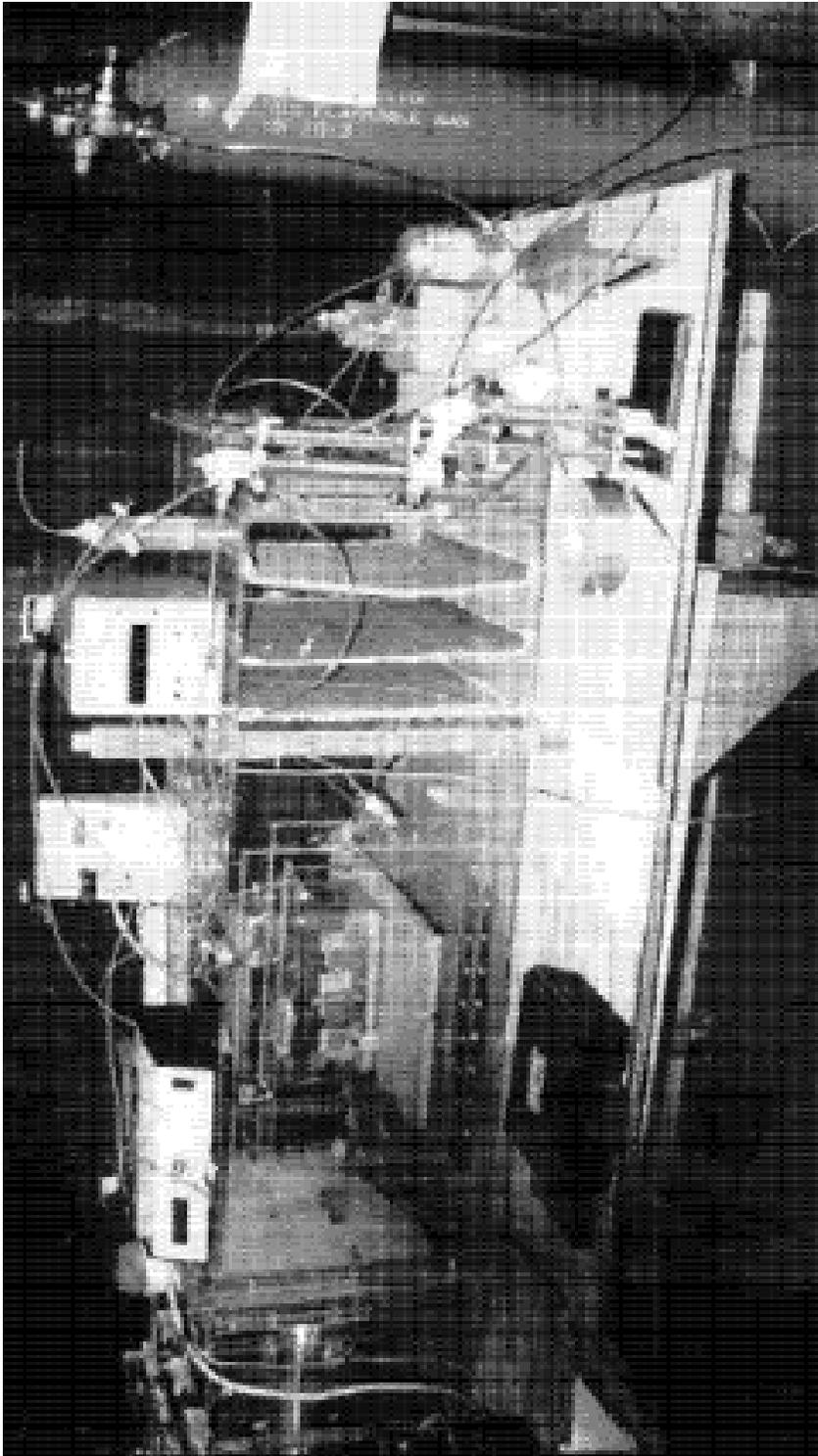
Figure 4.04 Wind Tunnel with Cage in Parallel Orientation.

SIDE VIEW

12----:2)\\ _ill

/ <=f /   r '-. Dulslclof Co

@   V   s1-ll?o.ar
o   o
L   cf   3.B

B dd' B

le peroic.r<' $<?rGen

-Air Veloc!tv IP sor

oll dir>>?nslorss in
cerrtlr>>?lm-s.

TOP VIE/   BoiiiF -.   Mori lu e

1;   c'X   .""::1   19 / (I)

H olr {j--- i   Tb
                         /. l
o   ! 3.B
                         19
Cog 7Tcp   T l
V'
Cog' Bot: ../ .U 8.9   8.9 /8.

Po roll t>I Vl>w - 1op On
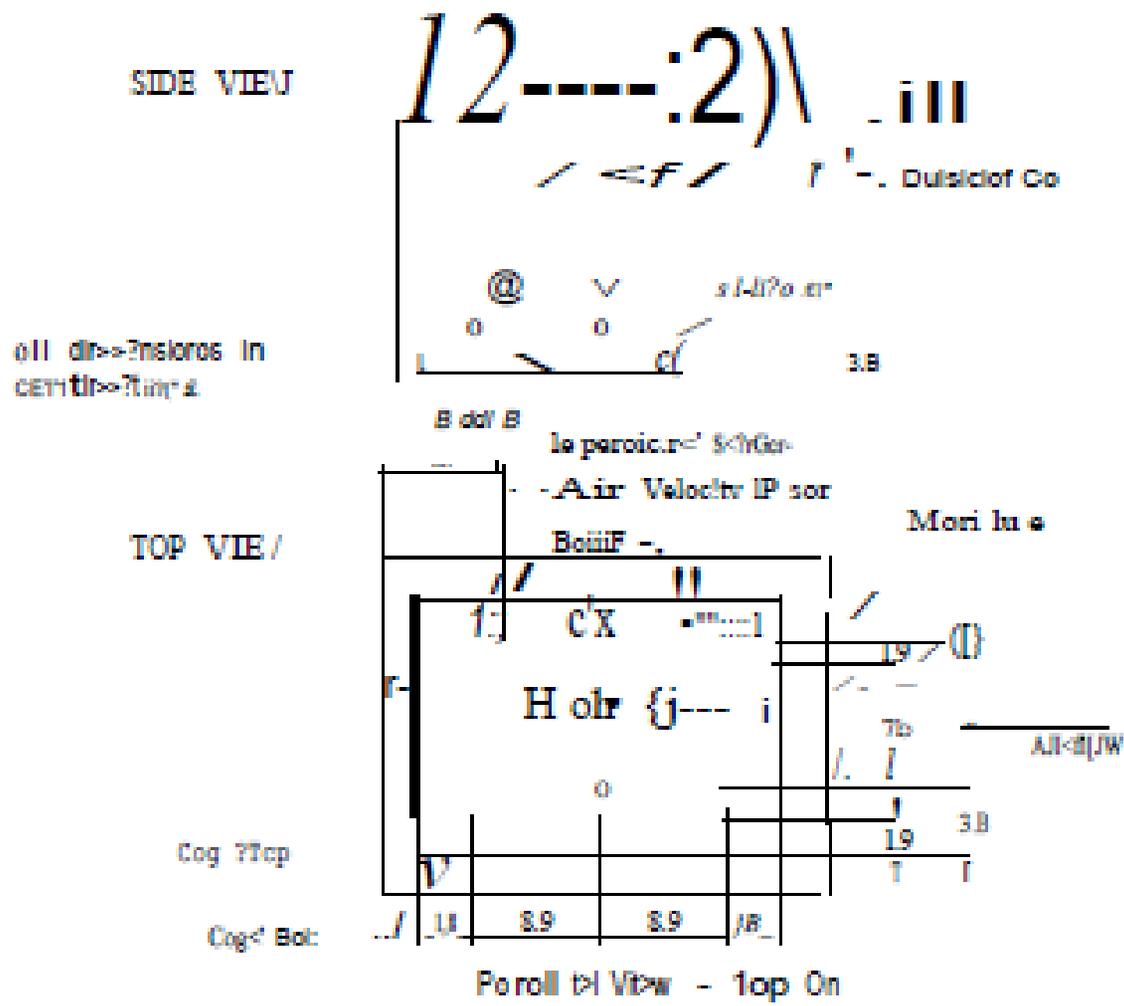
Figure 4.05 Sensor, air inlet and sampling location for cage parallel to horizontal airflow.
Mouse Heater Representation: DMH

Figure 4.06 Sensor, air inlet and sampling location for cage perpendicular to horizontal airflow.
Mouse Heater Representation: DMH

Figure 4.07 Source, air inlet and sampling location for cage vertical to horizontal airflow. Mouse Heater Representation. Draft.

SIDE VIEW

oll dimensions in
COnYtiPoriHE

TOP VIEW

Figure 4.08 Sensor, air inlet and sampling location for cage parallel to horizontal airflow.
Mouse Heater Representation: SMO.

SIDE VIEw'

oll dine-ns.ions in
c rd in<?te>..-s

TOP VIEV

Air V locrt'' ser-oss

Co9'' Top

GagBa''T1D

Pe-rpe-nclculo.-
Vi<?w – 1op Dr'
SA-10

Figure 4.09 Sensor, air inlet and sampling location for cage perpendicular to horizontal airflow.
Mouse Heater Representation: SMO.

SIDE VIEW

/OK]

oll edb-e->slor>s l>
centile>r s.

all dimensions in
centimeters.

IDP VIEW

Ve>r-iicol View - 1op On SMO

Figure 4.10 *Sensor, air inlet and sampling location for cage vertical to horizontal airflow. Mouse Heater Representation: SMO.*

Figure 4.11   Microisolator with Sampling Tube.
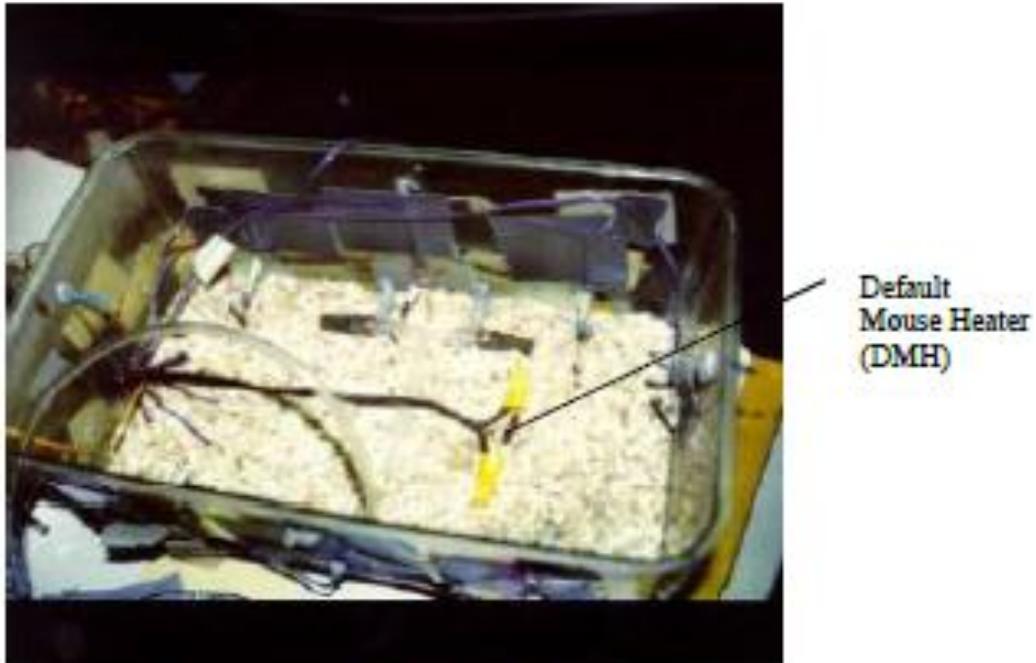
Figure 4.12   Default Mouse Heater (DMH).
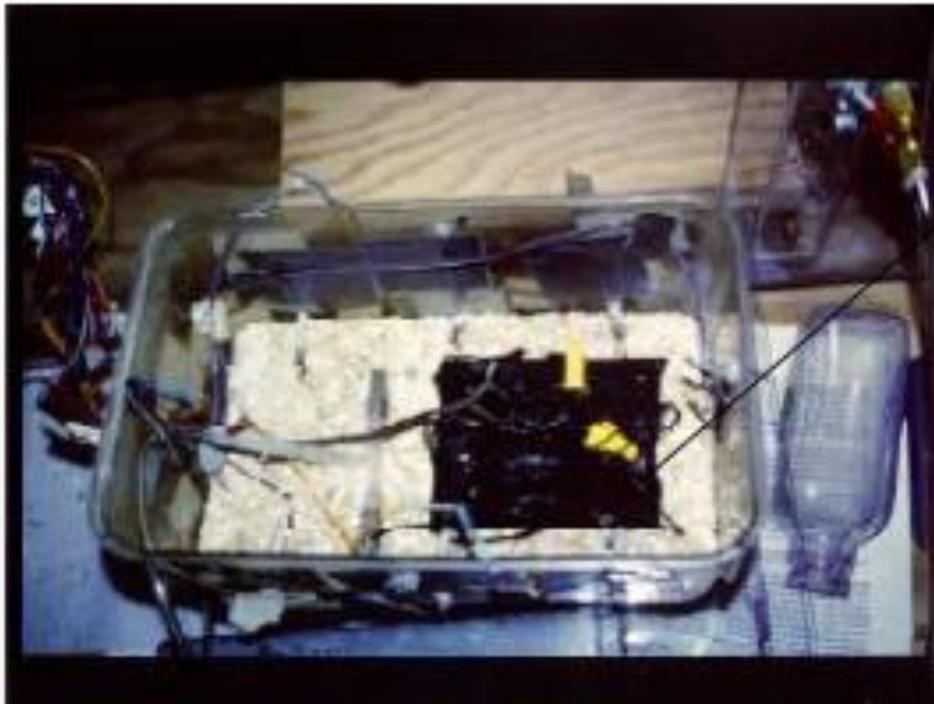
Figure 4.13   Simulated Mouse Heater (SMO).
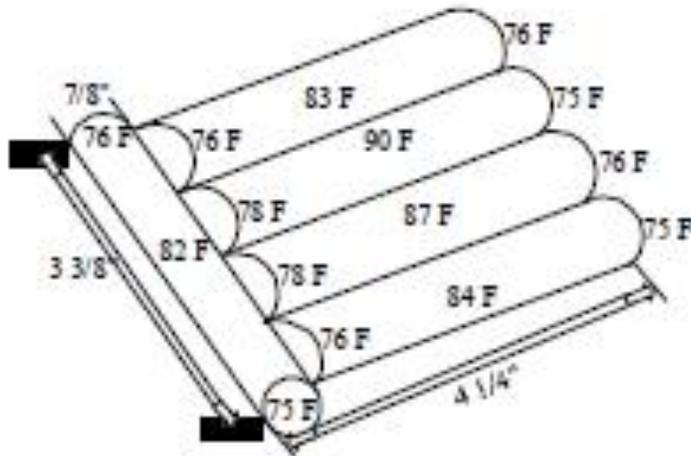
Figure 4.14   Simulated Mouse Object (SMO) with surface temperatures and dimensions.
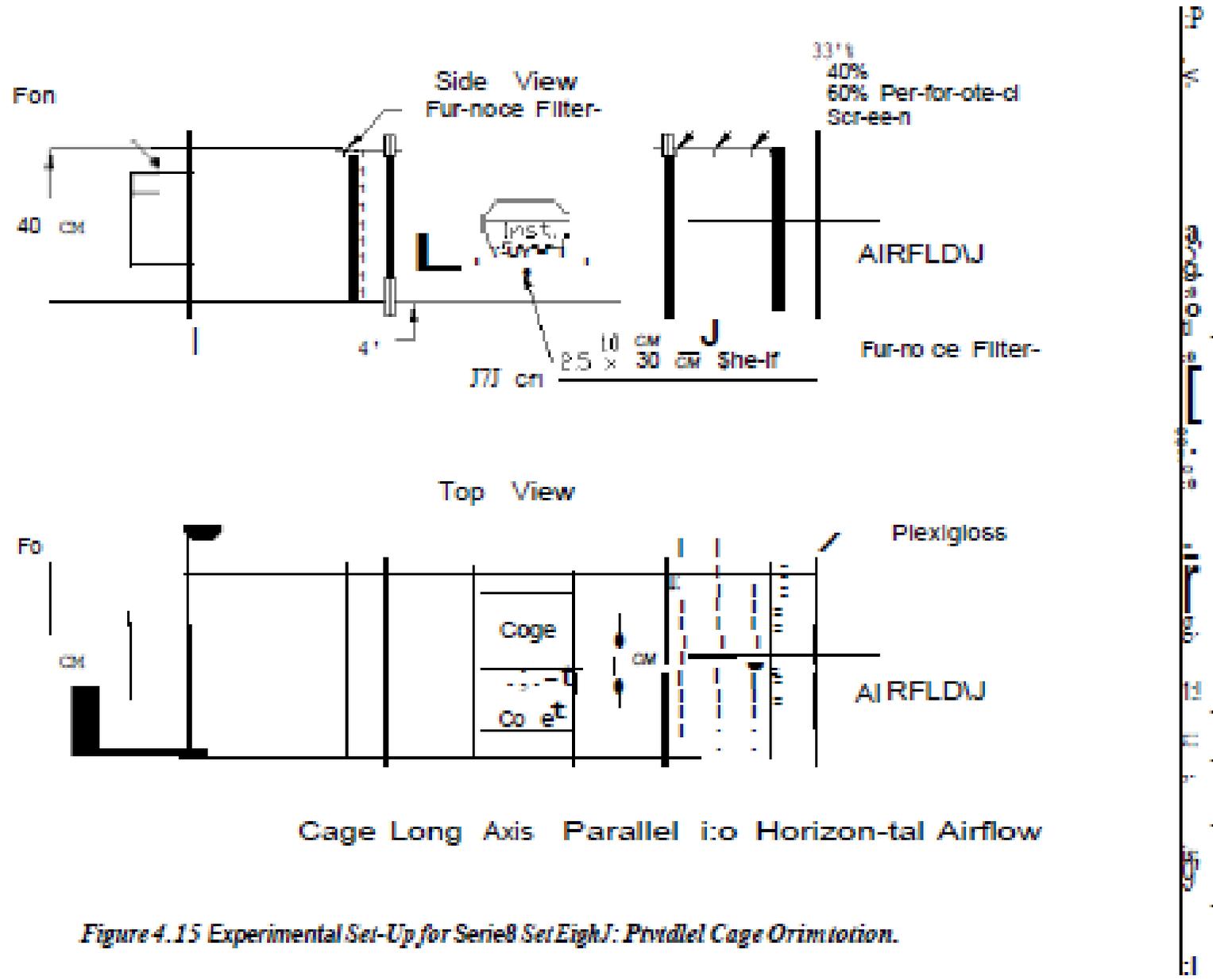
Figure 4.15 Experimental Set-Up for Series Set Eight: Parallel Cage Orientation.

Side View

Fon

40 cm

33%
40%
60% Per+'or(}teel
Screen

AIRFLD\V

(to(co   (>)

2.5 × 30 см Shel: |

171 cm

Top View

1.3 cм Thick
PlE")lgi()SS

50 см

2 . 1 c

q
[i]

A RFLD\V

Fo

JO см

Furnoce> Flite>r
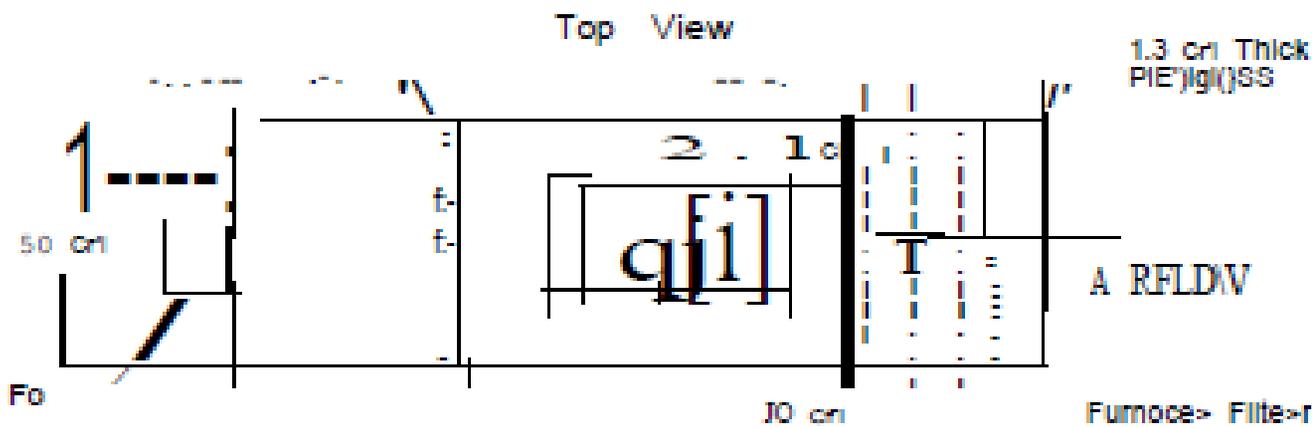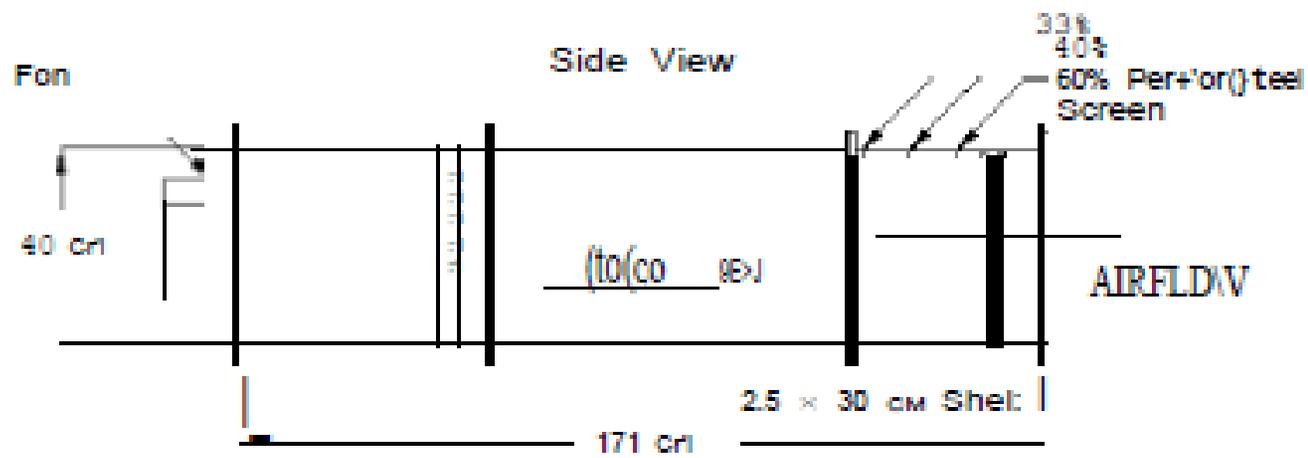
Cage Long Axis Perpendicular i:o Horizon-tal Airflow

Figwe 4.16 Elqmimmtol Set-Up for SerieB Sd Bight: Pe1'jleNtïcuJar Cage Orier tation.

Figure 4.17 Diagram of the closed-loop system used with precise velocity sensor calibration.
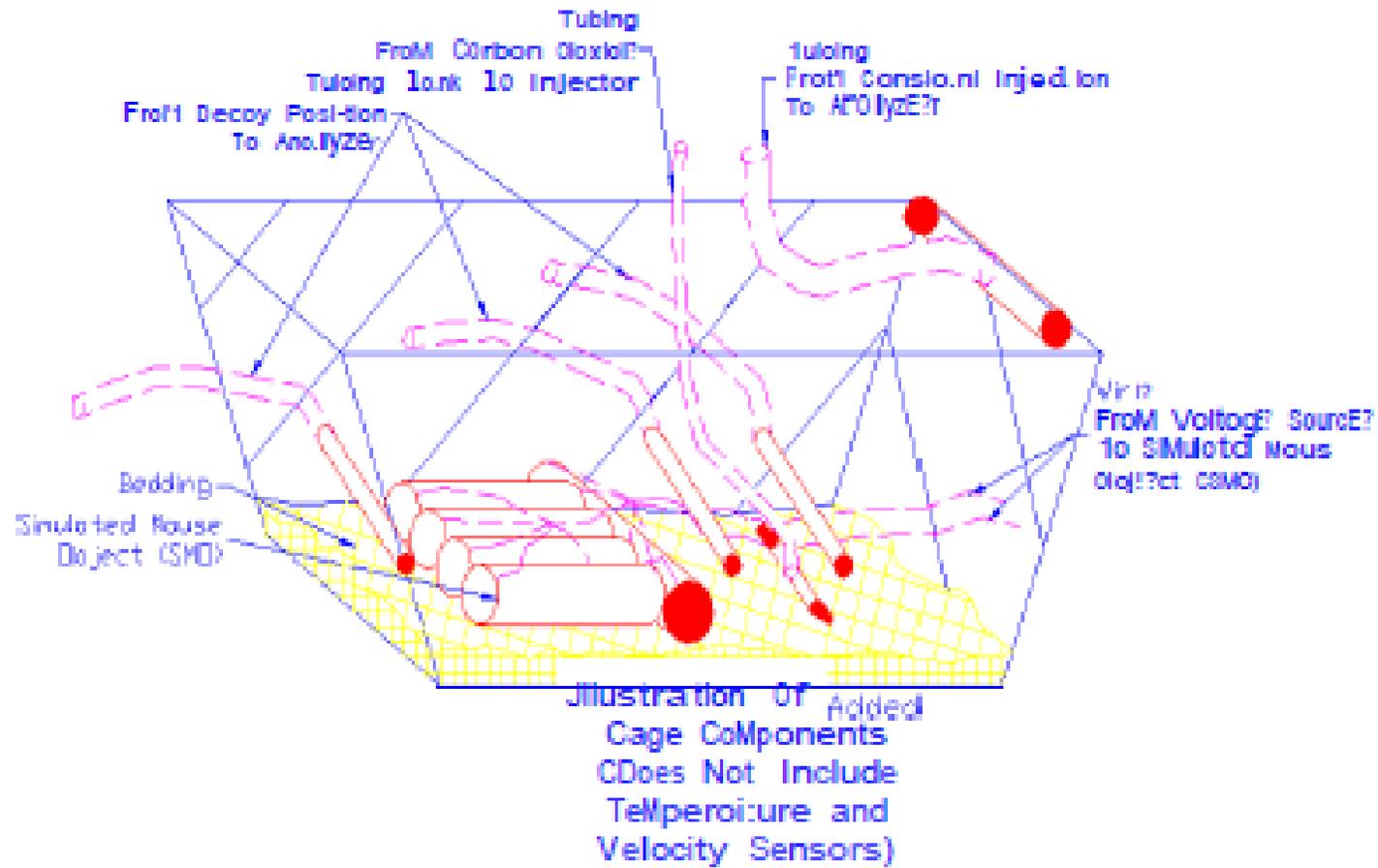
Figure 4.19 Model of the Cage with CO2 Injection/Retrieval Location and SMO.

Top of Bedding

Simulated Mouse Object (SMO)

Sampling Tube

Side View of Sampling Tubes

Simulated Mouse Object (SMO)

Decay Sampling Tubes Placed kmAbove Bedding

Section 1   **Section 2**   **Section 3**

Top View of Sampling Tubes
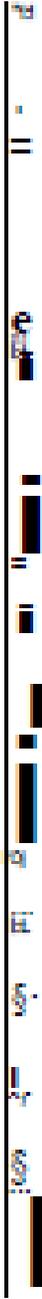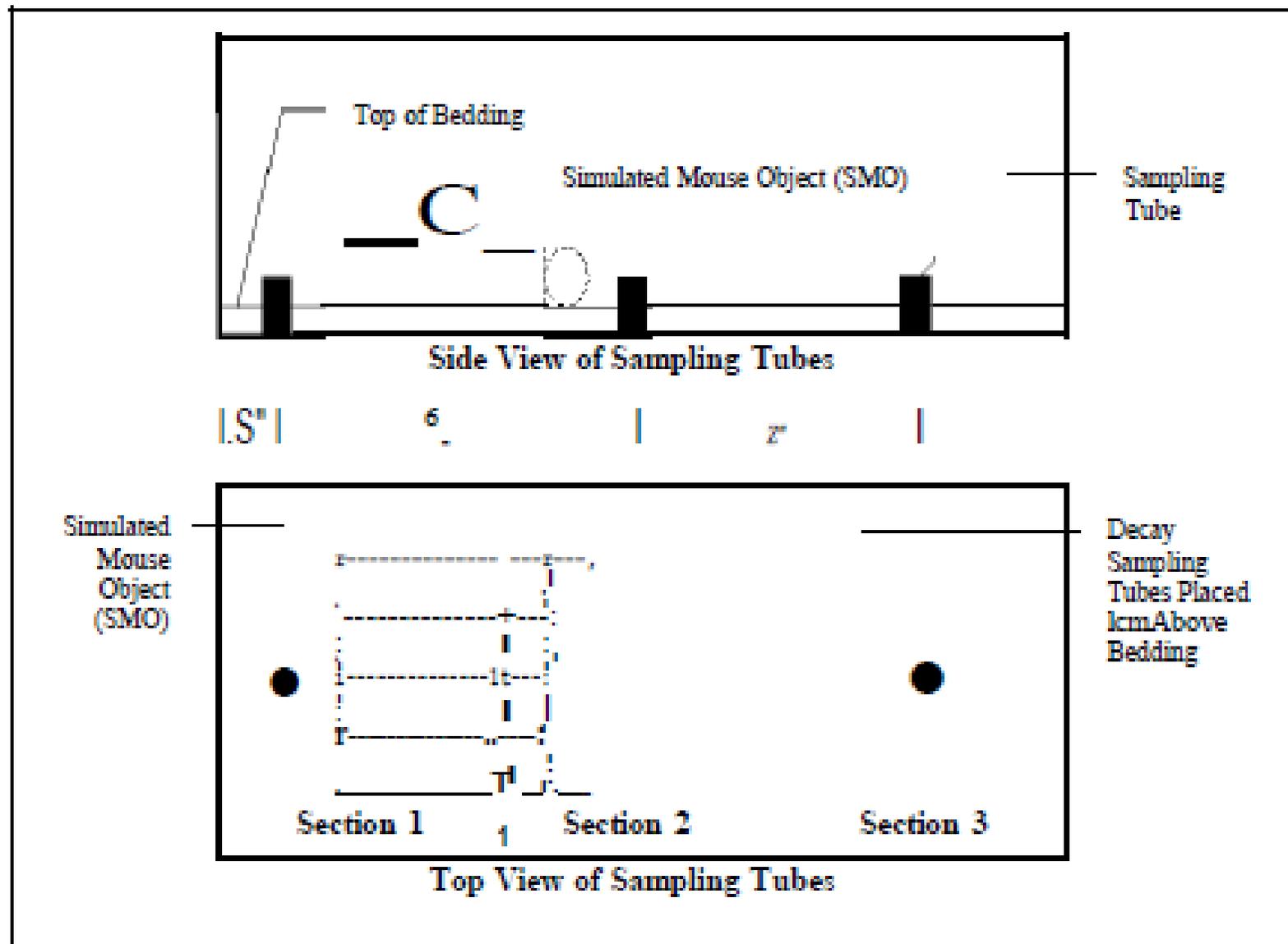
Figrue 4.20   Decay Sampling Poaition.

Figure 4.21   Cage Ventilation Rate vs. Approach Velocity. Series Set Base.
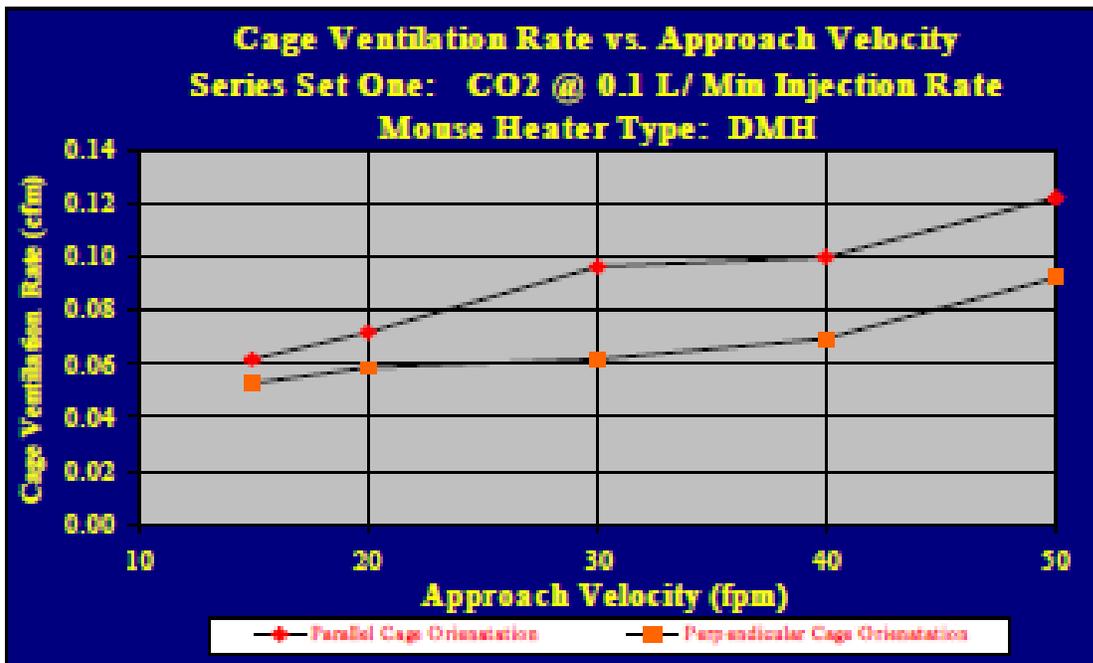
Figure 4.22   Cage Ventilation Rate vs. Approach Velocity. Series Set One.
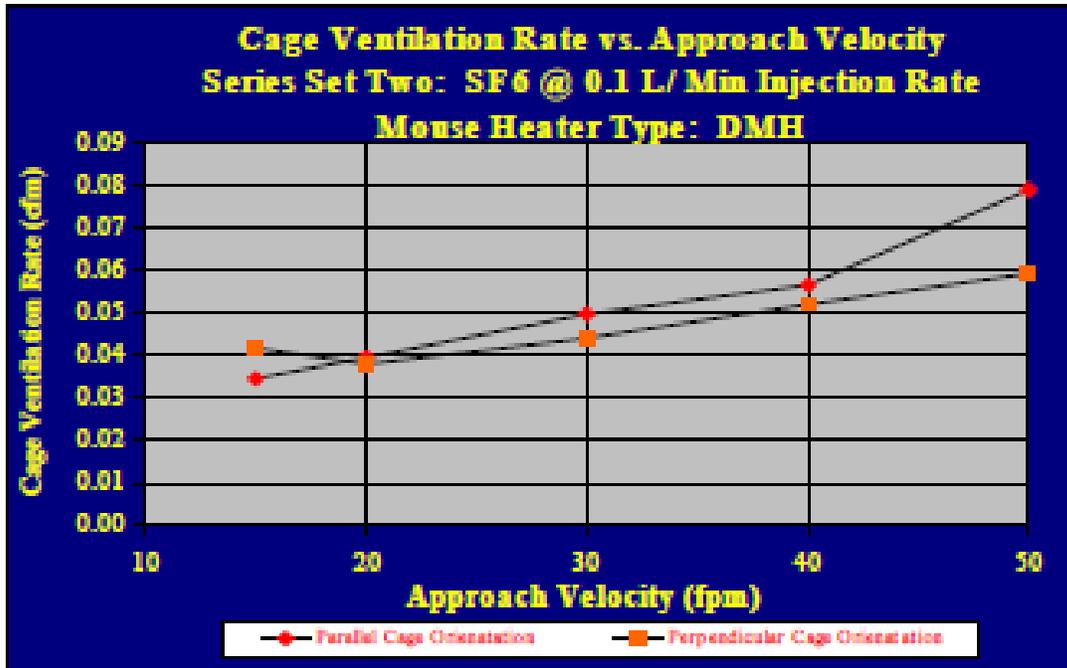
Figure 4.23   Cage Ventilation Rate vs. Approach Velocity. Series Set Two.
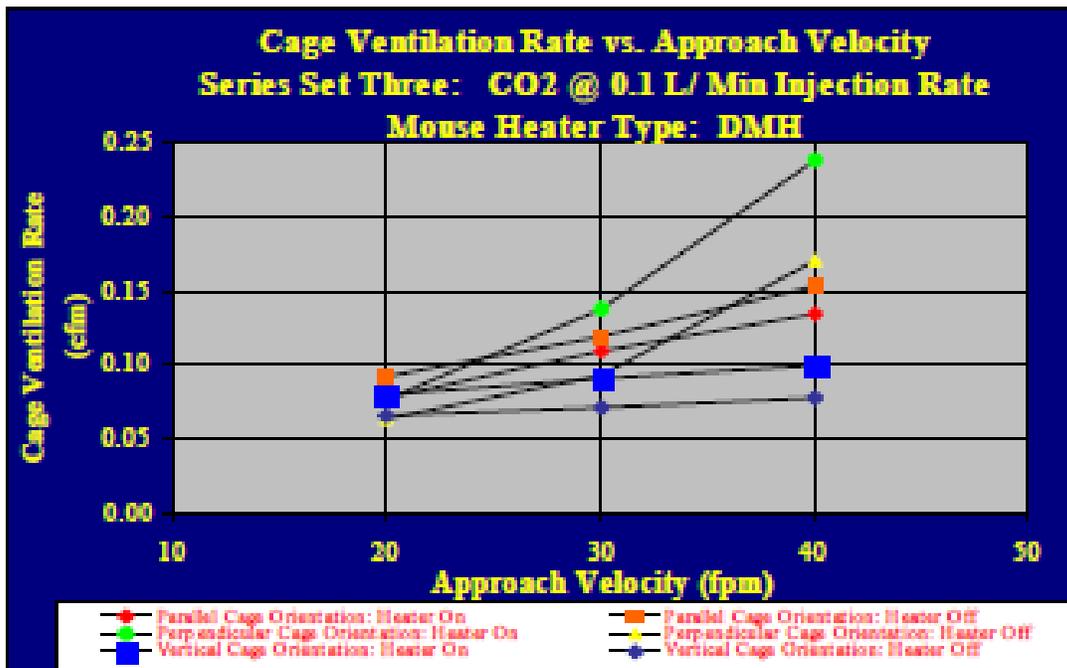
Figure 4.24   Cage Ventilation Rate vs. Approach Velocity. Series Set Three.
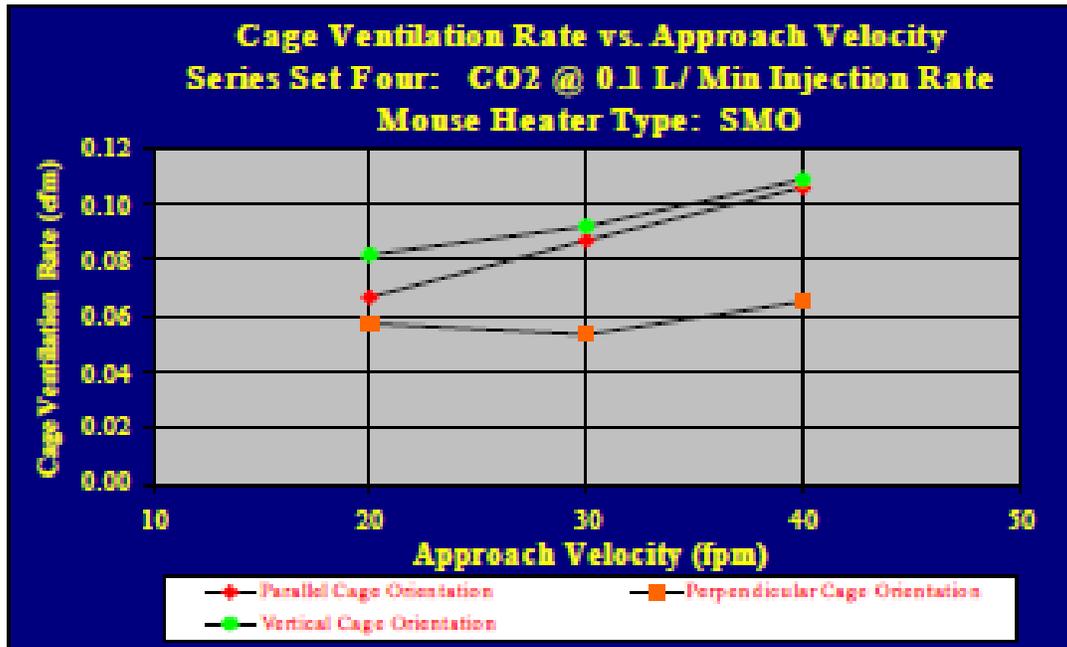
Figure 4.25   Cage Ventilation Rate vs. Approach Velocity. Series Set Four.
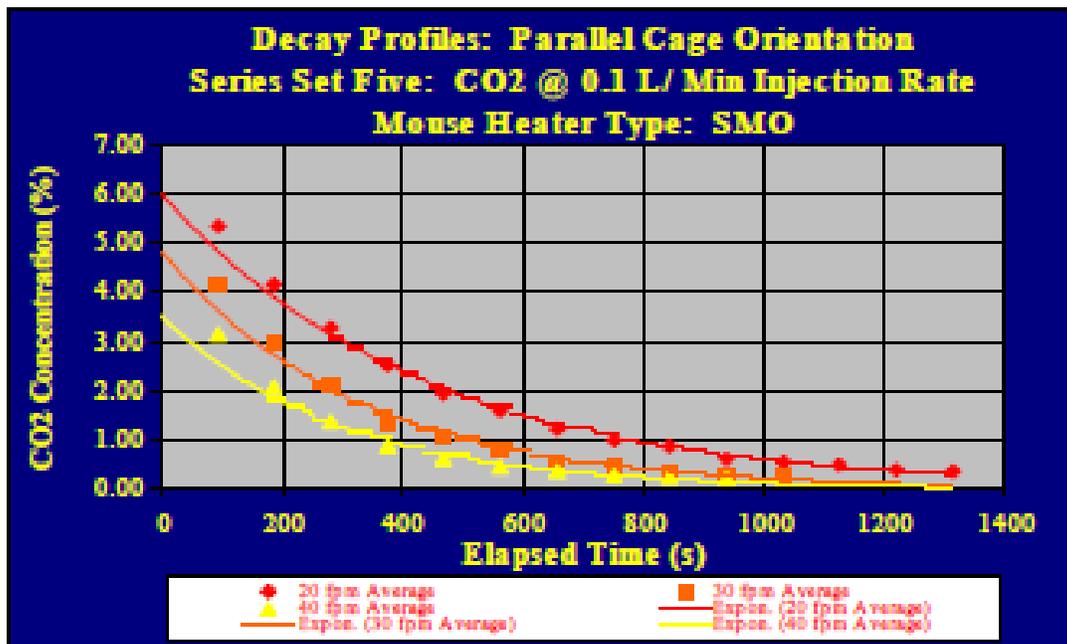
Figure 4.26   Decay Profiles: Parallel Cage Orientation. Series Set Five.
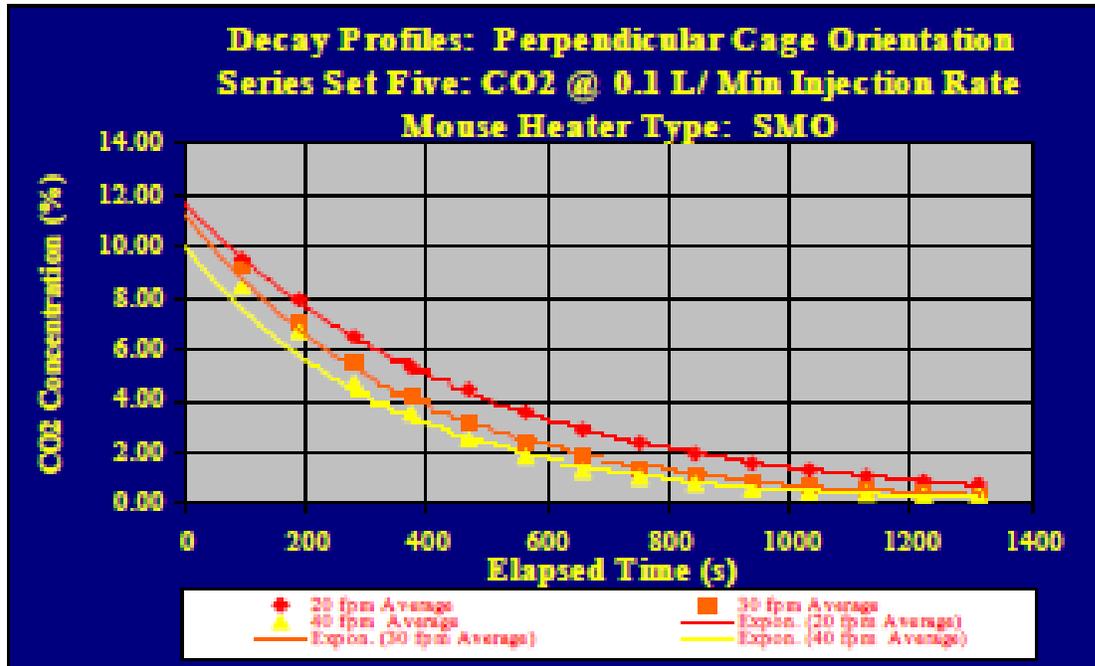
Figure 4.27   Decay Profiles: Perpendicular Cage Orientation. Series Set Five.
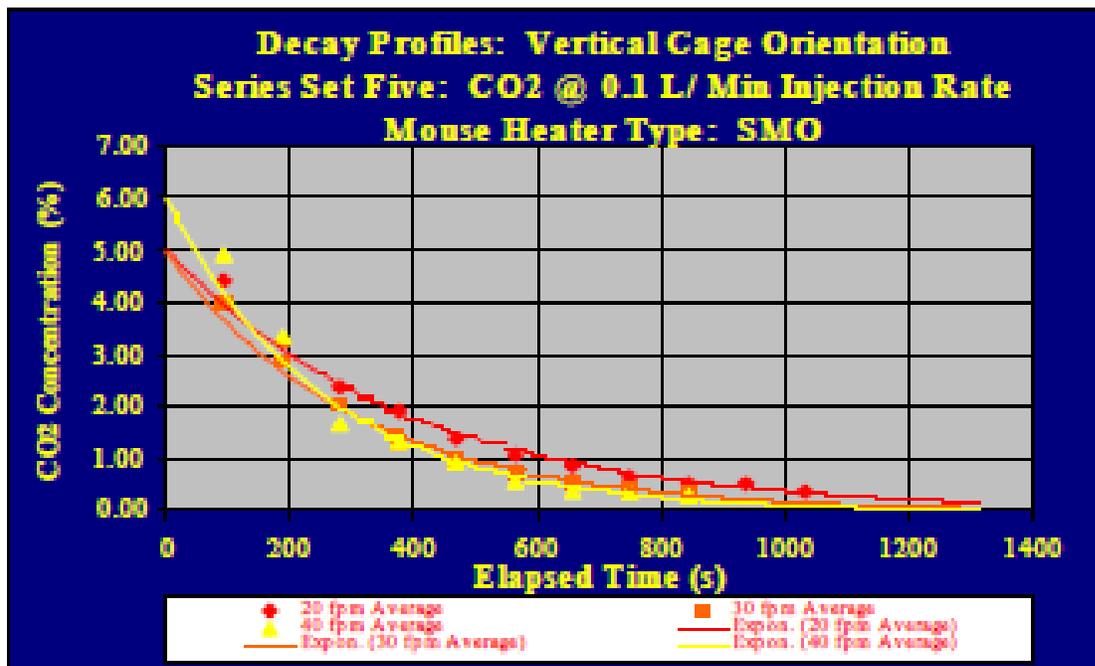
Figure 4.28   Decay Profiles: Vertical Cage Orientation. Series Set Five.
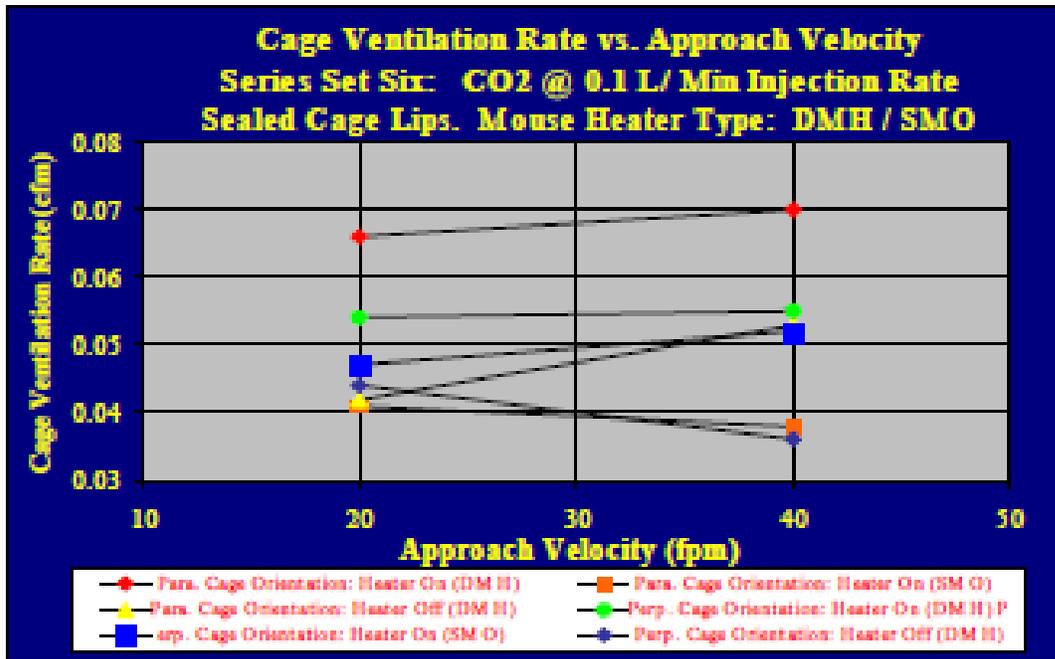
Figure 4.29   Cage Ventilation Rate vs. Approach Velocity.   Series Set Six.
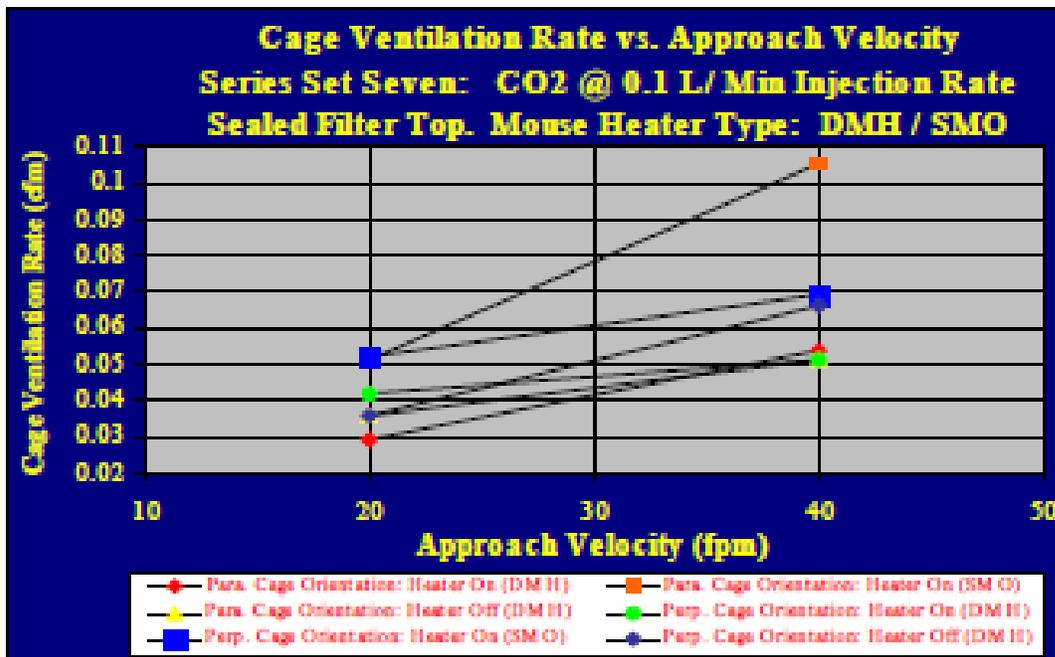
Figure 4.30   Cage Ventilation Rate vs. Approach Velocity.   Series Set Seven.
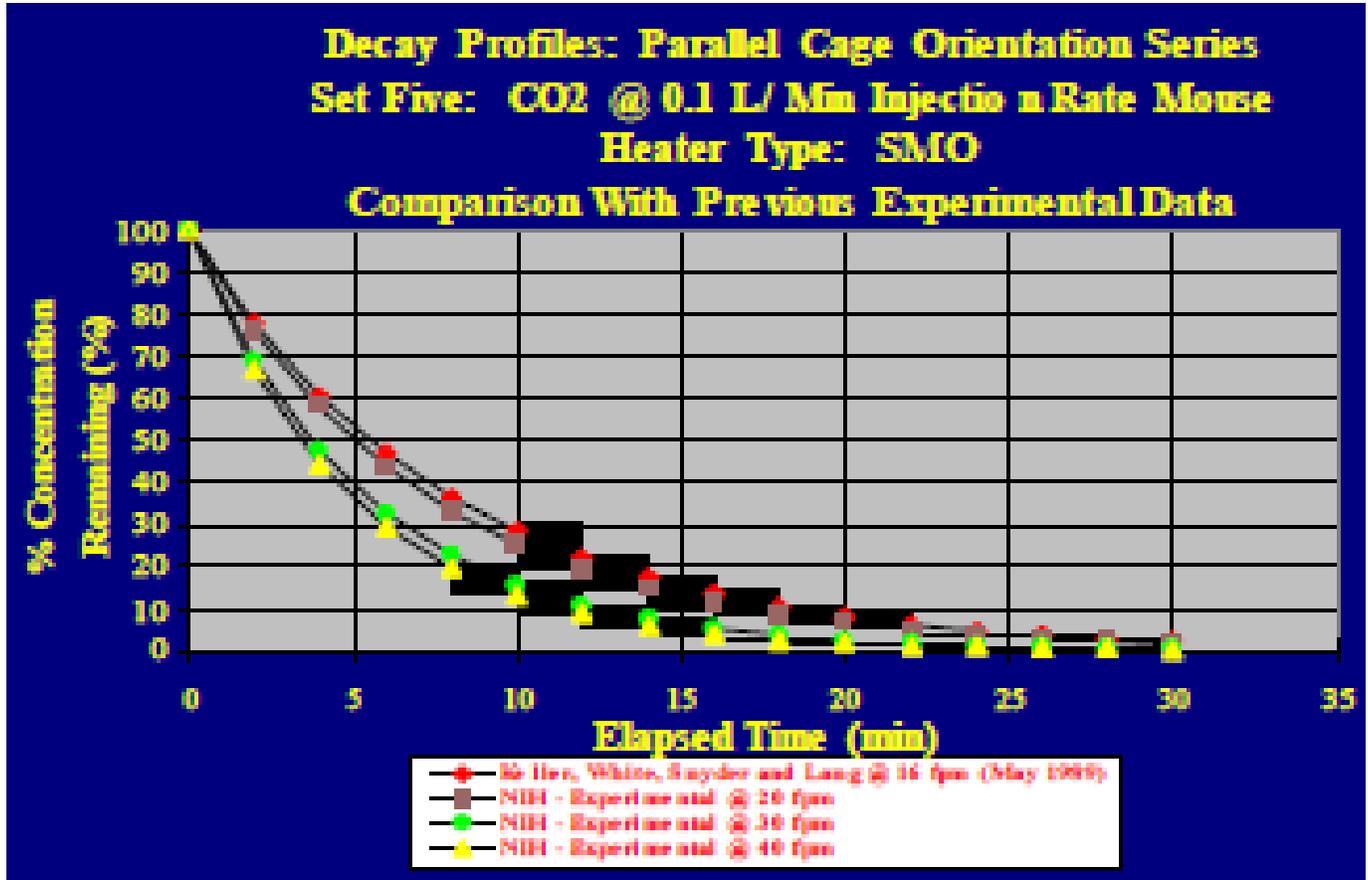
Figure 4.31   Comparison of Series Set Five: Parallel Orientation Sampling Method Results and Results from Keller, White, Snyder and Lang (1989)

4.1.2 CO_2, NH_3, H_2O and Heat Generation Measurements at Low and High Humidities

4.1.2.1 Introduction

This study was conducted at the Bioenvironmental Engineering Research Laboratory (BERL) and was intended to determine typical mass generation rates of CO_2, H_2O, and NH_3, and consumption of O_2 of mice in shoebox cages with bedding at two environmental relative humidities (35 percent and 75 percent). To determine the gas generation rates, animals and their cage habitat were placed within enclosed chambers (open-system calorimeters) with precisely controlled fresh air exchange rates. Cage bedding was not changed for longer than normal periods (10 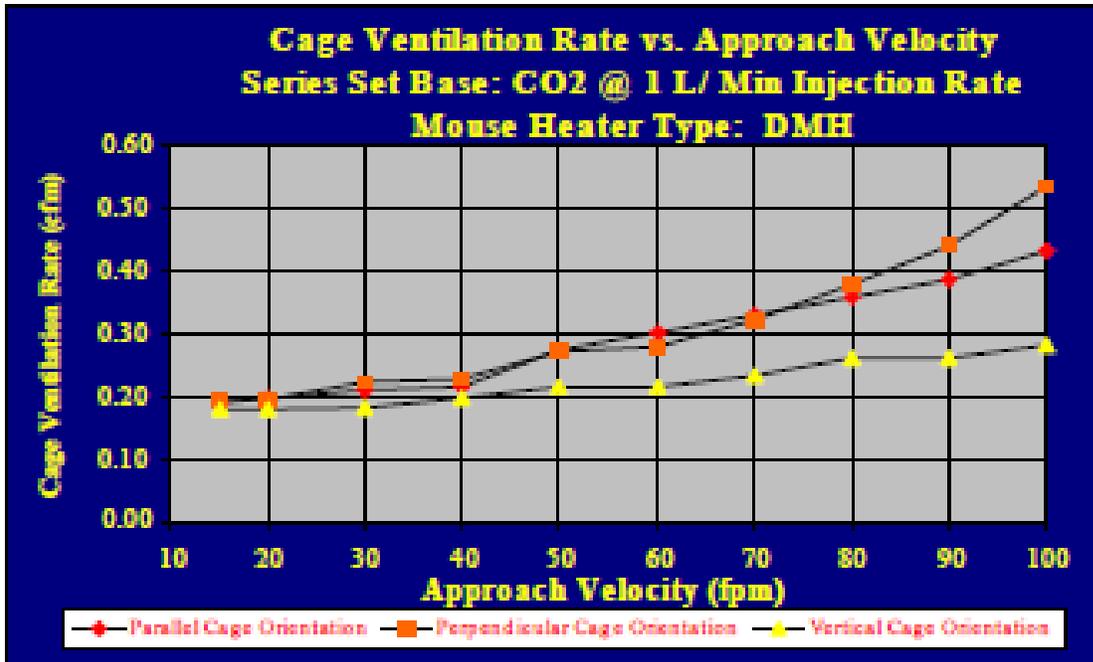days) to allow ammonia generating bacteria to develop within the bedding, that allowed us to obtain enough data to assess this time dependent process.

4.1.2.2 Mice and Husbandry Practices

Outbred mice (female, HSD-ICR, initial age of 4 weeks see figure 4.32) were placed in the shoebox cages for a 13-day period. The bedding type was hardwood (Beta chip) shavings. The cages and accessories were washed and sanitized prior to use using standard procedures for laboratory animal facilities. The number of mice per cage was the maximum allowable for the mouse weight and cage area (five mice/cage). The cages were housed in environmental chambers when not in the calorimeters. The environmental chambers and the chamber that the calorimeters were kept in were all approved for housing laboratory animals and were ventilated at 10-15 air changes per hour (ACH). The light period was 12 h light and 12 h dark; lights were turned on at 1:00 a.m. and off at 1:00 p.m. A white light and a blue light were on during the light period and only the blue light was on during the dark period. The light intensities of the light period and the dark period are presented in table 4.1.02. The mice received standard rodent diet and water *ad libitum*.

Table 4.1.03 Light intensities in mouse facilities

Calorimeter and Chamber	White and Blue Light On Light Intensities (lux)			White Light Off, Blue Light On Light Intensities (lux)		
Calorimeter 1	10			1		
Calorimeter 2	42			6		
Calorimeter 3	10			1		
Environmental Chamber #1 (RH 35 percent)	Top Shelf 25	Middle Shelf 7	Bottom Shelf 6	Top Shelf 2	Middle Shelf 1	Bottom Shelf 1
Environmental Chamber #2 (RH 75 percent)	Top Shelf 16	Middle Shelf 5	Bottom Shelf 4	Top Shelf 2	Middle Shelf 1	Bottom Shelf 1

The first three days after the mice arrived served as an acclimation period to allow the mice to adjust to their new surroundings and cage mates. The cages were kept at static conditions on

racks in two environmentally controlled chambers for acclimation. Both environmental chambers were kept at 24.0±1.5 °C (75.2±2.7 °F), but one was at 35±10 percent and the other at 75±10 percent relative humidity (RH). The temperature and relative humidity in each chamber were continuously monitored with hygrothermographs (Oakton, model 37250-00). Cage litter was changed after the 3-day acclimation period, that was just prior to the 10-day test period. After the experiment, the mice were euthanized in a container precharged with carbon dioxide.

4.1.2.3   *Calorimeter design*

Three indirect, convective calorimeters were used for this project (see figure 4.33). A brief introduction to the indirect calorimeter is given in appendix I: section 3.1. A flow diagram of the calorimeter is shown in figure 4.34.   Air temperature, velocity, and relative humidity were controlled in each calorimeter. The calorimeter boxes were constructed from 6.4e-3m (¼") thick plexiglass and were 0.356m high x 1.07m long x 0.585m deep (14" x 42.13" x 23"). Clear plexiglass was used to allow observation of animals and to allow light into the calorimeter from the environmental chamber.

The entire front panel was removable to allow access of workers and to move mice in and out. The inside edges of the front panel were coated with vacuum grease to form a seal and were clamped on the calorimeter with 10 clamps around the perimeter. A recirculation pipe, 200mm diameter plexiglass tube, exited from one side of the calorimeter box, went up and over the calorimeter, and attached to an in-line fan on the other side of the calorimeter box. This air recirculation system allowed for the control of air velocity past the cages without affecting the fresh airflow exchange rate.

Air Temperature Control

The calorimeter box and air recirculation system were completely sealed to maintain the gas balance. Therefore, heat generated within the calorimeter had to transfer through the box or tube surfaces. To enhance this heat transfer process, all three calorimeters were placed within an environmental chamber that was operated at a lower temperature than the calorimeter air temperature. Also, a plastic duct, which served as a heat exchanger, was placed around the outside portion of the air recirculation tube and conditioned air was forced between that duct and the air recirculation tube to create a heat exchange system. One separate air conditioning/heating unit per calorimeter was placed outside the environmental chamber. Air from the tube heat exchange surface was recirculated through these units to control the temperature of the air passing through the heat exchanger and, thus, the amount of heat leaving or entering the heat exchanger. This heat exchange system, plus a 150W electric heater bar placed in the air recirculation tube, allowed for precise control of air temperature entering the calorimeter boxes.

The heat exchanger, air conditioners, and heaters were controlled with a microprocessor PID temperature controller (Omega model CN9122A). Each calorimeter was individually controlled. Temperatures within the calorimeters were sensed with one type T thermocouple placed in the

center of the calorimeter box in front of the cages. The thermocouples were read with a Campbell data logger (model 21X). Air temperature was set at 24.0±1.5 °C (75.2±2.7 °F).

Figure 4.32   *Outbred Mice Female – HSD – ICR.*
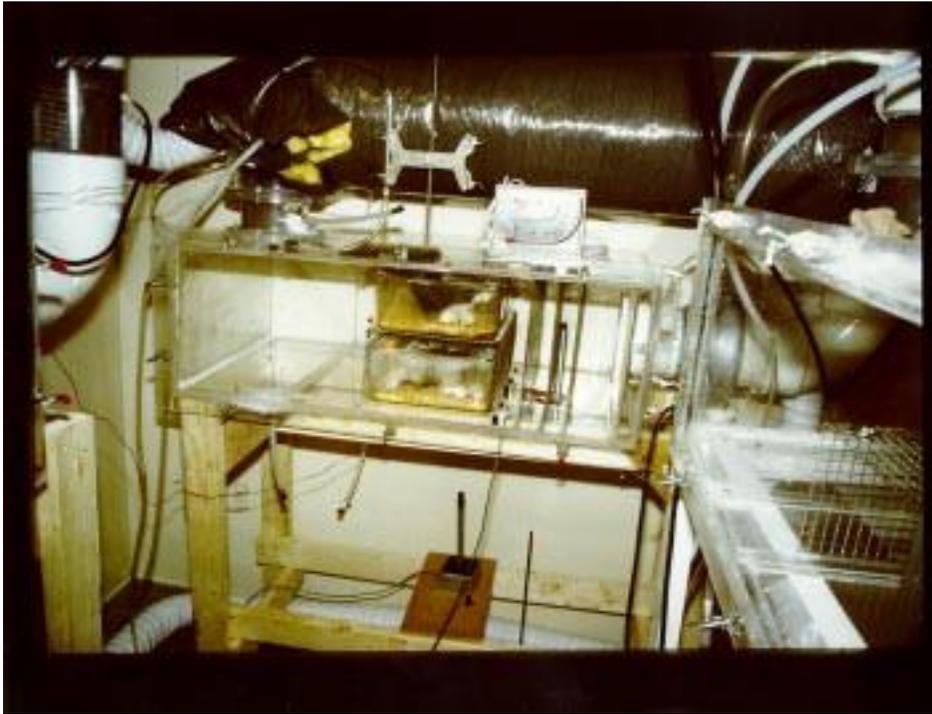
Figure 4.33 *An Indirect Convective Calorimeter*
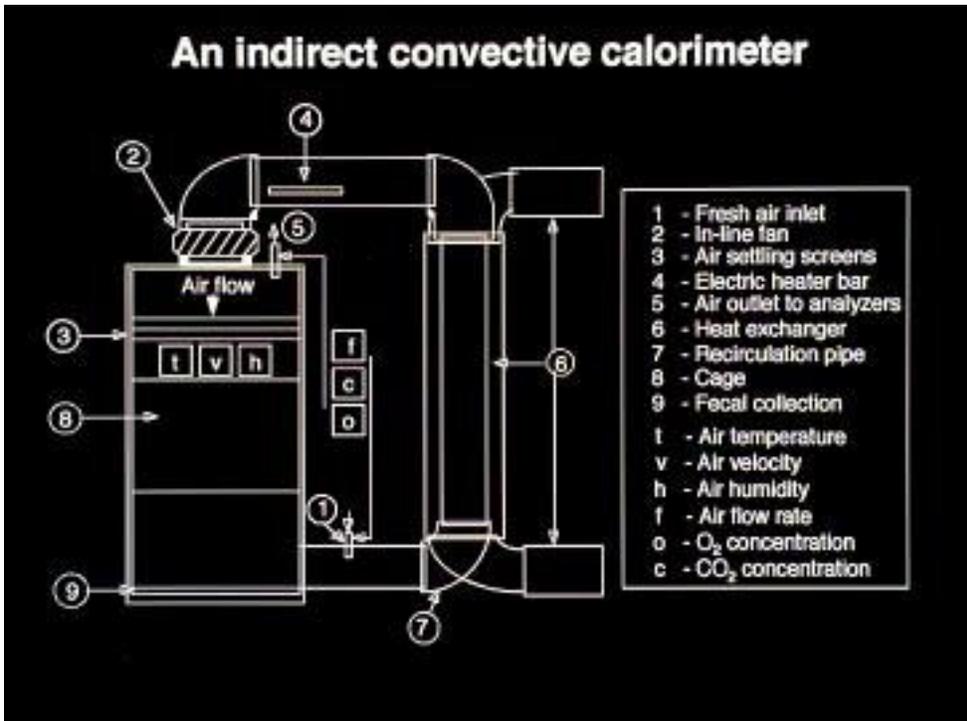
Figure 4.34 *Flow Diagram   - Indirect Convective Calorimeter*

Air Velocity Control

Air moved horizontally through the calorimeter so the movement was from front to back along the animal cages. Air movement was created by recirculating air through the air recirculation tube described previously. The airflow rate through the recirculation fan was controlled by adjusting the fan speed with a voltage controller. There was a square air diffuser at the air entry that distributed the air around the calorimeter cross-section. To further improve the uniformity of airflow across the cross-section, an air settling means was placed after the diffuser and before the animal cages, consisting of three perforated stainless steel sheets with 60 percent, 40 percent, and 30 percent open areas. To ensure that there was a uniform profile of air velocities approaching the animal cages, a 3 x 5 grid of air velocity measurements was taken between the air settling means and before the cages with a TSI air velocity meter (model 8738). The average air velocities approaching the mouse cages were set at 0.25±0.05 m/s (50±10 fpm) prior to each test (see appendix I: section 3.2.1 and 3.2.2 for calibration data).

Air Humidity Control

Relative humidity of the air within the calorimeters was controlled by three systems: 1) fresh air exchange, 2) desiccant drying system, and 3) humidification system.

1) Fresh air exchange (ventilation)–was provided to each calorimeter for several reasons: a) maintain appropriate O_2, CO_2, and NH_3 levels, b) remove moisture and help maintain appropriate relative humidity, and c) provide sample of air for gas analysis. Air was removed from the air entry part of the 0.20m (8") diameter air recirculation tube and passed through a Gilmont Instruments model GF1300 airflow meter (accuracy = 2 percent of reading). These fresh air exchange flow meters were calibrated prior to each test against a 1-liter bubble airflow meter (see appendix I: section 3.2.5 and 3.2.6 for calibration data). The air then flowed to a diaphragm pump that had a 500mL beaker in line to dampen the oscillation from the pump. Airflow rate was controlled by an air bypass system with a needle valve. Air flowed from the pump system to the gas analysis instruments, that were located in an adjacent environmental chamber.

Air drawn out of the calorimeters was precisely measured and used as flow rate in the O_2 consumption and CO_2 production calculations. A slight negative pressure was maintained within the calorimeters. This negative pressure would draw in the same amount of fresh air from the surrounding environmental chamber as was removed by the pump. A planned air inlet (8-mm diameter hole) was placed in the inlet part of the air recirculation tube, but some fresh air would have entered through unplanned inlets (leaks). Since the entire calorimeter was at a negative static pressure and a certain amount of air had to enter the calorimeter anyway, the leaks did not create a problem.

The air that entered the planned inlet passed first through a container of desiccant to remove its moisture. This fresh air was passed through a 30x10 cm desiccant cylinder filled with approximately 3500g of 100 percent $CaSO_4$, #8 mesh granules, to help control calorimeter relative humidity (see figure 4.34).

2)   Desiccant drying system–A separate air humidity control system was developed to remove moisture from the calorimeter air. To accomplish this, calorimeter air was recirculated through a desiccant drying system. The dehumidification system consisted of two diaphragm air pumps (approximately 10 L/min each) that pulled air from the calorimeter, passed it through a 0.30 x 0.10 m (12" x 4") desiccant cylinder filled with 100 percent $CaSO_4$, then returned the air back into the calorimeter (see figure 4.34; Dehumidification System). As the air passed through the desiccant, it effectively removed all of the moisture. The relative humidity exiting the bottom of the drying container was measured to be 0 percent with a Tri-Sense temperature/humidity meter (model 37000-00). The air pumps were operated manually based on the relative humidity in the calorimeter, which was sensed electronically with General Eastern (model RH-5-V) humidity transducers. The relative humidity sensors in each of the calorimeters and in the environmental chamber housing the calorimeters were calibrated prior to each 10-day run with a psychrometer. The signal from these sensors was collected on a Keithley Metrabyte DAS-8/PGA data acquisition system connected to an IBM compatible PC. The signals were analyzed with Keithley Metrabyte VIEWDAC software. After each calorimeter test, the desiccant was dried in an oven at 220 °C for 1.5 h and reused.

3)   Humidification system–For the high humidity calorimeters, water was added to the air as needed to control relative humidity by passing the recirculation air over an evaporative pad (see detailed operating procedure for humidification system in appendix I: section 3.3). Water was placed in a graduated cylinder above each calorimeter and flowed through a tube to an electric solenoid, then into the calorimeters to drip into an evaporative pad (figure 4.34; Humidification System). The solenoid valves were opened and closed manually based on the relative humidity readings (see detailed operating procedure for relative humidity measurements in appendix I: section 3.3).
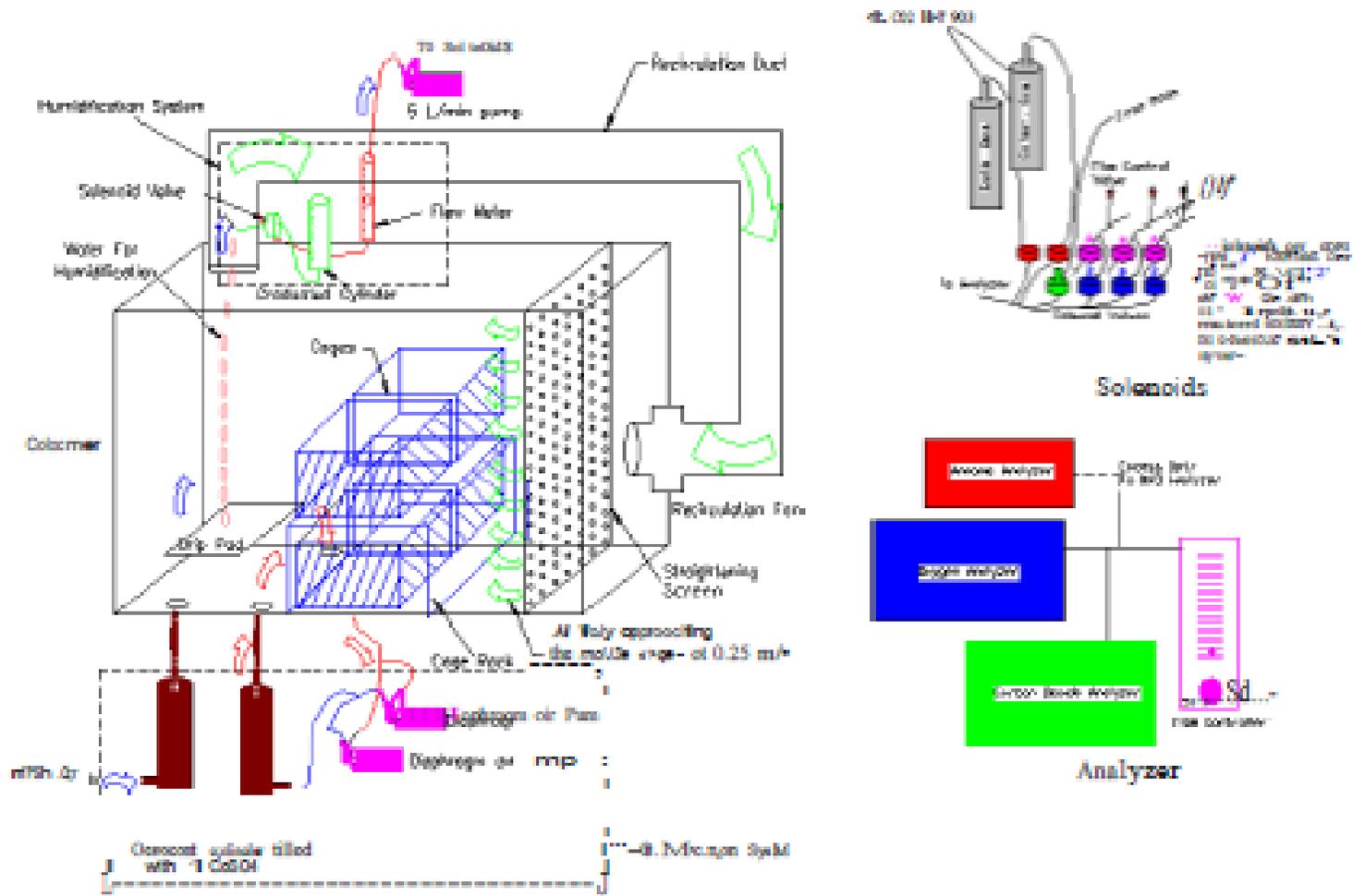
Figure 4.35 Experimental Apparatus for Mass Generation Rates of Ammonia in Mouse Cages at Low and High Relative Humidities.

Figure 4.35   Experimental Apparatus for Mass Generatitm Rates of.Ammtmia in Mouse Cages at Low and High Relative Humidities.

Oxygen, Carbon Dioxide, and Ammonia Analysis

Air flowed through a manually controlled solenoid valve switching system that controlled airflow to the O_2 and CO_2 analysis instruments (Beckman model OM-11 and LB-2, respectively). Air was analyzed from six sources—the three calorimeters, the environmental chamber that housed the calorimeters, and two standard gases. Each source was connected to a separate solenoid valve that directed air through the O_2 and CO_2 analyzers and either stopped airflow (standard gases) or redirected it into the outside room (calorimeter and chamber air). All of the solenoid valves were controlled manually. Certified standard gases (Matheson) were used to set the ranges of O_2 and CO_2 that were to be analyzed. Standard gas #1 was certified to have approximately 17.5 percent O_2 concentration and 0.55 percent CO_2 concentration. Standard gas #2 was certified to have 18.9 percent O_2 concentration and 1.58 percent CO_2 concentration. Output from the gas analyzers was continuously recorded on a strip chart recorder. Ammonia concentration of the sample air was measured with an ammonia gas detector (PhD model 1600W/1633, Biosystems, Inc.) that was calibrated to ammonia standard gases at 52.7 ppm. During the second test, calorimetric tubes (MAS, No. 487339) were also used as a check for ammonia levels.

Calibration of Calorimeters

Prior to each of the 10-day test periods, the calorimeters were calibrated by burning an ethanol lamp in the calorimeters to determine their mean recovery ratios of CO_2 and O_2. This procedure also served as an integrated check on all components of the calorimeter and determined the overall accuracy of the calorimeter. An ethanol lamp was filled with absolute ethanol (EtOH) and placed on an analytical balance that had been leveled on a platform inside a calorimeter. The lamp was ignited, the calorimeter door was sealed shut. After the ethanol lamp established a steady burn rate, the change in weight (g/min) of the ethanol lamp was measured with a stopwatch over several 10-minute periods (EtOH). Differences in percent O_2 content of air leaving the calorimeter (O_{2out}) was subtracted from O_2 content of air entering the calorimeter (O_{2in}) over the 10-minute periods (O_{2in}–O_{2out}). The same procedure for CO_2 analysis was simultaneously recorded (CO_{2out}–CO_{2in}). Accuracy, recovery, and calibration values for each calorimeter were obtained by comparison of respiratory quotient RQ = (CO_2 produced)/(O2 consumed) and recovery of gases obtained from the EtOH, O_2 percent, and CO_2 percent measurements. Calibration had RQ ranges from 0.64 to 0.81 in test 1. The accuracy of O_2 and CO_2 recovery ratio ranged from 83 percent and 94 percent to 121 percent and 117 percent, respectively, in test 1. Calibration had RQ ranges from 0.67 to 0.81 in Test 2. The accuracy of O_2 and CO_2 recovery ranged from 88 percent and 101 percent to 112 percent and 114 percent, respectively, in test 2. Calibration results are presented in appendix I: section 3.2.7 and 3.2.8.

4.1.2.4   Experimental Procedure

There were two environmental relative humidity treatments (low and high relative humidity) and three replications per treatment so there were six experimental units. Since there were only three calorimeters, this experiment was divided into two time periods. During test 1 (Oct. 18, 1997 to Oct. 27, 1997), two experimental units were at the 35 percent relative humidity treatment and one experimental unit was at the 75 percent relative humidity treatment. During test 2 (Dec. 13, 1997 to Dec. 22, 1997), two experimental units were at the 75 percent relative humidity treatment and one at the 35 percent treatment. When the mice first arrived, they were randomly assigned to 15 cages, then some adjustments were made to equalize average mouse weight among the cages. Only 12 cages were used in the tests, but extra mice were ordered to replace experimental animals if problems occurred. None of the extra mice were used. During test 1, 10 cages were randomly assigned to the 35 percent relative humidity treatment and five cages to the 75 percent relative humidity treatment. During test 2, 10 cages were assigned to the 75 percent and 5 cages to the 35 percent relative humidity treatments. The assignment of cages is shown in appendix I: sections 3.2.9 and 3.2.10.

After the 3-day acclimation period, there was a 10-day test period when the mice were placed in the calorimeters for 10 hours each day where the measurements were taken (see standard operating procedures in appendix I: section 3.3). During the rest of the day, the mice were kept in their respective environmental chambers. The same four cages were always randomly assigned to a different calorimeter each day and were an experimental unit (the randomized assignments are in appendix I: section 3.2.9 and 3.2.10). At the morning of every day of the tests, the mice, feed, water, and litter were weighed separately. Four cages with five mice each were placed in each calorimeter for a total of 20 mice in each calorimeter. The three calorimeters were operated at the same temperature (24.0±1.5 °C (75.2±2.7 °F). Data were collected three times during the photophase (approximately at 10:40, 11:20 and 12:00 a.m.) and three times during the scotophase (approximately at 3:15, 4:00 and 4:40 p.m.). Since the lights were shut off at 1:00 p.m., half of the data were obtained during the daily photophase and half during the scotophase, so effects of light could be determined.

The calorimeters were in the horizontal position so airflow approached the front of the cages (see figure 4.34). The four cages were positioned on two levels (as in a cage rack). The calorimeter static pressure was kept negative. The fresh air exchange rates for the calorimeters varied from 5 to 9.3 L/min. Fresh airflow rates were increased over the 10-day test period to keep ammonia levels low. After the mice were placed in the calorimeter and also after the lights were turned off, a dehumidification system was manually turned on for approximately one hour for the low humidity calorimeters to reduce the humidity. The dehumidification system was only operated for about one hour then the gas levels were allowed to stabilize for around two hours before readings were taken. Weights of the desiccant cylinders were determined at the start and end of each daily experiment so water balances could be calculated. At the beginning of each daily experiment, the cylinders were emptied and refilled with recharged desiccant. Water production was measured based on water added to calorimeter, different weights of desiccant cylinders in

the dehumidification system, and relative humidity and temperature readings of the calorimeters and chamber.

4.1.2.5   Recovery Ratio of CO_2 and O_2 Calculation.

Assumptions: EtOH has a molecular weight of 46.0694, 22.414 liters (L) of gas per mole, and 4.9 Kcalories of energy per L O_2 consumed, and 7.1 Kcal/g of heat of combustion.

According to:

$$C_2H_6O + 3O_2 \quad 2CO_2 + 3H_2O + Energy \tag{4.5}$$

$$RQ \quad \frac{2CO_2}{O_2} \quad 0.67 \tag{4.6}$$

Equation to calculate CO_2 generation rate and O_2 consumption rate from sample air:

$$P_{cco} \quad \frac{(CO_{2out} \quad CO_{2in}) \quad M}{100} \tag{4.7}$$

$$P_{cO2} \quad \frac{(O_{2in} \quad O_{2out} \quad M}{100} \tag{4.8}$$

Where:

P_{cco2}, P_{cO2}	CO_2 generation rate and O_2 consumption rate, L/min.
CO_{2out}, O_{2out}	CO_2 concentration and O_2 concentration of sample air, percent.
CO_{2in}, O_{2in}	CO_2 concentration and O_2 concentration of chamber air, percent.
M	Air exchange flow rate, L/min.

Respiratory quotient (RQ):

$$RQ \quad \frac{P_{cco2}}{P_{cO2}} \tag{4.9}$$

Equation to calculate CO_2 generation rate and O_2 consumption rate from burning EtOH:

$$EtOH \quad \frac{D \quad 22.414 \quad F}{10 \quad 46.069} \tag{4.10}$$

where:

EtOH	CO_2 generation rate and O_2 consumption rate from burning EtOH, L/min.
D	Burning EtOH weight in 10 minutes, g
F	Factor: 2 for CO_2 and 3 for O_2.

Equation to calculate recovery ratio:

$$\text{Recovery ratio} = \frac{P}{EtOH}$$

(4.11)

where:

P CO_2 generation rate and O_2 consumption rate from sample air, L/min

4.1.2.6   Mass Generation Rate Calculation
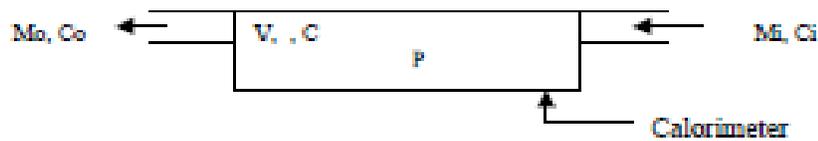
where:

mi, mo	Fresh air flow rate, kg/s
Ci,C, Co	Ammonia concentration, mg/kg
V	Volume of the calorimeter, m^3 ($0.225\ m^3$)
	Specific volume of air, m^3/kg
P	Ammonia production rate, mg/s

$$\frac{V}{v}\frac{dC}{dt} = miCi + P - moCo$$

(4.12)

Since mi = mo = m and C=Co, by solving the above equation we get the following result:

$$C = Ci + \frac{P}{m}(1 - e^{-\frac{mv}{V}t})$$

(4.13)

When the time goes to infinity, the calorimeter reaches the stable state, where the concentration is Ci + P/m. If we let =V/m , then when t=3 , the concentration will reach 95 percent of the stable state value. We ran our test mostly at 5 L/min flow rate. The volume of the calorimeter is 225 L. So   is 45 minutes and after 135 minutes, the concentration will reach 95 percent of its stable value. We measured the ammonia concentration at the stable state.

So:

$$C - Ci = \frac{P}{m} \qquad (4.14)$$

With the units transfer:

$$P = 0.7598 \times 0.001 \times 6 \frac{(C - Ci) \times m}{W_m} \qquad (4.15)$$

where:

P	Ammonia generation rate, g/hr/100g of mice.
C	Ammonia concentration in the calorimeter, ppm.
Ci	Ammonia concentration in the chamber, ppm.
m	Fresh air flow rate, L/min.
W_m	Mice weight in one calorimeter, g.

Using the same general equation to calculate carbon dioxide generation rate and consumption rate of O_2

$$P = 1.964 \times 60 \frac{(C - Ci) \times m}{W_m} \qquad (4.16)$$

where:

P	Carbon dioxide generation rate or oxygen consumption rate, g/hr/100g of mice.
C	Carbon dioxide concentration in the calorimeter, percent.
Ci	Carbon dioxide concentration in the chamber, percent.

1L CO_2 = 1.964 g, 1L NH_3 = 0.7598 g, 1-mole = 22.414 liters of volume, and mole weight of NH_3 = 17.03.

4.1.2.7   Water Production Calculation
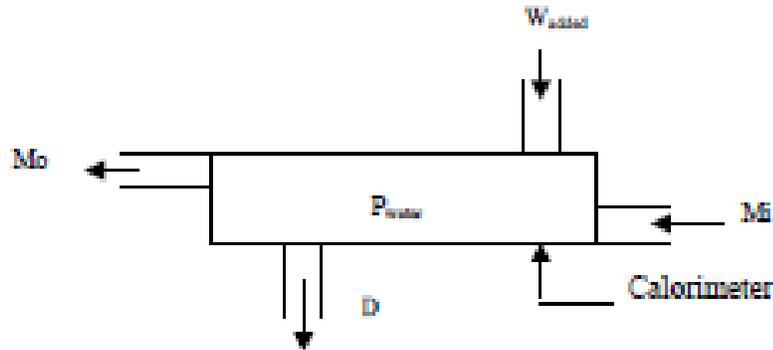
where:

P_{water}	Total water production, g/hr/100g of mice.
Mi	Leaking airflow rate, L/min.
Mo	Air exchange flow rate, L/min.
W_{added}	Water added to calorimeter, g.
D	Dehumidified water, g.

Equation to calculate water from air pumped out:

$$P_{out} = \frac{R_a \ M_o \ 1.1614 \ 6}{W_m} \qquad (4.17)$$

where:

P_{out}	Water production from pumped out air, g/hr/100g of mice.
R_a	Humidity ratio g moisture /kg dry air in calorimeter, g/kg.
W_m	Mice weight in calorimeter, g.
1.1614 x 6	Coefficient to convert units.

Equation to calculate water entering calorimeter through air leaking in:

$$P_{in} = \frac{R_r \ M_i \ 1.1614 \ 6}{W_m} \qquad (4.18)$$

where:

P_{in}	Water gain due to air leakage, g/hr/100g of mice.
R_r	Humidity ratio, g moisture/ kg dry air in chamber, g/kg.

Equation to calculate water added in caloirmeter (P_{added}, g/hr/100g of mice) over the 10 hr test period:

$$P_{added} = \frac{W_{added}}{10} \cdot \frac{100}{W_m} \tag{4.19}$$

Equation to calculate water removed by dehumidification system (P_d, g/hr/100g of mice) over the 10 hr test period:

$$P_d = \frac{D}{10} \cdot \frac{100}{W_m} \tag{4.20}$$

The total water production was summed:

$$P_{water} = P_{out} - P_{in} + P_d - P_{added} \tag{4.21}$$

4.1.2.8   Data Analysis and Results

4.1.2.8.1   Preliminary Data Tabulation, Collection and Analysis

All data referred to in this section are listed in tabulated and graphical form in appendix I.

In this experiment, data were collected three times during the photophase and three times during the scotophase every day, and this data is reported in appendix I: section 3.4.1 under raw data for test 1 and test 2. The averages of the three data points taken in the photophase and the scotophase each day are reported in appendix I: section 3.4 under individual calorimeter data for NH_3, CO_2, and O_2 concentration for test 1 and test 2. The mass generation rates were calculated based on these data.

The relative humidity sensors in each of the calorimeters and chamber sensed relative humidity every five minutes over the 10 hr test period each day and values are reported in appendix I: section 3.4 under relative humidity data for test 1 and test 2. The average values of relative humidity and temperature in the calorimeters and chamber over the 10-hour test period were used to determine the humidity ratio value of the air (g moisture /kg dry air) from a psychrometric chart. This data were used along with data on water added by the humidification system and water removed by the dehumidification system to calculate water production rates which are reported in the appendix I: section 3.4 under water production data for test 1 and test 2.

The individual weight of mice, feed, water, and litter were determined every day of the tests and reported in appendix I: section 3.4 under raw weight data for test 1 and test 2. Mice weight in individual cages and cage group were calculated and reported in the appendix I: section 3.4 under mice weight for test 1 and test 2.

Since test 1 had two experimental units at the 35 percent relative humidity and test 2 had two experimental units at the 75 percent relative humidity, the average value of the two experimental units at 35 percent relative humidity in test 1, and the average value of the two experimental units at 75 percent relative humidity in test 2 are reported in the appendix I: section 3.4 under Average Gas Mass Generation Rates for All Experimental Units in Test 1 and Test 2.

The data for all experimental units in test 1 and test 2 were averaged for both relative humidity treatments and are presented in the appendix I: section 3.4 under average data for all experimental units from both test 1 and test 2. There were higher mass generation rates of ammonia in the high relative humidity treatment (RH 75 percent) than in the low relative humidity treatment (RH 35 percent). Mass generation rate of ammonia during scotophase is higher than during photophase at the same relative humidity treatment. Water production data have some variation in each day. Average value of water production data for the low relative humidity treatment was higher than for the high relative humidity treatment.

4.1.2.8.2 CO_2, NH_3 and H_2O Data Preparation for Use in CFD Simulations

The data were regrouped and reanalyzed for general usage, and for use in the CFD simulations performed later. As demonstrated in appendix I: sections 3.4.1.9 and 3.4.1.10, the levels of mass generation were higher for the dark (scotophase) period than they were for the light (photophase) period. Emphasis has therefore been placed on the scotophase results for the purposes of this study.

For each test, the cage group data were collected for each of the days in the experiment, and the actual level of cage relative humidity (RH) (expressed as a percentage) was tabulated with each of the measured generation rates. For example, in Tables 4.1.04 and 4.1.05 below, the NH_3 generation rates on a day-by-day basis for the groups of cages are collected together. These data can then be rearranged in terms of the Desired RH level, as demonstrated in Tables 4.1.06 and 4.1.07. Plotting the data contained in tables 4.1.06 and 4.1.07 in a graph, the relationship between the NH_3 level and the day number can be represented as a polynomial approximation for both the low RH level (Desired 30 – 35 percent RH) and the high RH level (Desired 75 – 80 percent RH), as shown in figure 4.36. The generation rate of NH_3 can be then be calculated by interpolation between the two polynomial approximations on a given day for a given level of cage RH. It should be noted that the average level of cage RH achieved in the Desired 30 – 35 percent RH experiments was 60.86 percent (compared with the environmental RH average of around 39 percent), while the average level of cage RH in the Desired 75 – 80 percent RH experiments was 79.69 percent. Therefore, the interpolated value is only wholly accurate between 61 percent and 80 percent cage RH. It is interesting to note that the generation of NH3 is clearly dependent on the level of cage RH. However, this is not the case for temperature. In particular, figure 4.37 shows that there is no clear relationship between the generation rate of NH3 and temperature: there is significant scatter in the experimental data.

The levels of H_2O and CO_2 can also be rearranged for general usage for the CFD work. **Note:** Although the values have been considered for the scotophase, the H2O measurements were not noted for the scotophase or photophase individually; as noted above, water production was considered over a 10 hr period each day, with measurements taken in 5-minute intervals. Tables 4.1.08 and 4.1.09 show the variation of H_2O and CO_2 on a day-by-day basis for test 1 and test 2 respectively, while Tables 4.1.10 and 4.1.11 rearrange the data according to the Desired RH level. figure 4.38. to 4.41 show the variations of H_2O and CO_2 with the day in the experiment for the low RH level (Desired 30 – 35 percent RH) and the high RH level (Desired 75 – 80 percent RH) experiments respectively (Note that the erroneous negative H_2O generation rate, highlighted in black in table 4.1.08, has not been included in figure 4.38). The plots show that, based on the degree of scatter in the experimental measurements, the levels of CO_2 and H_2O can be considered constant throughout the days of the experiment. In particular, the average values are as follows:

Low RH Level:
CO_2 generation rate (g /hr/ 100g BW)   =   9.35e-1 g/ hr/ 100g BW
H_2O generation rate (g /hr/ 100g BW)   =   7.84e-1 g/ hr/ 100g BW

High RH Level:

CO_2 generation rate (g /hr/ 100g BW)	=	8.75e-1 g/ hr/ 100g BW
H_2O generation rate (g /hr/ 100g BW)	=	8.78e-1 g/ hr/ 100g BW

It can be noted that the generation rates of H_2O and CO_2 do not change significantly with the RH level. We can therefore further reduce the generation rates to two numbers, which we can regard as constant irrespective of RH or day in the experiment.

CO_2 generation rate (g /hr/ 100g BW)	=	9.05e-1 g/ hr/ 100g BW
H_2O generation rate (g /hr/ 100g BW)	=	8.31e-1 g/ hr/ 100g BW

Table 4.1.04   Tabular Variation of RH, NH_3 and $NH_{3\,(max)}$ with Day: Test 1, Lights Off

Cage Group	Day	RH actual (percent)	NH_3 (g/ hr/ 100g BW)	$NH_{3\,(max)}$ (g/ hr/ 100g BW)
1-4 (Desired RH = 30 – 35 percent)	1	71.3	4.69E-04	5.87E-04
	2	66.1	5.44E-04	7.32E-04
	3	70.4	8.30E-04	9.96E-04
	4	62.9	1.26E-03	1.52E-03
	5	61.4	0.00E+00	2.07E-04
	6	54.4	1.34E-03	1.38E-03
	7	52.6	1.96E-03	2.22E-03
	8	58.4	1.86E-03	2.06E-03
	9	61.4	4.31E-03	4.55E-03
	10	57.1	5.62E-03	6.28E-03
5-8 (Desired RH = 75 – 80 percent)	1	69.7	3.88E-04	4.76E-04
	2	84.8	5.23E-04	6.49E-04
	3	83.8	1.46E-03	1.91E-03
	4	78.2	3.73E-03	4.11E-03
	5	77.7	4.06E-03	4.68E-03
	6	79.6	4.27E-03	4.48E-03
	7	76.3	5.22E-03	5.39E-03
	8	81.1	7.30E-03	7.65E-03
	9	83.4	6.60E-03	6.70E-03
	10	80.6	5.02E-03	5.22E-03
9-12 (Desired RH = 30 – 35 percent)	1	68.0	5.67E-04	6.38E-04
	2	67.7	5.24E-04	7.59E-04
	3	62.8	6.99E-04	8.39E-04
	4	66.2	1.23E-03	1.44E-03
	5	56.8	1.29E-03	1.42E-03
	6	55.5	1.59E-03	1.65E-03
	7	62.4	2.59E-03	2.69E-03
	8	54.1	2.04E-03	2.24E-03
	9	60.2	4.71E-03	4.78E-03
	10	60.5	3.43E-03	4.01E-03

Table 4.1.05   Tabular Variation of RH, NH_3 and $NH_{3\,(max)}$ with Day: Test 2, Lights Off

Cage Group	Day	RH actual (percent)	NH_3 (g/ hr/ 100g BW)	$NH_{3\,(max)}$ (g/ hr/ 100g BW)
1-4 (Desired RH = 30 – 35 percent)	1	69.7	9.21E-05	1.11E-04
	2	59.6	0.00E+00	0.00E+00
	3	62.6	5.30E-05	1.06E-04
	4	63.7	2.89E-04	3.06E-04
	5	64.4	5.94E-04	6.29E-04
	6	58.0	1.05E-03	1.10E-03
	7	64.0	1.02E-03	1.41E-03
	8	50.3	-	-
	9	50.6	3.68E-03	4.66E-03
	10	52.4	2.75E-03	3.82E-03
5-8 (Desired RH = 75 – 80 percent)	1	73.9	1.28E-04	1.64E-04
	2	83.5	3.69E-05	5.53E-05
	3	79.5	9.19E-05	1.10E-04
	4	83.8	3.71E-04	4.24E-04
	5	86.9	2.15E-03	2.22E-03
	6	75.7	6.75E-03	7.19E-03
	7	87.5	8.16E-03	8.91E-03
	8	77.3	1.00E-02	1.04E-02
	9	75.2	1.39E-02	1.45E-02
	10	77.7	1.16E-02	1.21E-02
9-12 (Desired RH = 75 – 80 percent)	1	74.3	1.26E-04	1.61E-04
	2	80.4	3.53E-05	5.29E-05
	3	84.4	7.00E-05	1.05E-04
	4	79.4	5.29E-04	6.35E-04
	5	82.8	3.35E-03	3.54E-03
	6	81.1	6.38E-03	6.74E-03
	7	76.5	8.99E-03	9.36E-03
	8	76.8	1.14E-02	1.19E-02
	9	77.6	1.18E-02	1.23E-02
	10	81.0	1.03E-02	1.14E-02

Table 4.1.06 Tabular Variation of RH, NH_3 and $NH_{3\,(max)}$ with Day: Desired RH $= 30 - 35$ percent, Lights Off

Cage Group	Day	RH actual (percent)	NH_3 (g/ hr/ 100g BW)	$NH_{3\,(max)}$ (g/ hr/ 100g BW)
1 - 4 Test 1	1	71.3	4.69E-04	5.87E-04
	2	66.1	5.44E-04	7.32E-04
	3	70.4	8.30E-04	9.96E-04
	4	62.9	1.26E-03	1.52E-03
	5	61.4	0.00E+00	2.07E-04
	6	54.4	1.34E-03	1.38E-03
	7	52.6	1.96E-03	2.22E-03
	8	58.4	1.86E-03	2.06E-03
	9	61.4	4.31E-03	4.55E-03
	10	57.1	5.62E-03	6.28E-03
9 – 12 Test 1	1	68.0	5.67E-04	6.38E-04
	2	67.7	5.24E-04	7.59E-04
	3	62.8	6.99E-04	8.39E-04
	4	66.2	1.23E-03	1.44E-03
	5	56.8	1.29E-03	1.42E-03
	6	55.5	1.59E-03	1.65E-03
	7	62.4	2.59E-03	2.69E-03
	8	54.1	2.04E-03	2.24E-03
	9	60.2	4.71E-03	4.78E-03
	10	60.5	3.43E-03	4.01E-03
1 – 4 Test 2	1	69.7	9.21E-05	1.11E-04
	2	59.6	0.00E+00	0.00E+00
	3	62.6	5.30E-05	1.06E-04
	4	63.7	2.89E-04	3.06E-04
	5	64.4	5.94E-04	6.29E-04
	6	58.0	1.05E-03	1.10E-03
	7	64.0	1.02E-03	1.41E-03
	8	50.3	-	-
	9	50.6	3.68E-03	4.66E-03
	10	52.4	2.75E-03	3.82E-03

Table 4.1.07 Tabular Variation of RH, NH_3 and $NH_{3\,(max)}$ with Day: Desired RH = 75 − 80 percent, Lights Off

Cage Group	Day	RH actual (percent)	NH_3 (g/ hr/ 100g BW)	$NH_{3\,(max)}$ (g/ hr/ 100g BW)
5-8 Test 1	1	69.7	3.88E-04	4.76E-04
	2	84.8	5.23E-04	6.49E-04
	3	83.8	1.46E-03	1.91E-03
	4	78.2	3.73E-03	4.11E-03
	5	77.7	4.06E-03	4.68E-03
	6	79.6	4.27E-03	4.48E-03
	7	76.3	5.22E-03	5.39E-03
	8	81.1	7.30E-03	7.65E-03
	9	83.4	6.60E-03	6.70E-03
	10	80.6	5.02E-03	5.22E-03
5-8 Test 2	1	73.9	1.28E-04	1.64E-04
	2	83.5	3.69E-05	5.53E-05
	3	79.5	9.19E-05	1.10E-04
	4	83.8	3.71E-04	4.24E-04
	5	86.9	2.15E-03	2.22E-03
	6	75.7	6.75E-03	7.19E-03
	7	87.5	8.16E-03	8.91E-03
	8	77.3	1.00E-02	1.04E-02
	9	75.2	1.39E-02	1.45E-02
	10	77.7	1.16E-02	1.21E-02
9 - 12 Test 2	1	74.3	1.26E-04	1.61E-04
	2	80.4	3.53E-05	5.29E-05
	3	84.4	7.00E-05	1.05E-04
	4	79.4	5.29E-04	6.35E-04
	5	82.8	3.35E-03	3.54E-03
	6	81.1	6.38E-03	6.74E-03
	7	76.5	8.99E-03	9.36E-03
	8	76.8	1.14E-02	1.19E-02
	9	77.6	1.18E-02	1.23E-02
	10	81.0	1.03E-02	1.14E-02

Table 4.1.08   Tabular Variation of H_2O and CO_2 with Day: Test 1, Lights Off

Cage Group	Day	RH actual (percent)	CO_2 (g/ hr/ 100g BW)	H_2O (g/ hr/ 100g BW)
1-4 (Desired RH = 30 - 35 percent)	1	71.3	1.06E+00	1.22E+00
	2	66.1	8.02E-01	1.08E+00
	3	70.4	8.20E-01	9.46E-01
	4	62.9	1.01E+00	8.24E-01
	5	61.4	8.54E-01	7.85E-01
	6	54.4	7.52E-01	8.54E-01
	7	52.6	1.00E+00	8.08E-01
	8	58.4	1.03E+00	7.09E-01
	9	61.4	6.06E-01	6.97E-01
	10	57.1	7.61E-01	7.30E-01
5-8 (Desired RH = 75 - 80 percent)	1	69.7	8.48E-01	**-6.01E-01**
	2	84.8	8.82E-01	1.14E+00
	3	83.8	8.98E-01	7.92E-01
	4	78.2	7.86E-01	8.20E-01
	5	77.7	1.04E+00	5.31E-01
	6	79.6	1.05E+00	9.08E-01
	7	76.3	7.85E-01	5.75E-01
	8	81.1	9.89E-01	7.75E-01
	9	83.4	8.85E-01	8.20E-01
	10	80.6	6.76E-01	1.09E+00
9-12 (Desired RH = 30 - 35 percent)	1	68.0	1.22E+00	1.48E+00
	2	67.7	7.95E-01	1.09E+00
	3	62.8	9.99E-01	8.89E-01
	4	66.2	7.69E-01	8.49E-01
	5	56.8	6.95E-01	1.17E+00
	6	55.5	8.86E-01	8.58E-01
	7	62.4	9.44E-01	8.26E-01
	8	54.1	7.12E-01	7.40E-01
	9	60.2	7.98E-01	5.83E-01
	10	60.5	7.97E-01	7.44E-01

Table 4.1.09   Tabular Variation of H_2O and CO_2 with Day: Test 2, Lights Off

Cage Group	Day	RH actual (percent)	CO_2 (g/ hr/ 100g BW)	H_2O (g/ hr/ 100g BW)
1-4 (Desired RH = 30 - 35 percent)	1	69.7	9.86E-01	1.028E+00
	2	59.6	9.92E-01	1.097E+00
	3	62.6	9.76E-01	8.731E-01
	4	63.7	9.71E-01	8.599E-01
	5	64.4	7.90E-01	7.927E-01
	6	58.0	8.04E-01	8.988E-01
	7	64.0	1.02E+00	6.476E-01
	8	50.3	8.80E-01	7.398E-01
	9	50.6	7.58E-01	9.488E-01
	10	52.4	7.65E-01	5.782E-01
5-8 (Desired RH = 75 - 80 percent)	1	73.9	9.20E-01	8.224E-01
	2	83.5	1.06E+00	4.180E-01
	3	79.5	1.00E+00	7.288E-01
	4	83.8	9.13E-01	1.053E+00
	5	86.9	9.22E-01	7.567E-01
	6	75.7	8.63E-01	6.017E-01
	7	87.5	1.08E+00	7.605E-01
	8	77.3	9.76E-01	8.639E-01
	9	75.2	8.45E-01	7.348E-01
	10	77.7	7.94E-01	6.119E-01
9-12 (Desired RH = 75 - 80 percent)	1	74.3	9.79E-01	7.818E-01
	2	80.4	9.30E-01	7.737E-01
	3	84.4	1.11E+00	9.299E-01
	4	79.4	1.06E+00	9.155E-01
	5	82.8	8.48E-01	8.041E-01
	6	81.1	9.37E-01	7.828E-01
	7	76.5	1.09E+00	8.219E-01
	8	76.8	9.53E-01	8.713E-01
	9	77.6	9.80E-01	1.096E+00
	10	81.0	9.59E-01	1.523E-01

Table 4.1.10 Tabular Variation of H_2O and CO_2 with Day: Desired RH = 30 − 35 percent, Lights Off

Cage Group	Day	RH actual (percent)	CO_2 (g/ hr/ 100g BW)	H_2O (g/ hr/ 100g BW)
1 - 4 **Test 1**	1	71.3	1.06E+00	1.22E+00
	2	66.1	8.02E-01	1.08E+00
	3	70.4	8.20E-01	9.46E-01
	4	62.9	1.01E+00	8.24E-01
	5	61.4	8.54E-01	7.85E-01
	6	54.4	7.52E-01	8.54E-01
	7	52.6	1.00E+00	8.08E-01
	8	58.4	1.03E+00	7.09E-01
	9	61.4	6.06E-01	6.97E-01
	10	57.1	7.61E-01	7.30E-01
9 – 12 **Test 1**	1	68.0	1.22E+00	1.48E+00
	2	67.7	7.95E-01	1.09E+00
	3	62.8	9.99E-01	8.89E-01
	4	66.2	7.69E-01	8.49E-01
	5	56.8	6.95E-01	1.17E+00
	6	55.5	8.86E-01	8.58E-01
	7	62.4	9.44E-01	8.26E-01
	8	54.1	7.12E-01	7.40E-01
	9	60.2	7.98E-01	5.83E-01
	10	60.5	7.97E-01	7.44E-01
1 – 4 **Test 2**	1	69.7	9.86E-01	1.03E+00
	2	59.6	9.92E-01	1.10E+00
	3	62.6	9.76E-01	8.73E-01
	4	63.7	9.71E-01	8.60E-01
	5	64.4	7.90E-01	7.93E-01
	6	58.0	8.04E-01	8.99E-01
	7	64.0	1.02E+00	6.48E-01
	8	50.3	8.80E-01	7.40E-01
	9	50.6	7.58E-01	9.49E-01
	10	52.4	7.65E-01	5.78E-01

Table 4.1.11 Tabular Variation of H_2O and CO_2 with Day: Desired RH = 75 − 80 percent, Lights Off

Cage Group	Day	RH actual (percent)	CO_2 (g/ hr/ 100g BW)	H_2O (g/ hr/ 100g BW)
5-8 Test 1	1	69.7	8.48E-01	**-6.01E-01**
	2	84.8	8.82E-01	1.14E+00
	3	83.8	8.98E-01	7.92E-01
	4	78.2	7.86E-01	8.20E-01
	5	77.7	1.04E+00	5.31E-01
	6	79.6	1.05E+00	9.08E-01
	7	76.3	7.85E-01	5.75E-01
	8	81.1	9.89E-01	7.75E-01
	9	83.4	8.85E-01	8.20E-01
	10	80.6	6.76E-01	1.09E+00
5-8 Test 2	1	73.9	9.20E-01	8.22E-01
	2	83.5	1.06E+00	4.18E-01
	3	79.5	1.00E+00	7.29E-01
	4	83.8	9.13E-01	1.05E+00
	5	86.9	9.22E-01	7.57E-01
	6	75.7	8.63E-01	6.02E-01
	7	87.5	1.08E+00	7.61E-01
	8	77.3	9.76E-01	8.64E-01
	9	75.2	8.45E-01	7.35E-01
	10	77.7	7.94E-01	6.12E-01
9 - 12 Test 2	1	74.3	9.79E-01	7.82E-01
	2	80.4	9.30E-01	7.74E-01
	3	84.4	1.11E+00	9.30E-01
	4	79.4	1.06E+00	9.16E-01
	5	82.8	8.48E-01	8.04E-01
	6	81.1	9.37E-01	7.83E-01
	7	76.5	1.09E+00	8.22E-01
	8	76.8	9.53E-01	8.71E-01
	9	77.6	9.80E-01	1.10E+00
	10	81.0	9.59E-01	1.52E-01
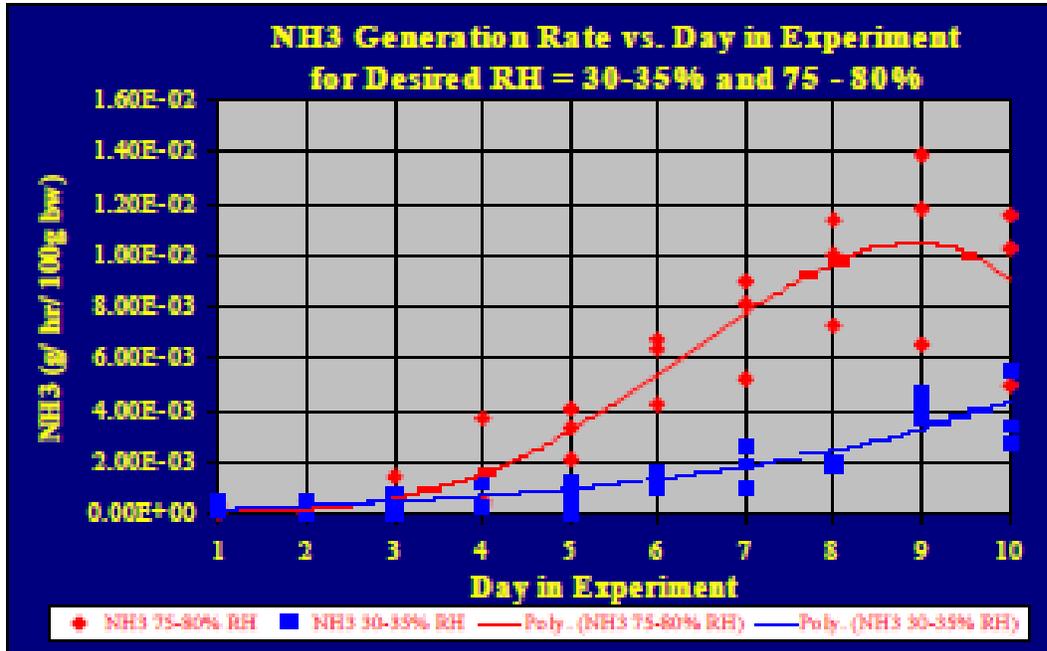
Figure 4.36   Variation of NH3 Generation Rate with Day in Experiment
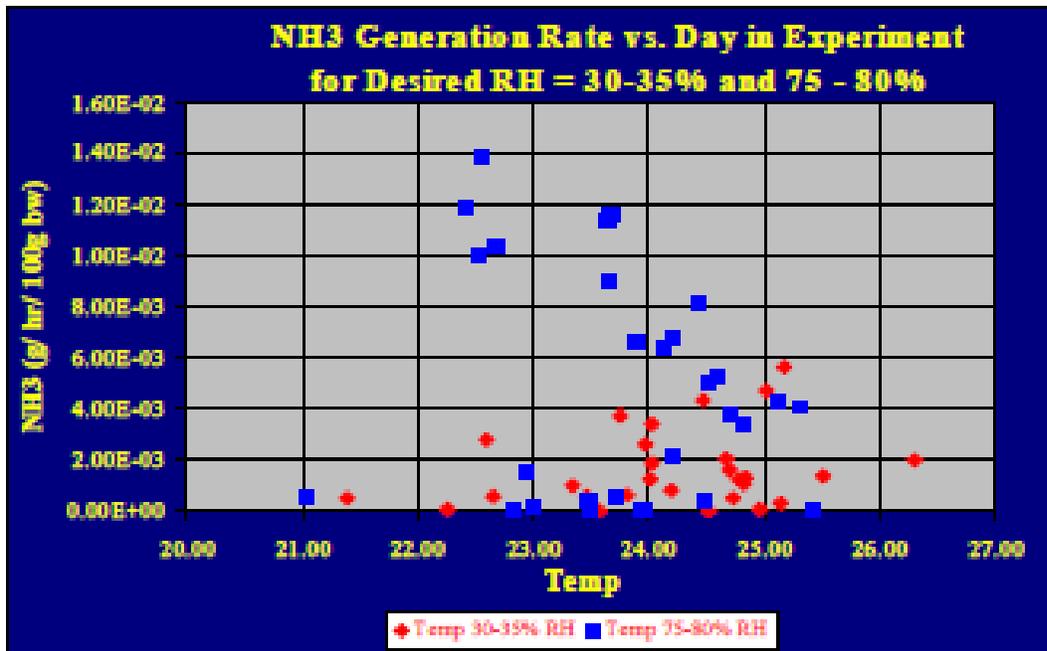
Figure 4.37   Variation of NH3 Generation Rate with Cage Temperature
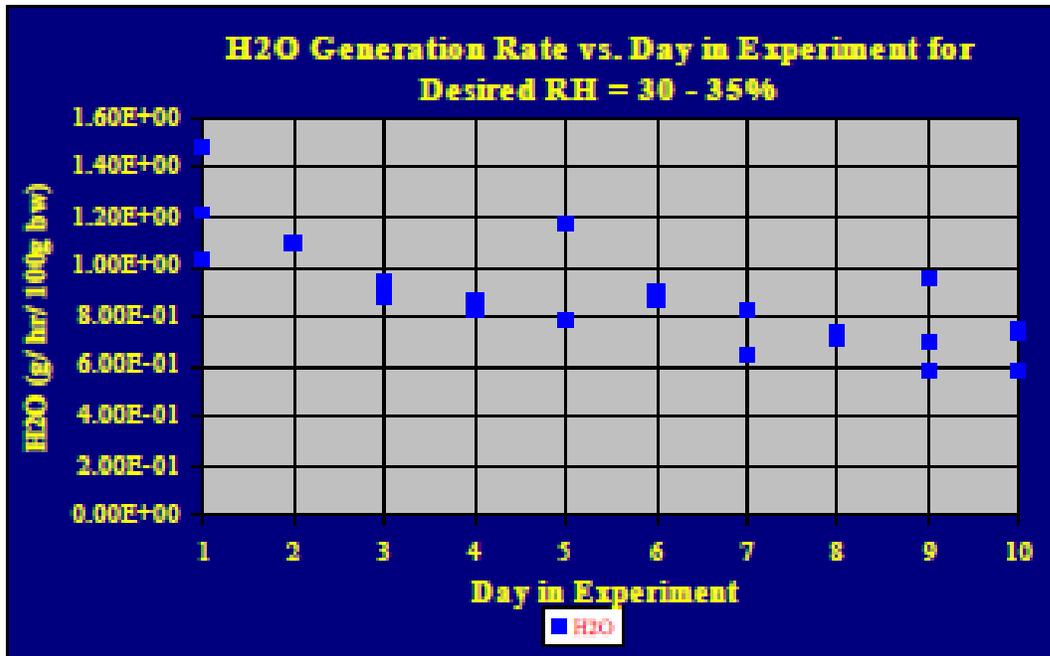
Figure 4.38   Variation of H₂O Generation Rate with Day in Experiment:
Desired RH = 30 – 35 percent.
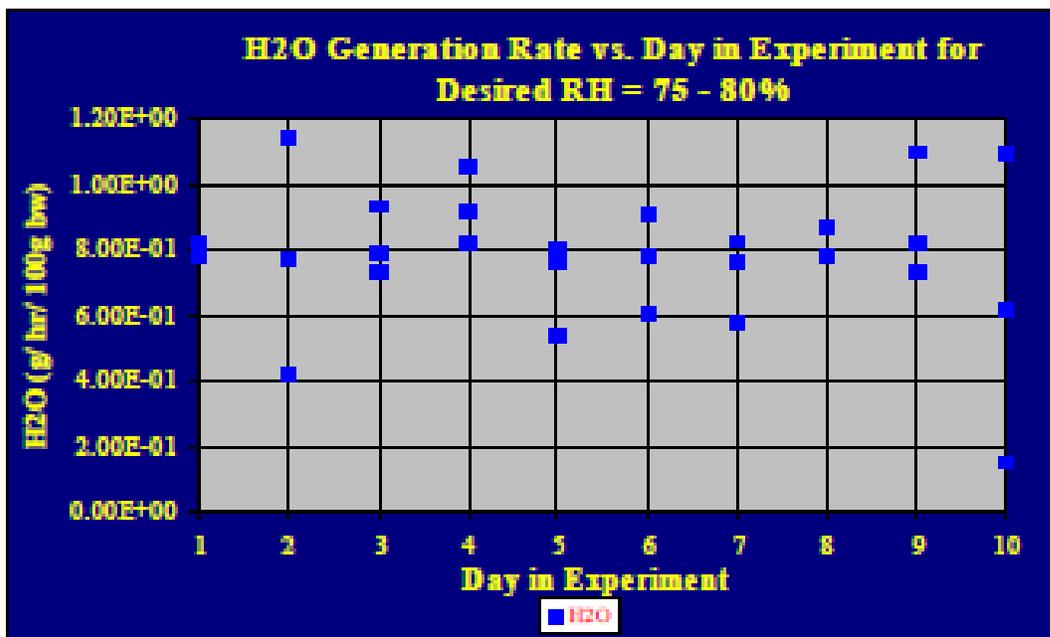
Figure 4.39   Variation of H₂O Generation Rate with Day in Experiment:
Desired RH = 75-80 percent.
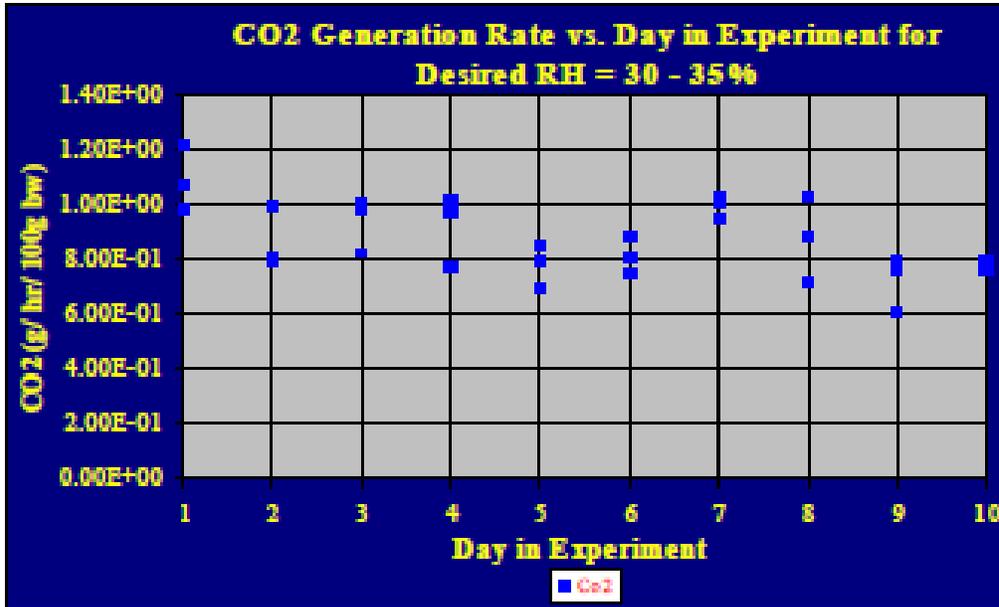
Figure 4.40   Variation of CO_2 Generation Rate with Day in Experiment: Desired RH = 30 –35 percent.
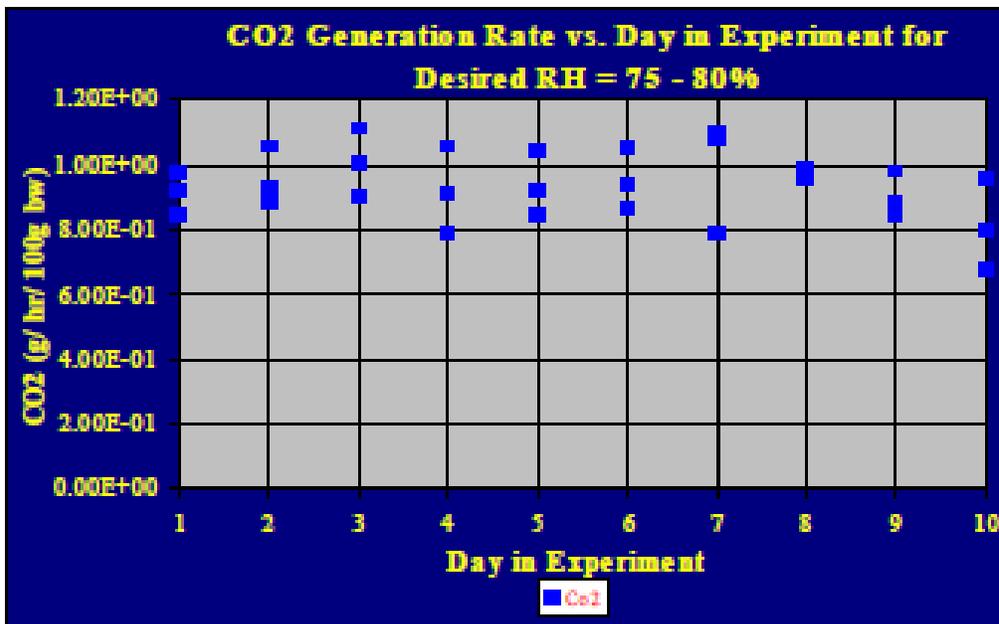
Figure 4.41   Variation of CO_2 Generation Rate with Day in Experiment: Desired RH = 75 – 80 percent.

4.1.2.8.3   Consideration of Heat Generation

Using the O_2 consumption data averages from the two tests for the different desired RH values, and the lights on/off conditions, the heat generation from the mice can be calculated. The results are shown in table 4.1.12 below, and are presented graphically in figure 4.42:

Table 4.1.12. Heat Generation Rates for Lights On/ Off Conditions in Tests 1 and 2.

|	O_2 Consumed (L/hr/ kg bw)	Heat Production (Kcal/hr/Kg BW)*	Heat Production per cage (W/ 100g bw)
Test 1:			
Desired RH 30–35 (Lights On)	3.49	16.83	1.96
Desired RH 30–35 (Lights Off)	4.16	20.06	2.33
Desired RH 75-80 (Lights On)	3.95	19.83	2.30
Desired RH 75-80 (Lights Off)	4.14	19.98	2.32
Test 2:			
Desired RH 30-35 (Lights On)	4.06	19.57	2.27
Desired RH 30-35 (Lights Off)	4.91	23.71	2.76
Desired RH 75-80 (Lights On)	5.46	26.34	3.06
Desired RH 75-80 (Lights Off)	6.00	28.94	3.36

*   Heat production was based on a heat production rate of 4.825Kcal/L O_2.

It can be noted that there is an increase in heat generation between the lights on and lights off conditions, and there is also an increase on moving from a low RH to a high RH cage condition. The average value from all the experiments is 2.55 W/100g bw, an 11 percent difference from the ASHRAE value of 2.3 W/ 100g bw, obtained from equation 4.1 (see section 4.1.1.2). This indicates that the current experiment is consistent with previous recommendations.

4.1.2.8.4   Summary of Experimental Data

The average mass generation rates of CO_2 and H_2O, the average consumption rates of O_2, and the generation rates of heat for the scotophase and photophase from all experimental tests are tabulated below in Table 4.1.13, and presented graphically in figure 4.43. The table and figure emphasize that the generation rates are higher during the scotophase than the photophase.

Table 4.1.13 Average Gas Mass Generation/ Consumption Rates, and Average Generation Rates of Heat for the Scotophase and Photophase from all Experimental Tests.

Variable	Scotophase	Photophase
CO_2 (g/ hr/ 100g bw)	9.05e-1	6.92e-1
CO_2 (ppm)	6147	4554
H_2O (g/ hr/ 100g bw)*	8.31e-1	
O_2 (g/ hr/ 100g bw)	6.60e-1	6.75e-1
Heat (W/ 100g bw)	2.69	2.40

*   No distinction was made between lights on/ off in calculation of water generation.

The NH3 data cannot be summarized in such a way, because the generation rate varies significantly with RH, light phase and the day in the experiment. figure 4.44 shows the variation of NH3 (ppm) with the day in experiment for different RH levels, and for scotophase and photophase.
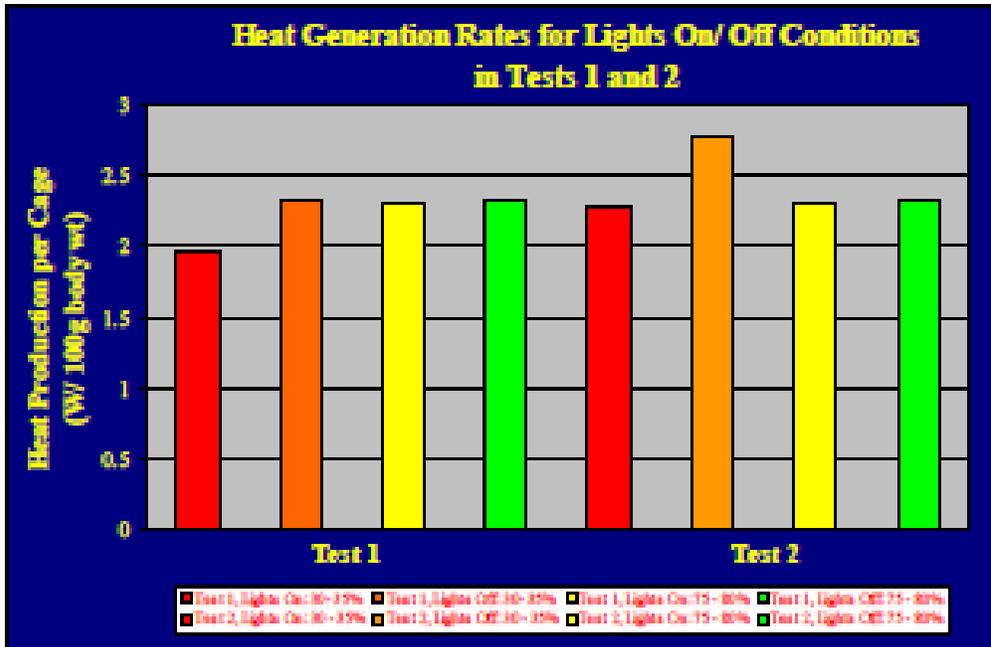
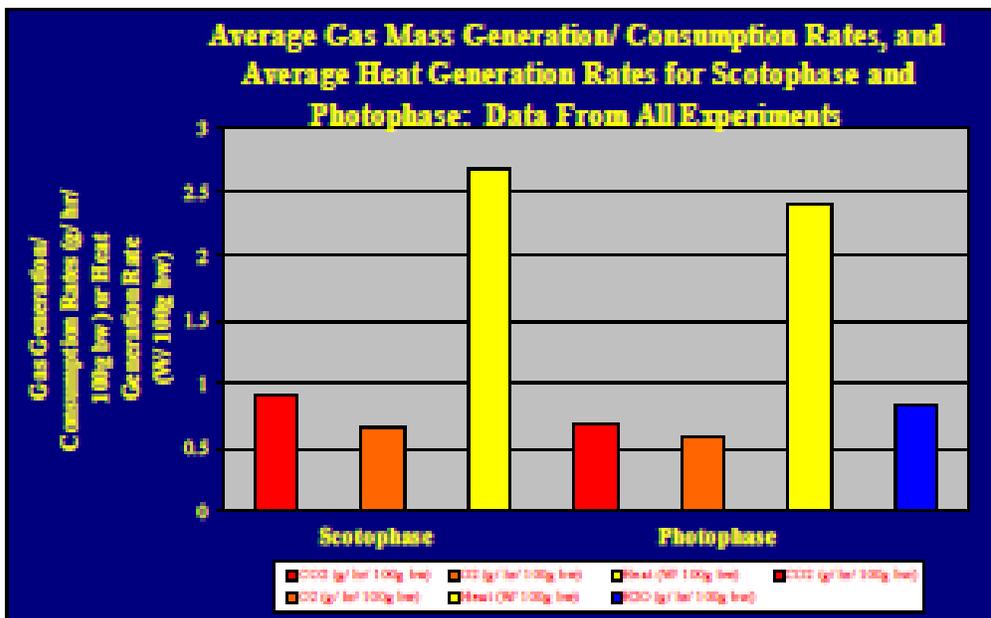*Figure 4.42   Heat Generation Rates for Lights On/ Off Conditions in Tests 1 and 2.*

Figure 4.43   Average Gas Mass Generation/ Consumption Rates, and Average Heat Generation Rates for Scotophase and Photophase: Data From All Experiments.
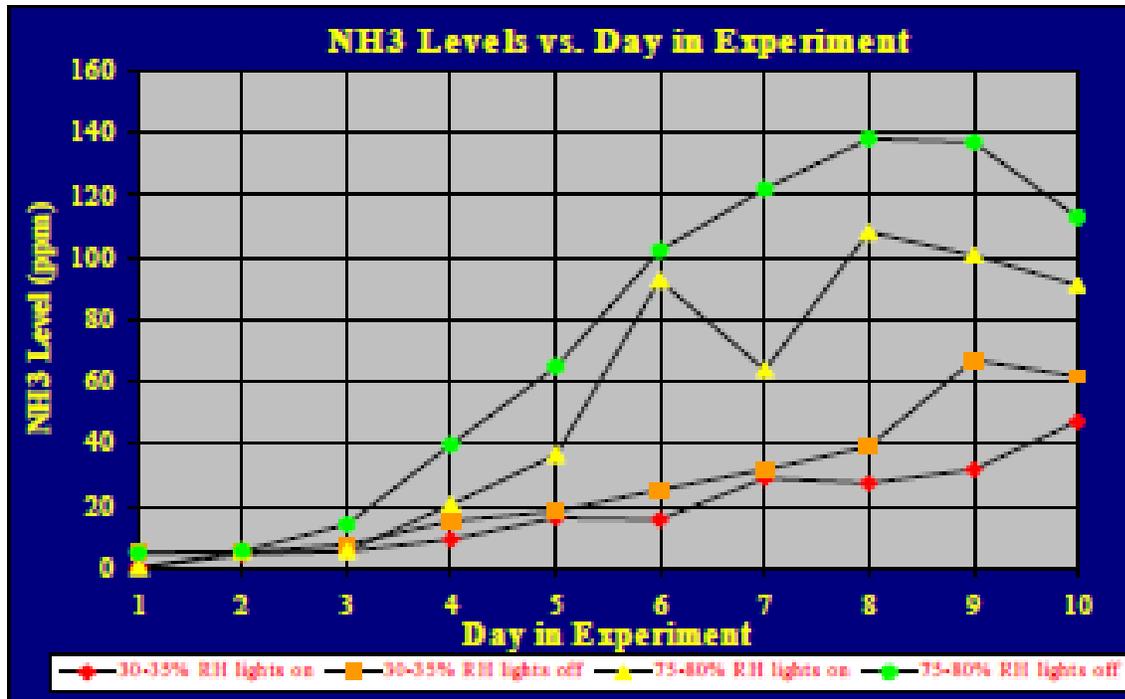
Figure 4.44   Variation of NH3 Level (ppm) with Day in Experiment

4.1.3   Room Condition

4.1.3.1   Experimental Cases

4.1.3.1.1   Empty Room: Description of Apparatus

The empty testing room, that measured 3.66m x 2.44m x 2.44m high (12' x 8' x 8'), was located within the larger air-conditioned UIUC room ventilation simulator (RVS). The room is shown in figure 4.45). The RVS is described in Wu et al., (1990). The placement of the room in the RVS allowed the supply air to the testing room to be precisely controlled. The RVS is capable of maintaining air temperature at any point between –25.0 to 40.0 ^{o}C (-13.0 to 104.0 °F) with an accuracy of   1.5 ^{o}C (2.7 ^{o}F), year around. In this study, room temperature in the RVS was maintained at 22.0 1.5 ^{o}C (71.6 2.7 ^{o}F). In this case, air was supplied by a TAD diffuser (Krueger 2-way total air diffuser), that was centered on the ceiling of the room. The diffuser, that measured 0.61m (24") long (east-west wise) and 0.57m (22.5") wide (north-south wise) was oriented to direct air towards the long axis of the room. The discharge surface of the diffuser was curved and the lowest point was 0.14m (5.5") below the ceiling. The room air exhaust was a 0.30m x 0.30m (12" x 12") aluminum grille with a 20 percent open area and was located in one corner of the ceiling. The exhaust outlet was 0.2m (8") away from both the west and north walls. The only other item of geometry in the room was the door, that measured 0.91m x 2.13m (3' x 7'), and was located centrally on the north wall. The door had a 6.4e-3m (¼") crack on its bottom, that allowed pressurization of the room.
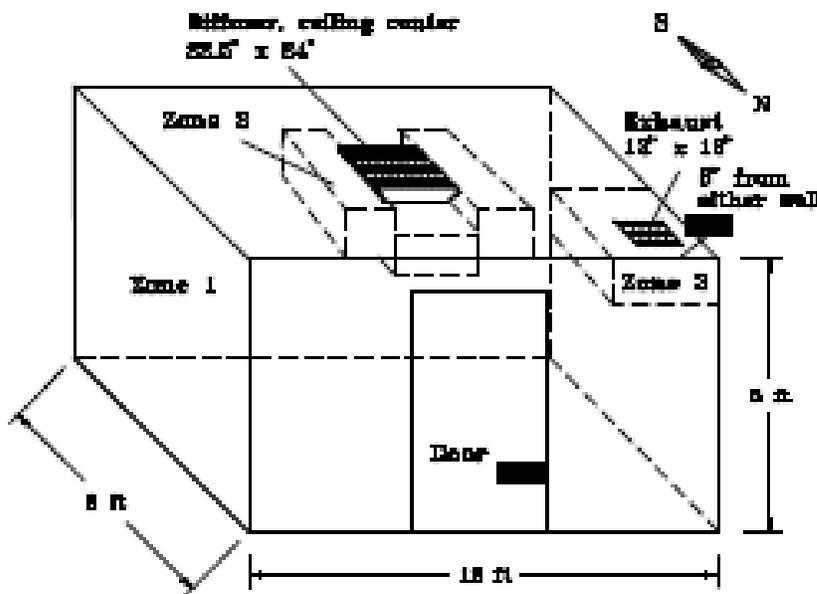
Figure 4.45   *Layout of the testing room and the zones used for data collection. Dashed lines show the borders of zones used in data collection.*

4.1.3.1.2   Empty Room: Test Procedure

The room air temperature was operated at 22.0 °C (71.6 °F) with a plus or minus tolerance of 1.5 °C (2.7 °F) throughout the room. Difference between the supply air temperature and the mean of the room surface temperatures was less than 1.5 °C (2.7 °F). The room surfaces were insulated and both the interior and exterior of the room were maintained at the same temperature. All surface temperatures were measured with an infrared thermographer (Cole-Parmer Instrument Co. model 39650-12). Surface temperatures were recorded at the beginning and end of each batch of data (approximately four hours). Measurements were taken at the center of each wall and the floor, and on the four sides of the ceiling halfway between the diffuser and the walls. These temperature measurements are tabulated in appendix I: section 4.3.1.

The room was operated at a slight positive pressure (at 10pa (0.04" of H_2O column) to eliminate incoming air currents other than the diffuser. The supply airflow rate was controlled at a constant value of 128 cfm (6.0e-2 m^3/s), that was 10 air changes per hour (ACH) for the testing room. The exhaust airflow rate was maintained at 102 2 cfm (appendix I: section 4.3.1).

Air volume flow rates into the room diffuser and out of the exhaust grill were measured with precision nozzles machined according to specifications given in the ANSI/ASHRAE Standard 51-1985. The nozzles were located in the ducts outside of the room. Airflows were controlled and measured continuously during each experimental run by measuring the pressure drop across the nozzles with a manometer. Duct fans were placed downstream of each nozzle. The supply fan was adjusted to provide the required airflow into the room and the exhaust fan was adjusted to provide the required static pressure in the room.

Three zones were used for data collection. The entire room airspace was zone 1. The air space 0.30m (1') from the diffuser surface was zone 2. The air space 0.30m (1') from the exhaust outlet was zone 3 (figure 4.45). The total number of measurement locations is shown in table 4.1.13. Temperature, air velocity, and turbulence intensity were measured every 5.1e-2m (2") within 0.30m (12") of the diffuser and exhaust, and every 0.15m (6") throughout the rest of the room. Temperature was measured with type-T thermocouples. The temperature sensors were calibrated in a temperature controlled water bath that was set according to a SAMA thermometer. The air velocity and turbulence intensity levels were measured with sensors that were designed and constructed at the Bioenvironmental Engineering Research Laboratory (BERL) at the UIUC. This air velocity sensor has a thermistor sensing head that is maintained at a constant temperature and is described in Li (1994). The accuracy is plus or minus 3 percent of reading or plus or minus 2 fpm, whichever is greater. The air velocity sensors were calibrated prior to the experiment in a TSI Certified Air Velocity Calibrator (model 8390). The air velocity sensor is omni-directional and has a fast response time so it can measure turbulence intensity as well as air velocity. Outputs from the temperature and air velocity sensors were collected on a data acquisition system (DAS-8 with EXP-16 expansion boards, Keithley-Metrabyte, Inc.) and an IBM compatible computer.

To determine turbulence intensity, air velocities were measured at a sampling rate of 40 Hz. Justifications of this sampling frequency are in appendix I: section 4.1. Preliminary data were collected at different sampling frequencies to verify the validity of using 40 Hz for this overall study. Air velocity data were collected for 6 seconds to obtain 240 data samples at each point.

Table 4.1.13 Number of Collection Points and Data Numbers for Empty Room Measurements

Zone	Number of Collection Points	Number of Variable Data Collected[a]	Number of Air Velocity Data Collected[b]
Zone 1	5625	33750	6.75e+6
Zone 2	3240	19440	3.888e+6
Zone 3	1920	11520	2.304e+6

a   -   number of collection points * number of variables (6)

b   -   number of collection points * number of air velocity variables * 240 (40Hz sampling over 6 seconds)

Sensors were mounted on a traverse system (positioned to minimize airflow interference) that moved the sensors throughout the room, see figures 4.46 and 4.47. The traverse was computer controlled to ensure the accuracy of locations of each measurement point. No people were in the test room during or 10 minutes prior to any measurements to ensure the room air was not disturbed and in a steady state. All heat generating devices (e.g., traverse power supply, amplifiers) were kept out of the room except for the sensing system. Measurements were not taken until after the door was closed for 10 minutes and room airflow reached steady-state conditions. The room air velocity field and temperature achieved steady-state 4 minutes after the door was closed.

Figure 4.46 *Automatic traverse system.*
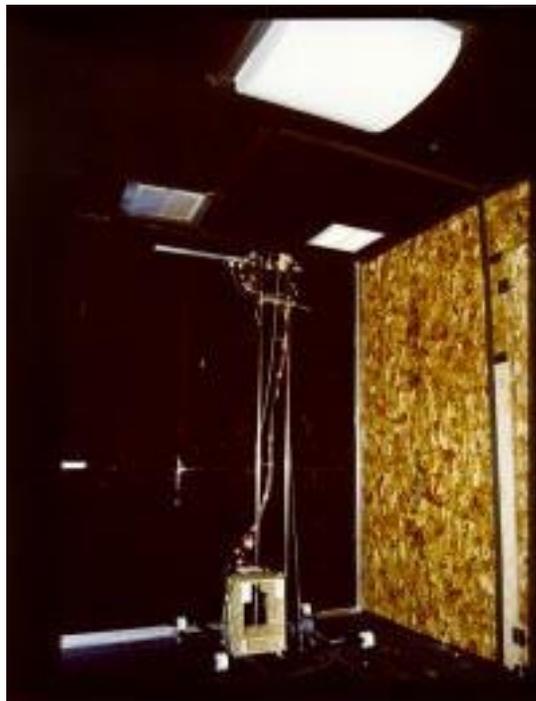
Figure 4.47 *Empty Room Measurement Taking.*

4.1.3.1.3   Room With Racks, Cages and Simulated Animals: Apparatus Description

The same room used in the empty room analysis with the same supply and exhaust flow rates and diffuser and exhaust were outfitted with three racks, rodent cages, and a sink (figure 4.48). Each rack was 0.61m D x 1.52m H x 1.83m W (24" x 60" x 72") with 6 solid shelves (figure 4.49). The shelf at the top of the rack was 1.52m (60") from the floor. The distances between two shelves (center to center) was 0.28m (11"), while the shelves themselves were 1.25e-2m (½") thick. All racks were filled to capacity with mouse cages (7 cages per shelf; 42 cages per rack) and the cages were shoebox type with were 1.25e-2m (½") of hardwood shavings bedding. The sink cabinet size was 0.61m W x 0.61m D x 0.81m H (24" x 24" x 32"). A 200 ohm precision resistance heater was placed in each cage to generate 2.42 W to simulate the heat load of the mice. CO_2 was supplied through diffuser stones at 3.75e-2m (9.5") above the bedding level towards the front of each cage near the heaters. The total CO_2 rate supplied to the room was 990 mL/min. Water bottles and simulated feed obstruction were included in each cage.
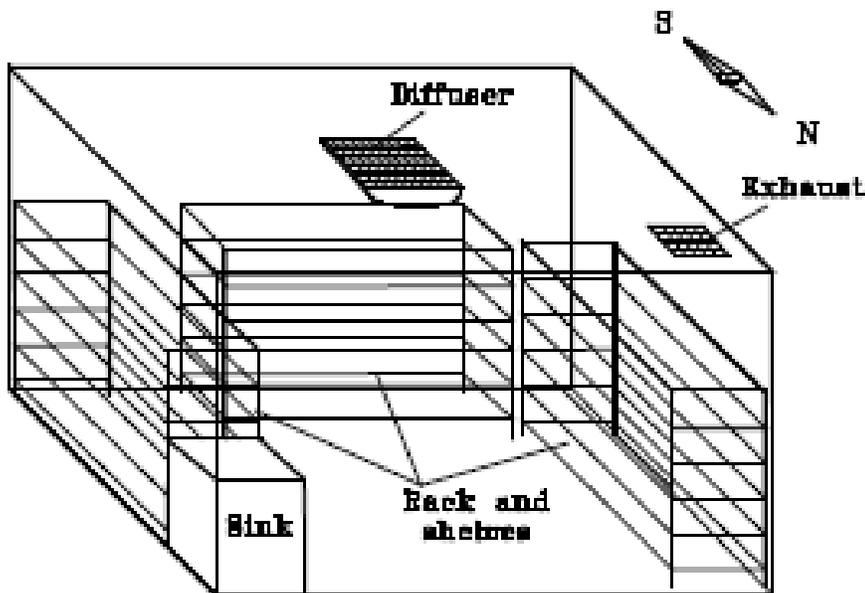
Figure 4.48   *Layout of the testing room with racks and sink. Each rack had six shelves and each shelf had seven cages.*

4.1.3.1.4   Room With Racks, Cages and Simulated Animals: Test Procedure

The test room was divided into seven zones for data collection, as indicated in figure 4.50. The total number of measurement locations is shown in table 4.1.14. The room mean air velocity, median air velocity, range of air velocity, temperature, TI, and CO_2 concentration patterns were determined at 0.30m (12") increments throughout the room. Measurements started 0.05m (2") from racks and walls. Temperature measurements were obtained with type -T thermocouples, air velocity with the BERL air velocity sensors, and CO_2 with the Fuji gas monitor (Fuji Electric Co., model ZEP5YA31). This equipment and their calibration procedures were described section 4.3.1.2. All sensors were calibrated prior to the start of this experimental sequence except for the thermocouples. The sensors were moved around the room with a traverse system as described earlier so no people entered the room during or 10 minutes prior to any measurements. A view of the measurement sensors on the traverse system is shown in figure 4.51.
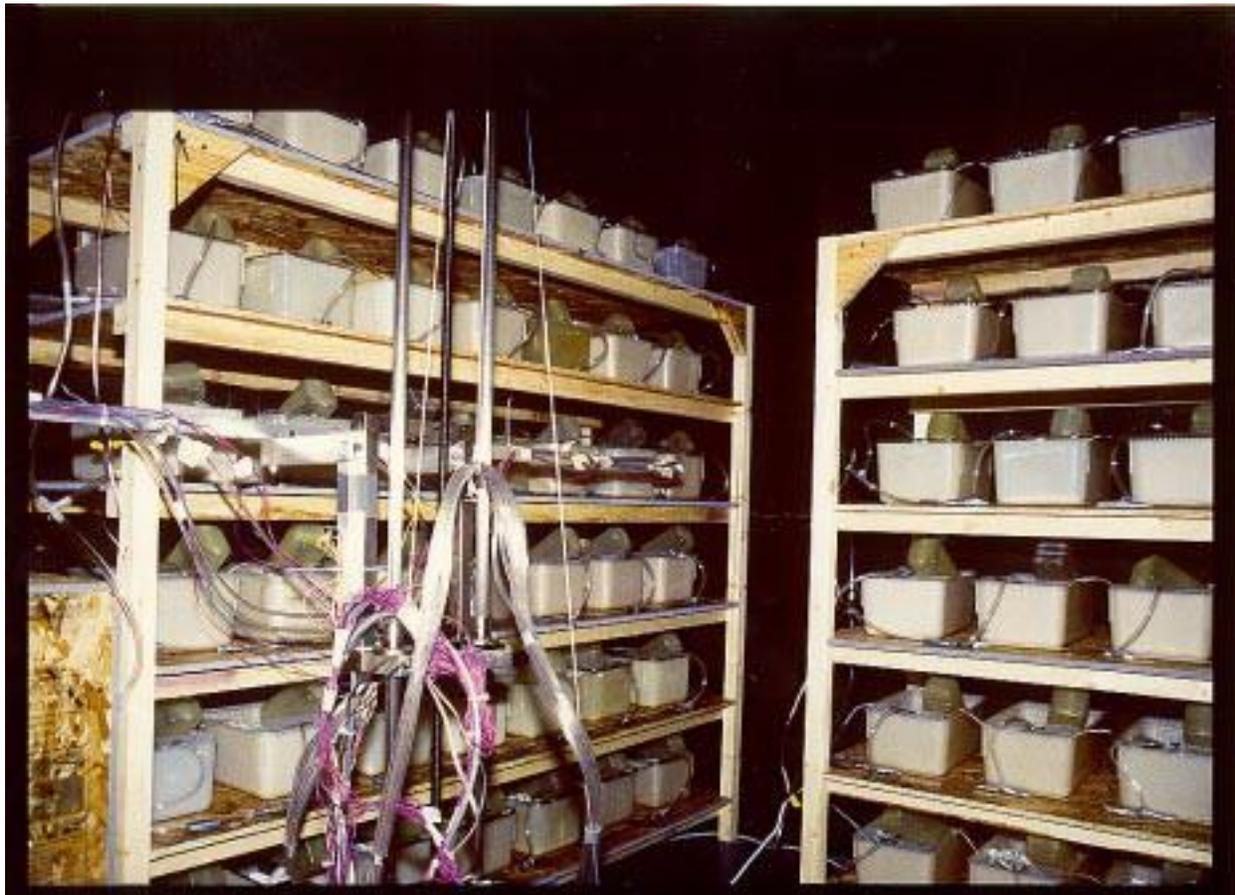
Figure 4.49   *Animal Room Macroenvironmental Measurements: Cage Rack.*
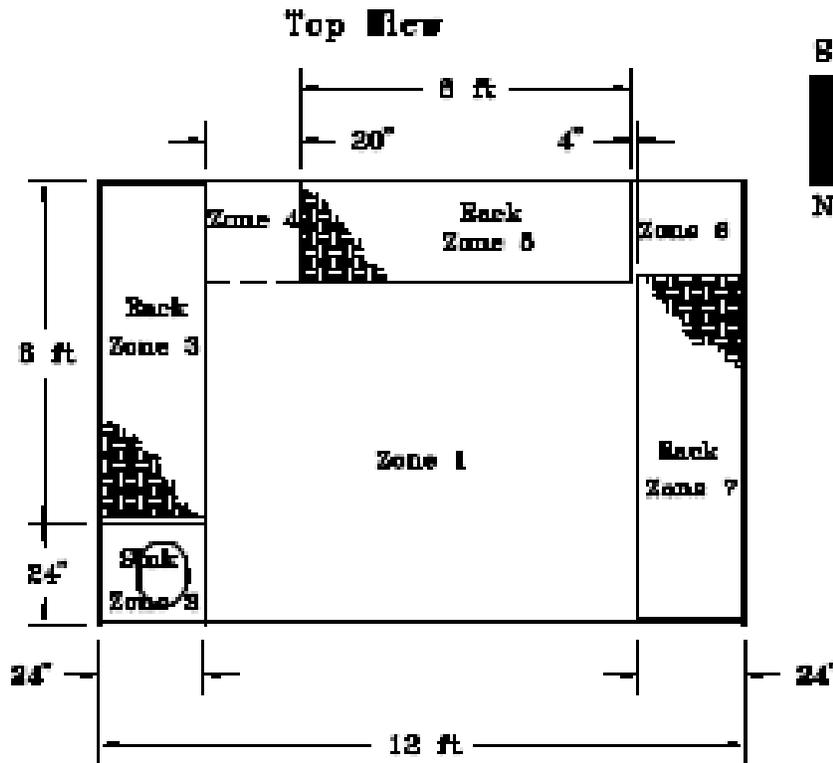
Figure 4.50   Top view of zones in the room: Three racks are identical, each rack has six shelves and each shelf supports seven mouse cages.

Table 4.1.14 Number of Collection Points and Data Numbers for Populated Room Measurements

Zone	Number of Collection Points	Number of Variable Data Collected[a]	Number of Air Velocity Data Collected[b]
Zone 1	441	3087	5.292e5
Zone 3	28	196	3.36e4
Zone 5	52	364	6.24e4
Zone 7	28	196	3.36e4

a   -   number of collection points * number of variables (7)
b   -   number of collection points * number of air velocity variables * 240 (40Hz sampling over 6 seconds)
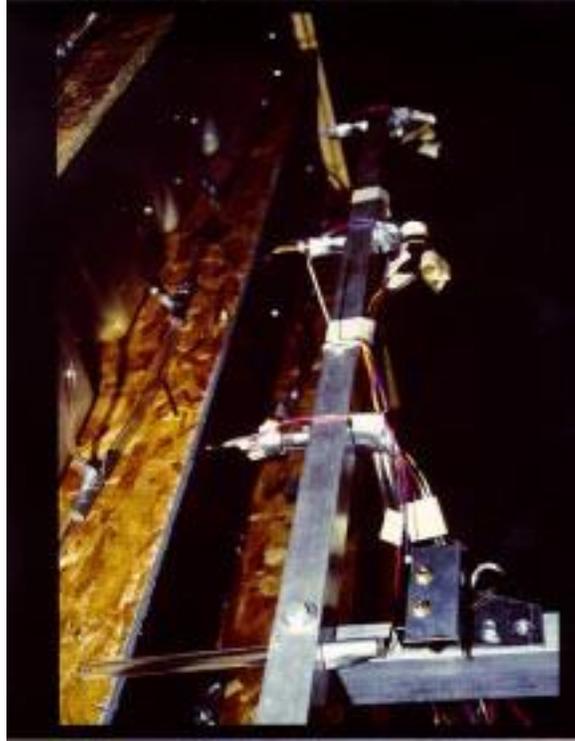
Figure 4.51 *Animal Room Macroenvironmental Measurement Sensors.*

4.2   CFD Simulations and Validation against Experimental Data

4.2.1   Cage Condition

A series of CFD models was constructed to simulate the cage wind tunnel experiments**.** The accurate modeling of the cage is an important stage in the project. In particular, the CFD cage model, as validated against the experimental data obtained in the wind tunnel, is used in the CFD animal research facility models as part of the racks. The two sets of boundary conditions that are of most concern are those associated with the transfer mechanisms into and out of the cage, namely the side cracks and the top of the cage, that includes the filter.

4.2.1.1   Description of CFD models

All the models contained the same basic components and modeling philosophy: changes between the models reflected the different experimental procedures.

The walls of the tunnel were specified to define the shape of the experimental wind tunnel. Typical CFD models for the tunnels are shown in figures 4.52 to 4.54. The ventilation system specification for the tunnel was the definition of a 0.4 m x 0.5 m (15.75" x 20") opening at the entrance of the tunnel, and an extract at the opposite end. The size of the extract, 0.14m x 0.14m (5.3" x 5.3"), was defined such that the cross-sectional area was the same as in the physical situation. The mass flow rate set through the exhaust was varied to produce the same air velocities through the tunnel section as in the experiments, with the value dependent on the desired speed. The three screens and two filters in the tunnel were modeled using 0.4 m x 0.5 m (15.75" x 20") planar resistances. The loss coefficients for each were set according to the free area ratio of the object. The values are listed below in Table 4.2.01, and are based on Idelchik (1989):

Table 4.2.01. Free Area Ratios and Loss Coefficients Used for Tunnel Straightening Media

Device	Free Area Ratio	Loss Coefficient
Screen 1	0.6	2.00
Screen 2	0.4	8.25
Screen 3	0.33	14.35
Filters 1,2	0.5	4.00

The shelf on that the cage sits was defined as a rectangular block of dimension 2.5e-2m x 0.30 m x 0.50 m (1" x 11.8" x 20"). The shelf was located 0.10m (4") from the floor of the tunnel for the parallel and perpendicular orientation experimental measurements, with the center of the shelf located at the center of the tunnel section. In the vertical orientation experiments, the shelf was located centrally within the tunnel.

Placed on the shelf was the CFD model representation of the cage. A typical representation of the cage, without instrumentation, is shown in figure 4.55. The dimensions of the cage were set as 0.27 m x 0.16m x 0.21m (10.7" x 6.38" x 8.39"): these dimensions retained the same volume as in the physical case. The sides of the cage were modeled as thin plates, with the thickness and conductivity of the plates set to those of the cage polycarbonate. The bottle was represented using a combination of rectangular prisms and cuboid blocks. The volume of the bottle was retained, as was the location of the bottle in the cage. A food supply was modeled using two triangular prisms. The bedding was represented as a dimension 0.27m x 0.16m x 1.3e-2m (10.7" x 6.38" x 0.5") rectangular block. The alternative representations of the mice heater were modeled using rectangular blocks. In particular, the original heater was modeled as a 1.59e-2m x 0.32e-2m x 0.32e-2m (5/8" x 1/8" x 1/8") block, with the heat flux set to 2.3W, while the huddled mice were modeled as a block of dimension 0.11m x 8.6e-1m x 2.2e-2m (4 1/4" x 3 3/8" x 7/8"), with the surface temperature set to 26.7°C (80.0°F).

There are two transfer mechanisms for the air and tracer gas to enter/ leave the cage, namely the top of the cage, that includes filter media, and the side cracks of the cage.

The top of the cage has two constituent parts that had to be represented using CFD boundary conditions: the filter media; and the top of the cage itself, that consists of regular arrays of holes in the polycarbonate material. The filter material was identified as Reemay #2024, 12 mils, 2.1 oz/ yd^2. Using manufacturer's data, a pressure drop vs. wind tunnel speed graph could be plotted in figure 4.56. The profile was then approximated to a polynomial expression that could be converted to CFD boundary conditions. In particular, the polynomial expression can be expressed as:

$$DP = 70.277 \, v^2 + 307.37 \, v \hspace{4cm} (4.22)$$

As the average velocities through the filter are relatively small (of the order of 0.17 cfm (8e-4 m/s)), the linear contribution dominated the pressure drop. Using boundary conditions defined in section 5.1.6.2, the first term of the right hand side was represented using a planar resistance, while the second term was represented using a planar source of momentum. The loss coefficients were set appropriately for each boundary condition to replicate the polynomial expression. As the flow through the filter media is laminar, the turbulent viscosity at the plane of the media was reduced to very low levels. To achieve this, the value of k (the turbulent kinetic energy) was set at 1e-5 at the planar source, while (the rate of dissipation of k), was set to 1e5.

The cage top material itself was represented through the calculation of the free area ratio of the top surface, and the addition of the loss coefficient to the planar resistance term. The free area ratio was calculated to be 0.35, that gives a loss coefficient of 12.35 (Idelchik (1989)).

The settings for the side crack boundary conditions were the most problematical to specify because of physical uncertainties. In particular, the top lid of the cage does not fit well on the lower section of the case because the meshing is often deformed. The first step was to define

these cracks as planar resistances of height 6.4e-3m (¼"). Initially using the results of the series set base experiments, the values for the loss coefficients on the side cracks were varied until the predicted CFD values for the cage ACH reasonably matched the experimental data over a range of tunnel velocities for each of the three orientations. These loss coefficient values were then tested against the lower injection rate experimental series (series sets one to four, to eight) to ensure good agreement. Any adjustments to the loss coefficients were then tested over the a range of experimental data sets to ensure that the values were applicable to all possible conditions that the cage could be presented within the animal facility room environment.

4.2.1.2 Results from CFD Simulations

In this section, variable plots from a typical cage will be considered, then the comparison of the CFD results with the experimental data will be presented.

4.2.1.2.1 Plots from Typical Cage CFD Simulation

A single CFD simulation will be considered to indicate the physical features that can be predicted using CFD, which are otherwise difficult to determine using experimental procedures. In particular, the CFD allows the determination of flow patterns within the cage, as well as temperature and concentration distributions.

The close-up plot of the vector field at the plane halfway through the tunnel for the Series Sets Six: Parallel Orientation, Heater On (SMO) 40 fpm (0.2 m/s) case is shown in figure 4.57. Note that the key accompanying the plot indicates speed in m/s (to convert to fpm, multiply by 200). Externally from the cage, the most prominent feature is the recirculation region immediately behind the cage. Internally, the main feature is the buoyant plume resulting from the SMO. However, it is noticeable that, apart from the plume, there are few flow patterns present within the cage of any great magnitude. In particular, although there is obviously strong external flow that is impinging directly onto the side of the cage, relatively small amounts of flow actually enter it.

The equivalent close-up plots of the temperature and CO_2 concentration fields are shown in figures 4.58 and 4.59 respectively. Note that the keys indicate the temperature in °C and concentration in kg of species/ kg of air (to convert to ppm multiply by 1e6*(28.96/44)) respectively. The temperature plot shows the distinct plume resulting from the SMO. This plume dominates the distribution of the concentration also, as the CO_2 is entrained into this flow feature. The concentration plot also indicates the clear stratification of the CO_2 in the cage. That is due to the density difference between the CO_2 and air. This stratification makes the matching of the CFD results to the experimental data difficult, as relatively small spatial changes result in marked differences in the level of concentration.

4.2.1.2.2 Comparison of CFD Results vs. Experimental Data

Presented below, in tables 4.2.02 to 4.2.12, are a series of comparisons between the experimental data sets and equivalent CFD simulation cage ACH for the chosen optimal values for the cage side crack loss coefficients. Note that, because of time constraints, only a representative sample could be considered from the wide range of experimental data available. The focus of the sample was to pick orientations that the cage was more likely to experience in the animal facility room environment, in particular, parallel cage orientation, and appropriate air velocities, in particular, 40 fpm (0.2m/s) and below.

A complete listing of the experimental cage ACH data is given in appendix I: section 2.2.

The comparisons show good agreement between the experimental data and CFD simulation results for the range of experimental series considered. In the majority of cases considered, the difference between the experimental and CFD results is under 20 percent. This error can be considered reasonable for this set of validation and calibration exercises. In particular, the CFD results show that the calculated value for the cage ACH is sensitive to the exact location of the sampling tubes, and the sampling tube holes themselves: this is because of the stratification of the CO_2 or SF_6 concentrations in the cages (see figure 4.59). Relatively small variations from the quoted location of the experimental sampling tubes would translate to errors in the CFD calculation. Further, as table 4.2.02 demonstrates, some level of error should be accepted in the experimental procedure.

Table 4.2.02. Comparison of CFD results against Series Set Base: Parallel Orientation Results.

Tunnel Velocity (FPM)	Ventilation Rate (CFM) 1 l/min CO_2 *Parallel - Heater On*		
	CFD	**Series Set Base**	**Series Set Base (Repeat)**
20	0.15	0.19	--
30	0.17	0.21	0.18*

* The percent difference between the two separate experimental readings is 14.3 percent.

Table 4.2.03. Comparison of CFD results against Series Sets Two: Parallel Orientation, SF_6 Results

Tunnel Velocity (FPM)	Ventilation Rate (CFM) 0.1 l/min SF_6 _Parallel - Heater On_	
	CFD	**Set Two**
20	0.04	0.04
30	0.05	0.05
40	0.06	0.06

Table 4.2.04. Comparison of CFD results against Series Sets Two: Perpendicular Orientation, Heater On, SF_6 Results

Tunnel Velocity (FPM)	Ventilation Rate (CFM) 0.1 l/min SF_6 _Perpendicular - Heater On_	
	CFD	**Set Two**
20	0.05	0.04
30	0.05	0.05
40	0.06	0.05

Table 4.2.05. Comparison of CFD results against Series Sets One and Three: Parallel Orientation, Heater On Results.

Tunnel Velocity (FPM)	Ventilation Rate (CFM) 0.1 l/min CO_2 Parallel - Heater On		
	CFD	**Series Set One**	**Series Set Three**
20	0.07	0.07	0.08
30	0.09	0.10	0.11
40	0.10	0.10	0.13

Table 4.2.06. Comparison of CFD results against Series Sets Three: Parallel Orientation, Heater Off Results.

Tunnel Velocity (FPM)	Ventilation Rate (CFM) 0.1 l/min CO_2 Parallel - Heater Off		
	CFD	**Series Set Three**	**Series Set Three (Repeat)**
20	0.10	0.09	--
30	0.10	0.12	0.09*
40	0.12	0.15	--

* The percent difference between the two separate experimental measurements is 25 percent

Table 4.2.07. Comparison of CFD results against Series Sets Three: Perpendicular Orientation, Heater On Results.

Tunnel Velocity (FPM)	Ventilation Rate (CFM) 0.1 l/min CO_2 *Perpendicular - Heater On*	
	CFD	**Series Set Three**
20	0.15	0.08
30	0.18	0.14
40	0.21	0.24

Table 4.2.08. Comparison of CFD results against Series Sets Three: Perpendicular Orientation, Heater Off Results.

Tunnel Velocity (FPM)	Ventilation Rate (CFM) 0.1 l/min CO_2 *Perpendicular - Heater Off*	
	CFD	**Series Set Three**
20	0.15	0.06
30	0.18	0.09
40	0.21	0.17

Table 4.2.09. Comparison of CFD results against Series Sets Six: Parallel Orientation, Heater On (DMH) Results

Tunnel Velocity (FPM)	Ventilation Rate (CFM) 0.1 l/min CO_2 *Parallel - Heater On (DMH)* *Sealed Lip*	
	CFD	Series Set Six
20	0.06	0.07
40	0.06	0.07

Table 4.2.10. Comparison of CFD results against Series Sets Six: Parallel Orientation, Heater On (SMO) Results

Tunnel Velocity (FPM)	Ventilation Rate (CFM) 0.1 l/min CO_2 *Parallel – Heater On (SMO)* *Sealed Lid*	
	CFD	Series Set Six
20	0.04	0.04
40	0.06	0.04

Table 4.2.11. Comparison of CFD results against Series Sets Six: Perpendicular Orientation, Heater On (SMO) Results

Tunnel Velocity (FPM)	Ventilation Rate (CFM) 0.1 l/min CO_2 *Perpendicular – Heater On (SMO)* *Sealed Lid*	
	CFD	Series Set Six
20	0.05	0.05
40	0.06	0.05

Table 4.2.12. Comparison of CFD results against Series Eight Results

Cage Orientation	Ventilation Rate (CFM) 0.1 l/min CO_2 *Parallel/ Perpendicular – Heater On (SMO)*	
	CFD	Series Set Eight
Parallel	0.10	0.10
Perpendicular	0.09	0.08

Fan

33% Open
Perforated
Screen

Cage

Shelf

40% Open
Perforated
Screen

60% Open
Perforated Screen
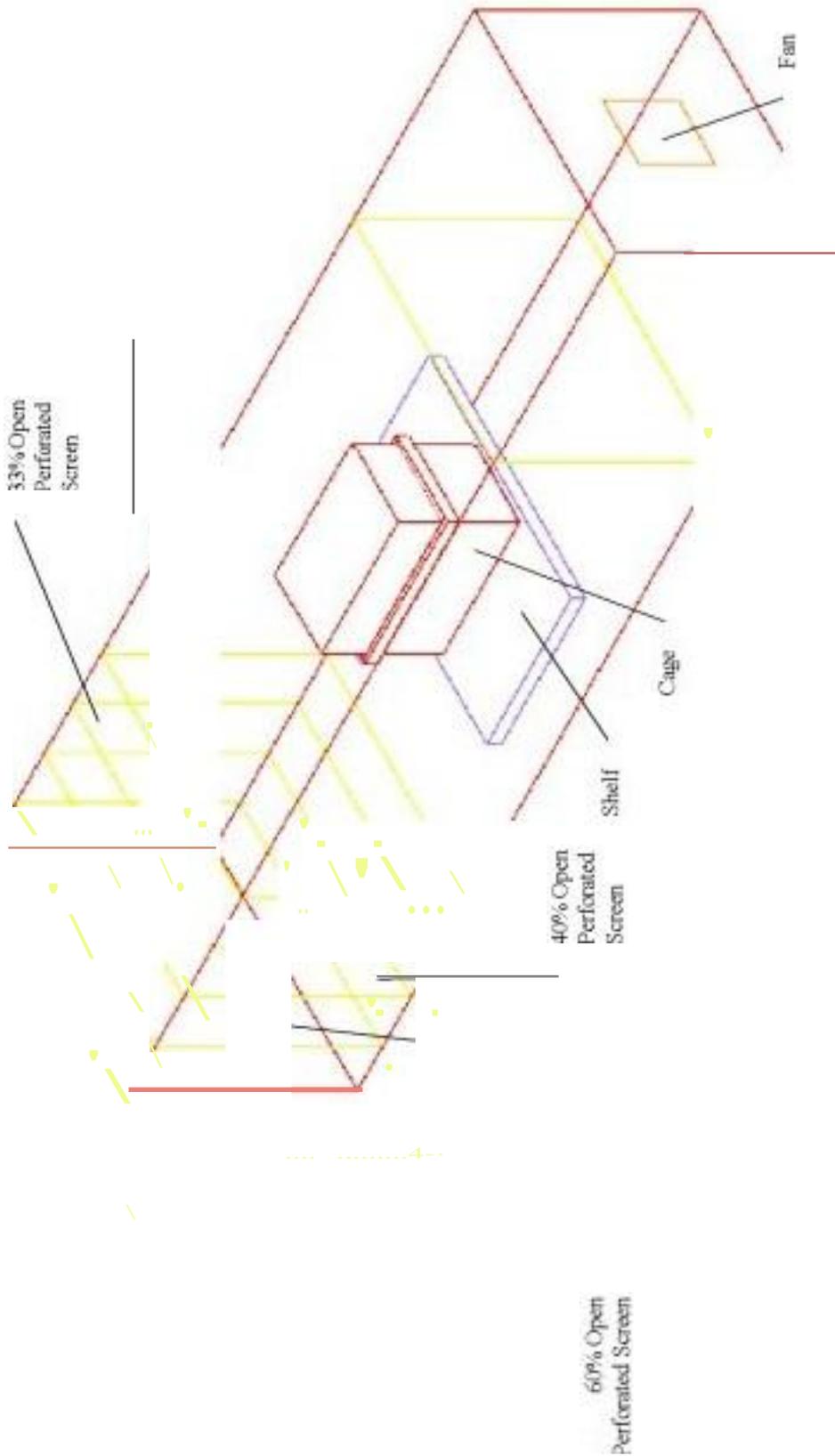
Figure 4.52　　*Parallel Cage Orientation CFD Model.*
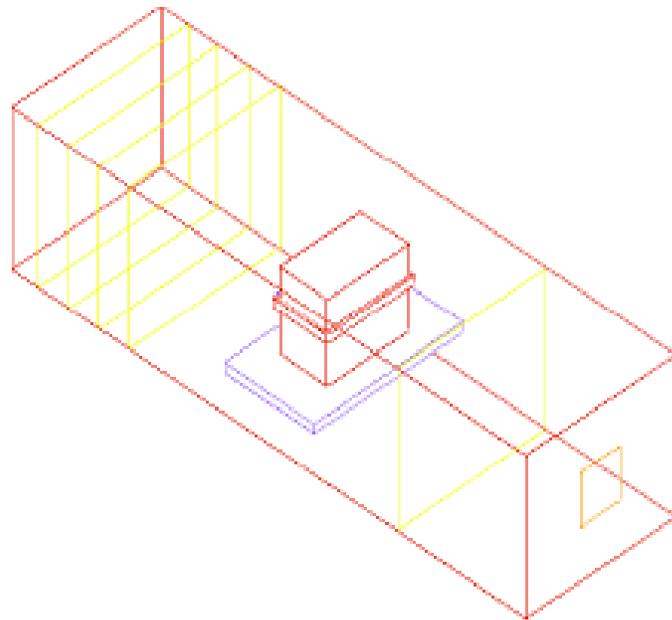
Figure 4.53   Perpendicular Cage Orientation CFD Model.
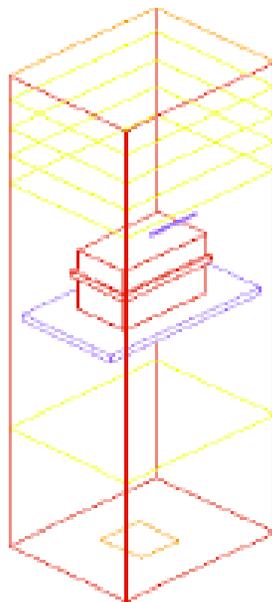
Figure 4.54   Vertical Cage Orientation CFD Model.
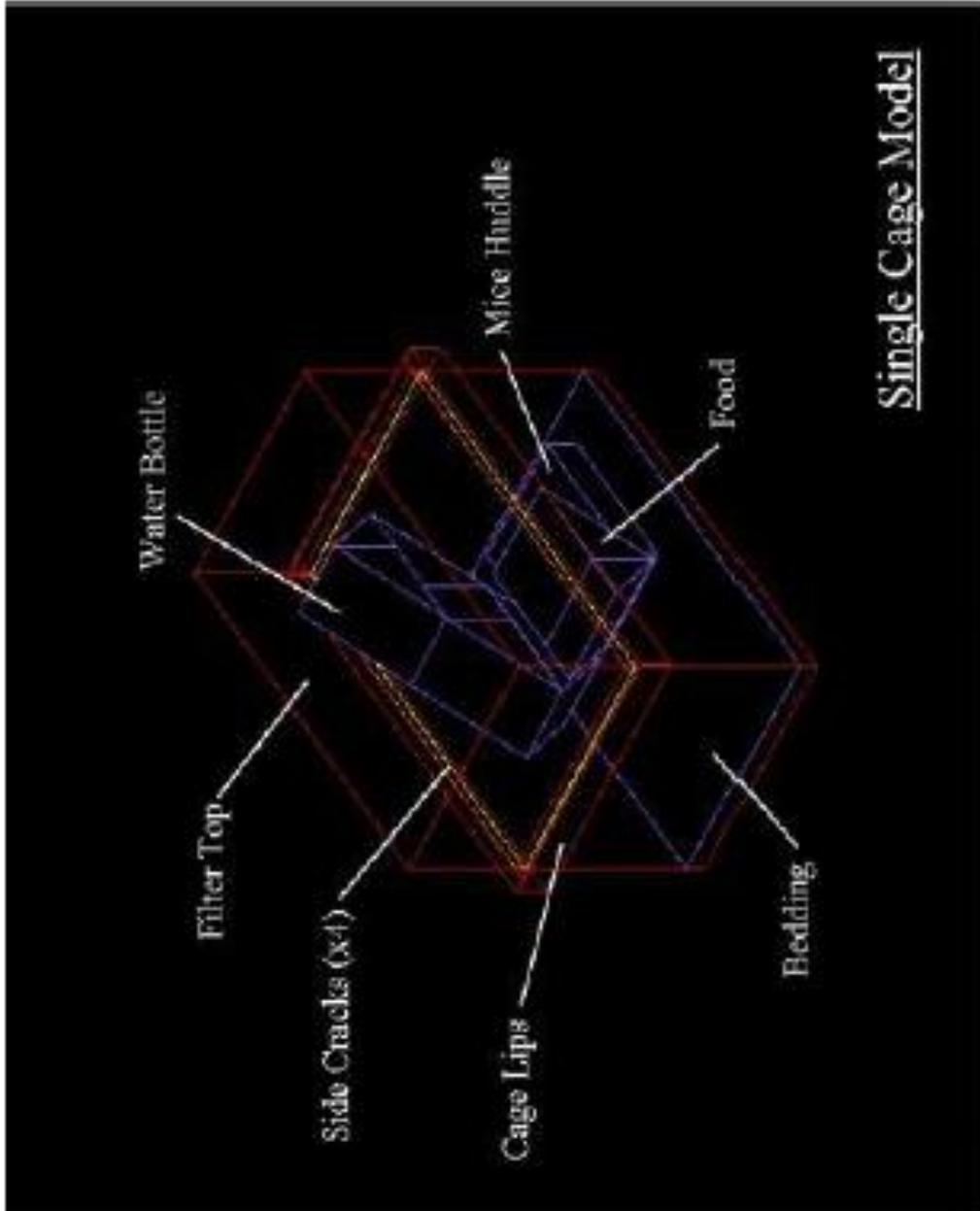
Figure 4.55   CFD Model of Single Cage. Sampling Tubes and Injection Diffuser Stones Not Shown. Mouse Heater Representation: SMO.
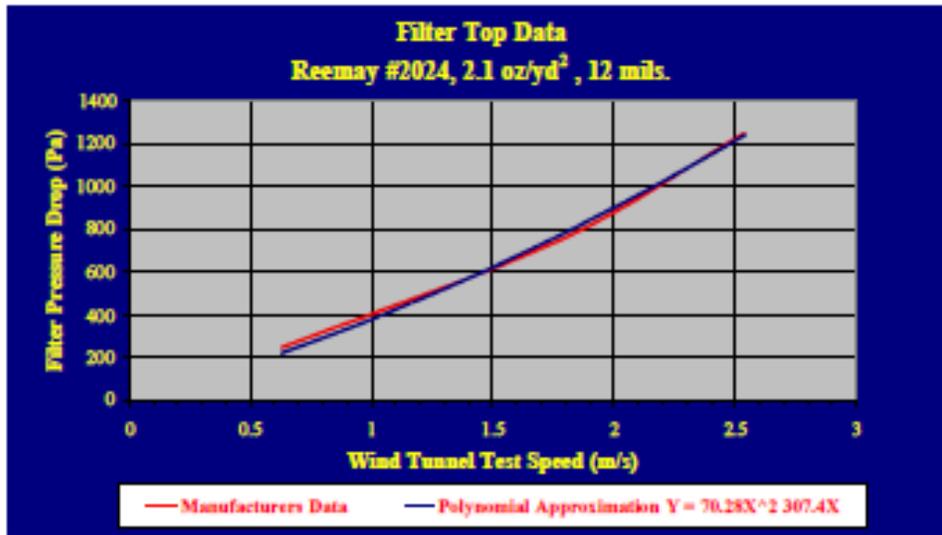
Figure 4.56   Filter Material Test Data and Polynomial Approximation.
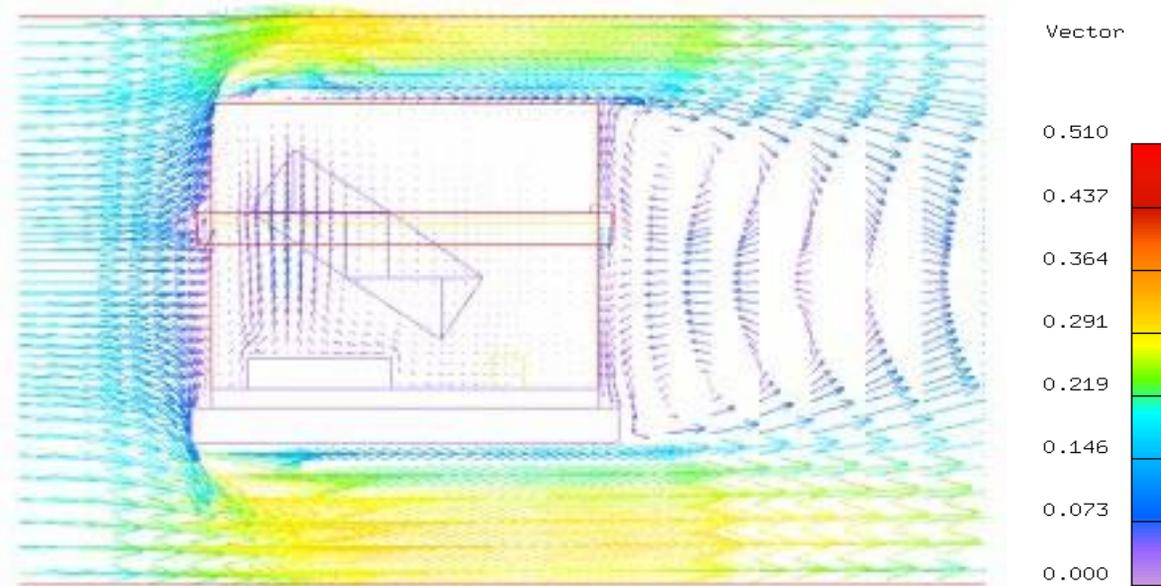
Figure 4.57   *Close-up Plot of the Vector Field at Mid-plane of Tunnel.   Series Sets Six: Parallel Orientation, Heater On (SMO) 40 fpm (0.2m/s).*
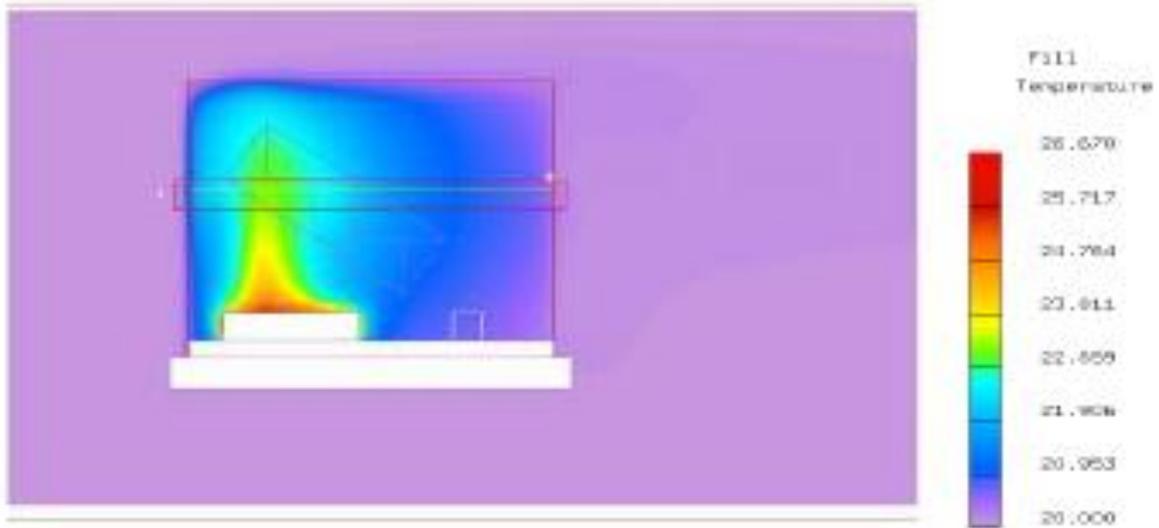
Figure 4.58   *Close-up Plot of the Temperature Field at Mid-plane of Tunnel. Series Sets Six: Parallel Orientation, Heater On (SMO) 40 fpm (0.2m/s).*
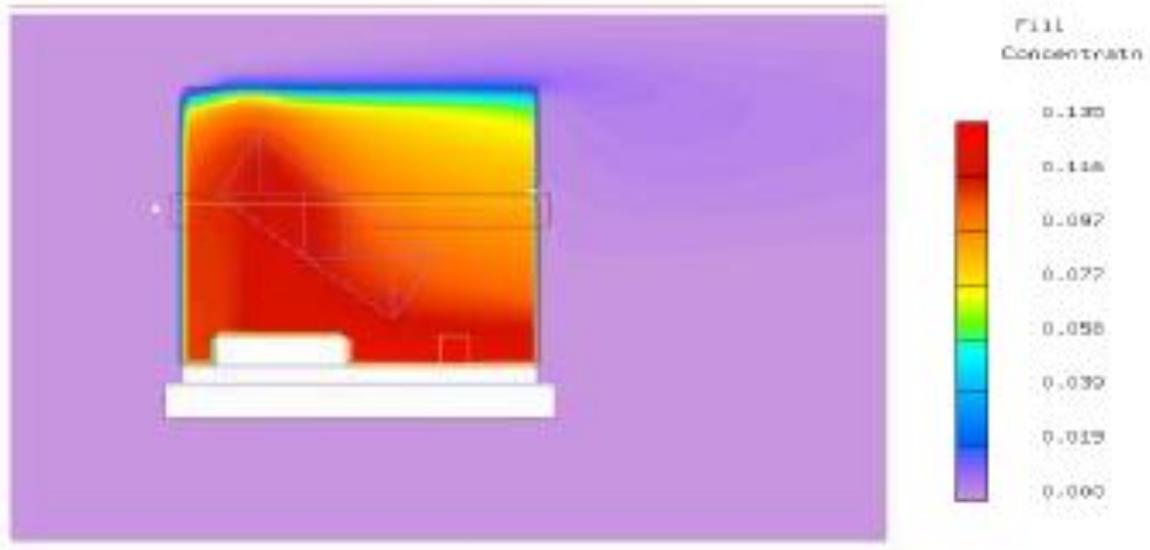
Figure 4.59   *Close-up Plot of the Concentration Field Mid-plane of Tunnel. Series Sets Six: Parallel Orientation, Heater On (SMO) 40 fpm (0.2m/s).*

4.2.2   *Calibration of CFD Diffuser model against Manufacturers Data*

When a diffuser is modeled using CFD it is essential to calibrate the model against manufacturer's data. This is essential because small details in the geometry of the diffuser, the method of construction, etc., can change the jet characteristics. Of course, the detailed geometry of the diffuser could itself be modeled, but the level of detail required in full room models would make the model computationally impractical. This calibration allows the modeler to identify the jet characteristics close to the face of the diffuser where they can be expected to be virtually unaffected by room conditions. The three diffuser types were: a radial diffuser; a slot diffuser; and a low induction diffuser.

4.2.2.1   *Radial Diffuser*

The diffuser is so named because it is designed to provide an airflow pattern that spreads in a fan shaped (or radial) fashion perpendicular to the center line of the diffuser as demonstrated in figure 4.61. The intention of this is to prevent the formation of recirculation zones either side of the diffuser that could potentially retain contaminants. For this reason, this type of diffuser/flow pattern has become increasingly popular in animal rooms, was chosen for the base case whole room simulation, and was used in the experimental empty and populated room scenarios. It should be noted however, that the sideways throw characteristics could be compromised when strong thermal effects are present.

The radial diffuser used in these simulations is as manufactured by Krueger (known in their literature as a TAD, total air diffuser) is shown in figure 4.60. The manufacturer's test facility for this diffuser measured 3.66m (12') x 3.66m (12') x 2.74m (9') high. The diffuser is located centrally in the ceiling of the test room. Two 0.30m (1') high exhausts are located at floor level. The manufacturer's data indicated the vertical and horizontal distance of the 0.25m/s (50 fpm) throw isovel (line of constant velocity) from the diffuser, that was used in the validation exercise, for various flow rates.

In the CFD representation of the test facility, advantage was made of symmetry: the right side of figure 4.61 represents the symmetry plane. The flow rate that was chosen from the manufacturer's data for validation purposes was that nearest the base case flow rate through a single radial diffuser. In particular, the base case flow rate was 270 cfm, while the nearest manufacturer's data point is for 300 cfm. Further, the effect of temperature was also considered. The data point chosen was for a 2.8 °C (5.0 °F) rise in the air temperature between the discharge and the exhaust. Heat sources were applied to the walls of the CFD model to provide such a temperature rise.

Figure 4.61 indicates that the CFD representation of the radial diffuser matches the location of the vertical and horizontal 0.25m/s (50 fpm) isovel data very well. Confidence can therefore be placed in the representation of the CFD radial diffuser in the animal facility simulations.

4.2.2.2   Slot Diffuser

A typical slot diffuser is shown in figure 4.62. The slot diffuser provides high shear flow conditions at inlet, that result in high entrainment of the surrounding air into the jet flow, and consequently highly mixed conditions.

The manufacturer's (Gilberts) test facility in this instance measured 5m x 7m x 3m high (16.4' x 22.97' x 9.84'). The diffuser is centrally located in the ceiling of the test room. The manufacturer's data indicated the vertical distance of the 0.25 m/s (50 fpm) throw isovel from the diffuser, that was used in the validation exercise, for various flow rates.

In the CFD representation, the flow rate that was chosen from the manufacturer's data for validation purposes was that nearest the base case flow rate through a single radial diffuser. In particular, the base case flow rate was 270 cfm, while the nearest manufacturer's data point was 350 cfm.

Figure 4.63 demonstrates that the CFD representation of the slot diffuser matches the location of the 0.25 m/s (50 fpm) isovel data very well. Confidence can therefore be placed in the representation of the CFD slot diffuser model in the animal facility simulations.

4.2.2.3   Low Induction Diffuser

A typical low induction diffuser is shown in figure 4.64. The low induction diffuser provides low shear flow conditions at inlet that result in low induction of the surrounding air into the jet flow. This diffuser therefore provides a solid column of clean air, purging the space of contaminants immediately below it. The disadvantage is then that large recirculations are formed either side of the diffuser jet.

The manufacturer's (Gilberts) test facility in this instance measured 5m x 7m x 3m high (16.4' x 22.97' x 9.84'). The diffuser is centrally located in the ceiling of the test room. The manufacturer's data indicated the vertical distance of the 0.25 m/s (50 fpm) throw isovel from the diffuser, that was used in the validation exercise, for various flow rates.

In the CFD representation, the flow rate that was chosen from the manufacture's data for validation purposes was that nearest the base case flow rate through a single radial diffuser. In particular, the base case flow rate was 270 cfm, while the nearest manufacturer's data point was 325 cfm.

Figure 4.65 demonstrates that the CFD representation of the low induction diffuser matches the location of the 0.25 m/s (50 fpm) isovel data very well. Confidence can therefore be placed in the representation of the CFD low induction diffuser model in the animal facility simulations.

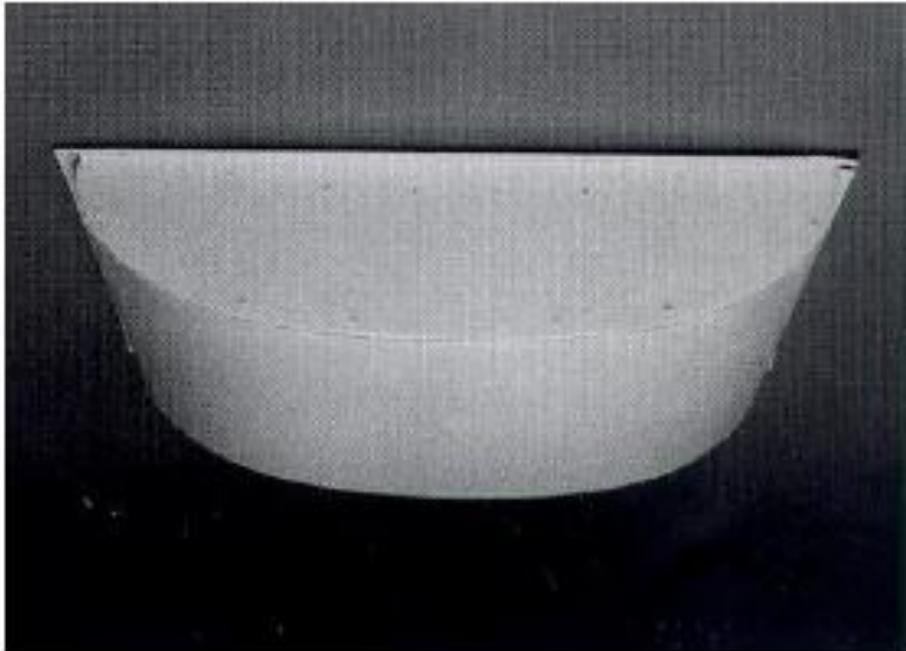*Figure 4.60   Radial Diffuser.*

Figure 4.61   Comparison of CFD and Manufacturers Data for Radial Diffuser.
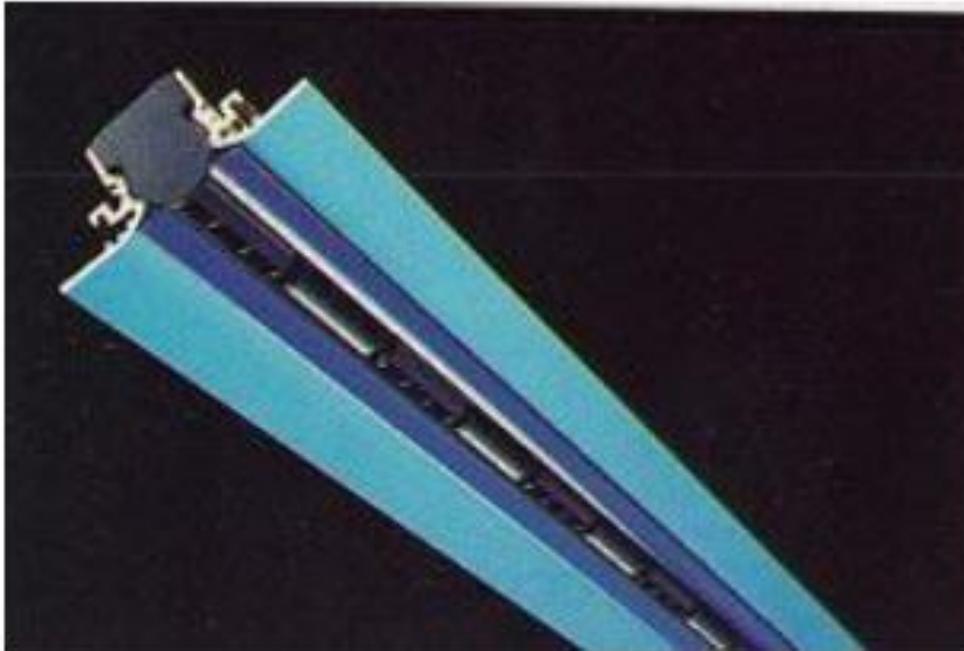
Figure 4.62   Slot Diffuser.

CFD 0.25 m/s Speed Contour
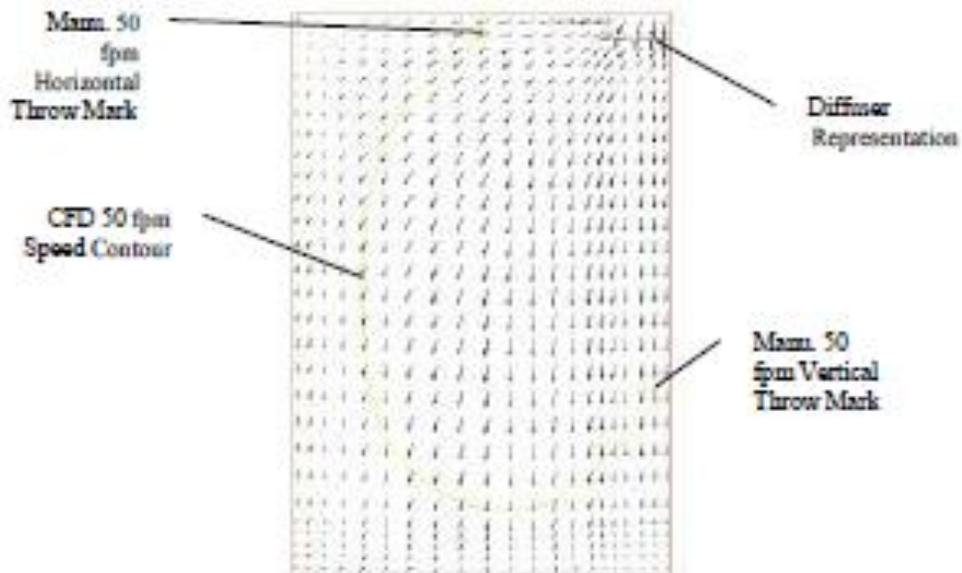
Manu. 0.25 m/s Throw
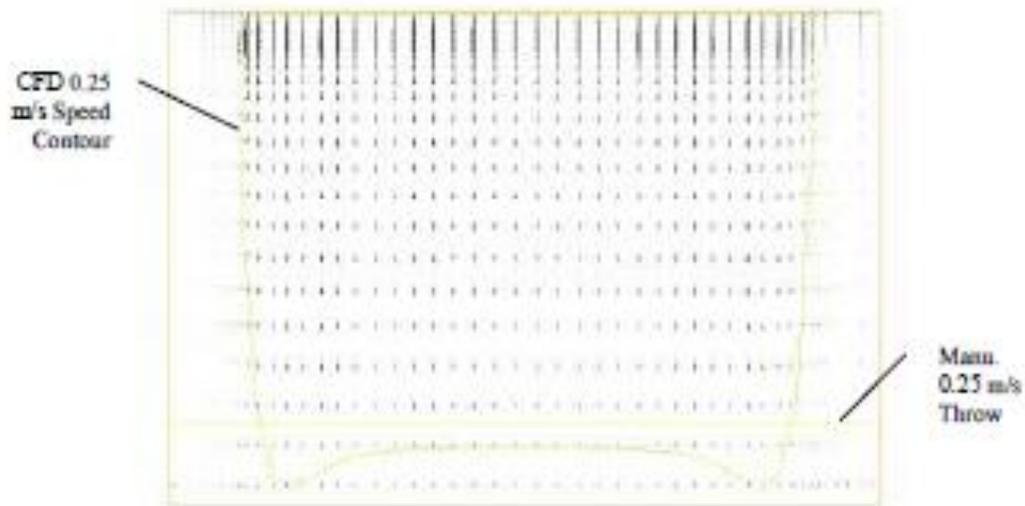
Figure 4.63   Comparison of CFD and Manufacturers Data for Slot Diffuser.
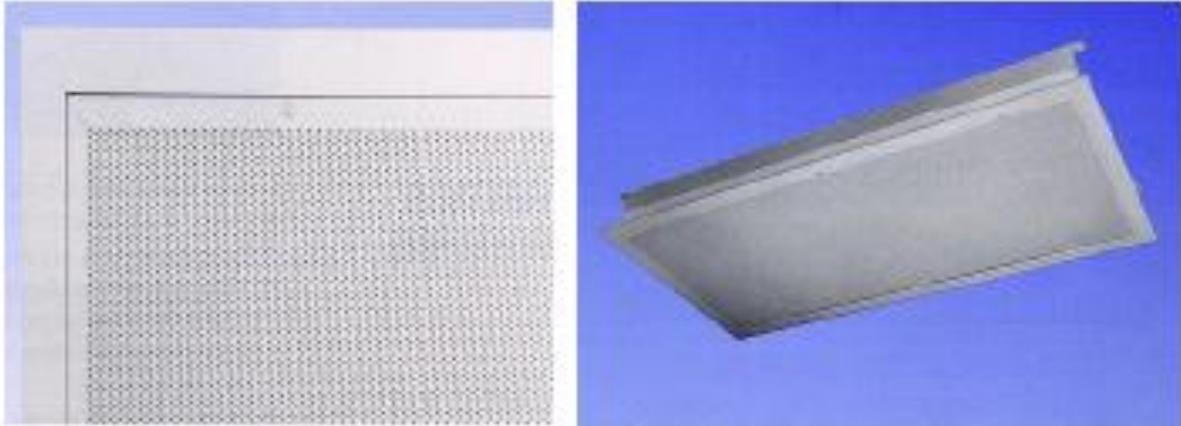
Figure 4.64   Low Induction Diffuser.
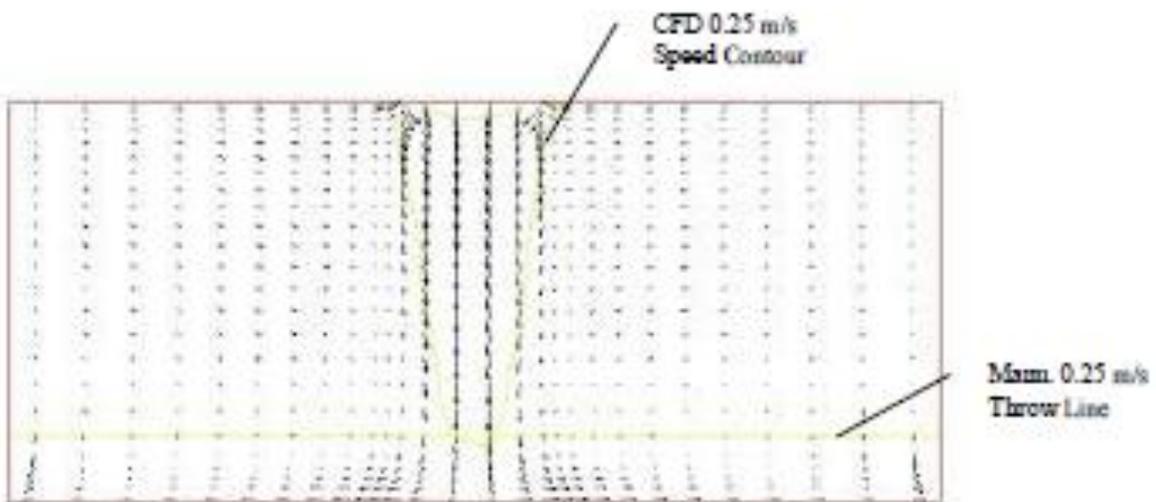
Figure 4.65   Comparison of CFD and Manufacturers Data for Low Induction Diffuser.

4.2.3 Room Condition

4.2.3.1 CFD Simulations

Two CFD models were constructed to replicate the experimental testing room scenarios as closely as possible. Isometric views of the two rooms are shown in figures 4.66 and 4.67. The overall size of the solution domain of both models was high 2.44m x 3.66m x 2.44m (8' x 12' x 8'). The 0.61m x 0.57m (24" x 22.5") centrally located radial diffuser was constructed using a combination of a supply and a series of planar resistances, with the loss coefficients for the planar resistances set such that the representation matched the available manufacturer's data (see section 4.2.2). The supply was specified to provide a flow rate of 128 cfm (7.27e-02 Kg/s).

The 0.30m x 0.30m (12" x 12") exhaust, modeled using an extract, was located 0.20m (8") from the north and west walls, and was specified to exhaust 102 cfm (5.8e-02 Kg /s). The mass imbalance was accounted for through a 6.4e-2m (¼") crack at the bottom of the 0.91m x 2.13m (3' x 7') door, that was centrally located on the north wall.

In the populated room case, the 0.61m x 0.61m x 0.81m (24" x 24" x 32") sink, located in the NE corner of the room, was modeled using a solid rectangular block. The sink recess was not modeled.

The shelves of the 0.61m x 1.83m x 1.52m (24" x 72" x 60") rack were modeled using 1.27e-2m (0.5") thick rectangular blocks. The top shelf was located 1.52m (60") above the floor, and the experimental shelf-to-shelf distance of 0.28m (11") was maintained. The sides of the 0.27m x 0.16m x 0.21m (10.7" x 6.38" x 8.39") shoebox cages were modeled using thin plates, with conductivity and thickness of the plate set to that of the polycarbonate. The water bottle in the cage was constructed from a series of rectangular blocks and triangular prisms: the volume of the water bottle was maintained compared with the physical bottle. The rack was modeled as a planar resistance, with the loss coefficient set to 0.25, corresponding to a free area ratio of 0.85 (Idelchik (1989)). The heater was modeled using a fixed flux rectangular block, with the block specified to dissipate 2.42 W. The diffuser stones were modeled using volume sources, with the injection rate of the CO_2 concentration set to 990 mL/min (3.01 E-5 kg/s) total, or 7.86 mL/min per cage (2.39 E-7 kg/s).
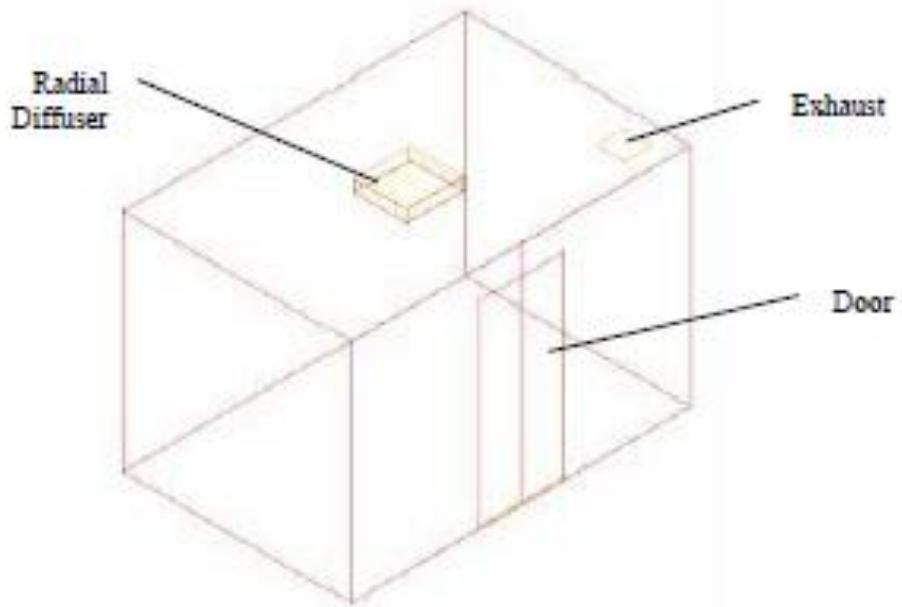
Figure 4.66   CFD Model Empty Room.
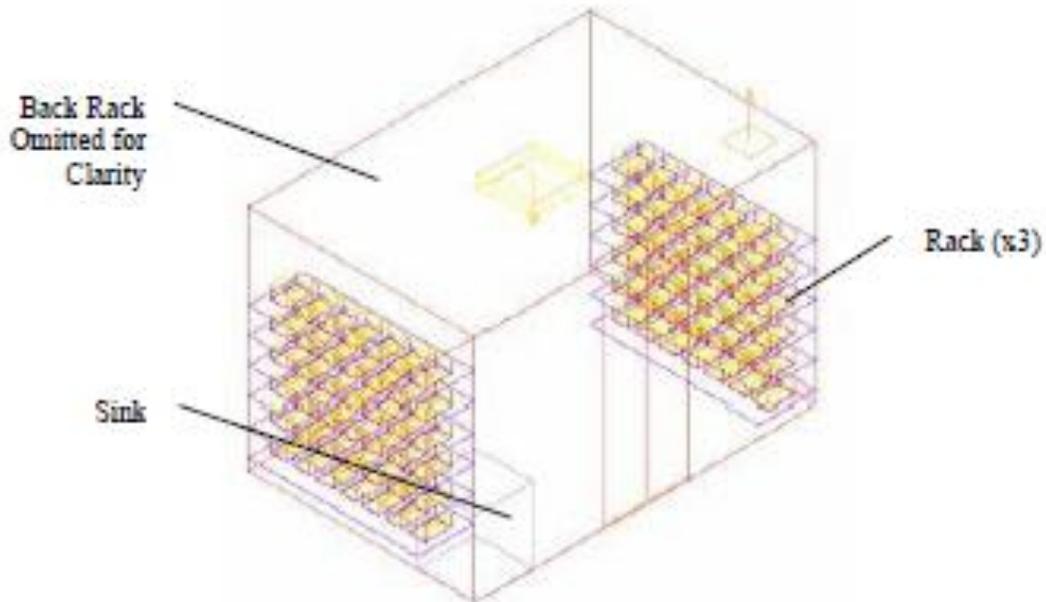
Figure 4.67   CFD Model: Populated Room.

4.2.3.2 Comparison of Experimental Data and CFD Results

This section compares data for two different room configurations, air velocity and temperature for an empty room, and air velocity, temperature and concentration for a stocked room. The challenge with this task largely relates to the measurement of the predominantly low air velocities. This is the case for two reasons. Firstly, the predominant air velocities are low and quite difficult to measure. Secondly, but probably more importantly, small temperature effects or infiltration can easily cause air currents of the order of the air speeds of interest. As a result CFD provides a good understanding of the key flow patterns and comparison is most easily made between the scalar quantities such as temperature and concentration. These are compared for the stocked or populated room

4.2.3.2.1 Empty Room

Due to the large amount of data, only two planes are considered for this experimental scenario. The two planes are plane 1, that is the experimental plane 0.15m (6") from the north wall and so is near the corner exhaust, and plane 8, that is experimental plane 1.22m (48") from the north wall, and so is located mid-way through both the room and the supply diffuser. For a full explanation of the experimental plane locations, see appendix I: section 4.3.2.

Speed Results

The fill plot of the experimental mean air velocity (speed) at experimental plane 1 (i.e. the plane 0.15m (6") from the north wall) is displayed in figure 4.68. Note that the left-hand side of the plot indicates the east wall, and the key range is between 0 and 40 fpm (0.2m/s). The plot clearly shows the locations of the various measurement zones. In particular, the upper left-hand side of the plot shows a region of relatively uniform speed flow, with the magnitude of the airflow velocity being typically around 0.15m/s (30 fpm) and higher. The spots of white in this region indicate velocity measurements that are higher than this: the peak velocity at this plane is 0.28m/s (55 fpm). This region can be clearly seen to be the zone 1, upper east measurement region (see appendix I: section 4.3.2). Also in this plot, the upper right corner of the plot should show a clear increase in velocity near the ceiling, as this plane is close to the corner exhaust of the room. There is no such feature present in the plot. Moving further into the room, the fill plot of the experimental speed field at experimental plane 8 (i.e. 1.22m (48") from the north wall) is displayed in figure 4.69. The white region at the center near the ceiling is the location of the diffuser, with the speeds here being above 0.20m/s (40 fpm). This is an expected feature. However, there are several spots within the plot that are either above or near 0.20m/s (40 fpm), that are well away from the diffuser region. In both plots, the appearance of the high speed sections in the experimental data is unexpected. In particular, appendix I: section 4.1.2 states that, based on theoretical considerations, the air velocity should not exceed 0.11m (22 fpm) outside the jet zone (within 0.30m (12") of the central diffuser), unless there is disturbance to the airflow. As plane 1 is furthest from the jet zone, and the room is fundamentally empty apart from the supply and exhaust, the higher speed values are subject to doubt.

The fill plot of the speed field at plane1 for the CFD simulation is shown in figure 4.70. The plot does not show the same blocks of high speed that are shown in the equivalent experimental plot. Further, the plot also indicates the clear acceleration of air towards the exhaust located in the upper right corner of the plot, that is an expected feature at this plane. The fill plot of the speed field at plane 8 for the CFD simulation is shown in figure 4.71. The plot shows a more consistent flow field associated with the diffuser than the experimental data. In particular, although higher speed flow exists close to the diffuser itself, this flow is quickly slowed as air is entrained into the jets. There are no spots of higher velocity away from this region as there are in the experimental plot.

Temperature Results

The fill plot of the experimental temperature field at experimental plane 1 (i.e. the plane 0.15m (6") from the north wall) is shown in figure 4.72. Note that the left-hand side of the plot indicates the east wall, and that the key range is between 21.1 to 25.0 °C (70.0 and 77.0 °F). The plot clearly shows the demarcation of the various experimental measurement zones. In particular, there are sections of the plot that show same color blocks that indicate regions of approximately the same temperature: others sections show different temperature regions. The reason for this is that the experimental data in the individual zones were taken with different wall surface conditions, as outlined in appendix I: section 4.3.1. This effect is even more marked on consideration of figure 4.73, that displays the fill plot of experimental temperature field at experimental plane 8 (i.e. the plane halfway through the room, 1.22m (48") from the north wall).

However, in the CFD simulation, the boundary walls were defined as being at an average surface temperature. As a result, the fill plots for the temperature fields do not exhibit the dominant effect of the wall surface temperature. Figure 4.74 displays the fill plot of the temperature field at plane 1 (i.e., the plane 0.15m (6") from the north wall). As the flow field exhibits essentially well mixed, isothermal conditions here, the temperature field shows relatively little variation. At the center plane of the room, plane 8 (i.e., the plane 1.22m (48") from the north wall), the shape of the incoming diffuser air is evident, as shown in figure 4.75.

Despite the apparent differences in the two sets of data, the levels of difference between the data is reasonable, as demonstrated in tables 4.2.13 and table 4.2.14. In particular, the average difference at plane 1 is around 11.6 percent, while that at plane 8 is around 16.8 percent. These are well within normally accepted experimental uncertainty.

Discussion and Conclusions

The above comparison demonstrates that reasonable agreement was obtained with regards to the temperature field, while the experimental speed field displayed several features and values that were subject to doubt.

The experimental temperature and speed fields highlight the difficulty of maintaining isothermal conditions in a test facility, despite the adherence to rigorous experimental protocol. This has a

significant impact on the airflow and temperature distributions. This is particularly important when using a diffuser of the radial type since they have inherently low momentum, so the jet is easily affected by small, induced air currents.

The problems are clearly identified by the fact that measured values of air speed are well in excess of the theoretical limit of 0.11m/s (22 fpm) well away from the diffuser jet (see appendix I: section 4.1.2). The CFD results only show these larger air speeds where they would be expected – close to the supply air diffuser and the room exhaust. The advantage of the computational fluid dynamics approach is that, by definition, the predicted values for the parameters in the analysis have to be consistent since the approach is based on the fundamental laws for the conservation of mass, momentum, and energy. The experimental approach does not benefit from any such luxury since the measurements are each independently recorded by parameter and by location. Air velocities of the low speeds seen in a room (in this case typically below 0.10 m/s (20fpm)), for example, are inherently difficult to measure for several reasons:

> The low velocities are very susceptible to fluctuations as well as variations in the boundary conditions over the period of the experiment. Extending the sampling period for individual points to obtain a more representative average can be counterproductive since it increases the total period of the experiment and makes it more difficult to maintain the boundary conditions for the experiment.

> The constant temperature thermistor based sensing head (used in hot film anemometers) becomes inaccurate at low speeds because the heating of the head causes local air velocities of a similar order.

> The presence of the measurement equipment, and any traversing equipment (see figures 4.32 and 4.33) can influence the local velocities.

The scalar quantities such as temperature and concentration are easier to measure, and as this section (and the following section, section 4.2.3.2.2 show) shows good correlation can be seen between the measured and predicted data.

Given that the predictions of temperature and concentration are good then, by the laws of conservation the air velocities must also be well predicted, with the discrepancies between measured and predicted data being accounted for by difficulty in measurement outlined above.

It should be also be remembered that the CFD model of the radial diffuser was found to accurately predict the manufacturer's throw data (see section 4.2.2), and so a good degree of confidence should be place in the CFD representation of the diffuser.

As far as the temperature measurements are concerned, the experimental data plots, for example, figure 4.72, highlight the difficulty in maintaining isothermal conditions within test facilities. In this example, the differing boundary wall temperatures have a marked impact on the internal room temperatures.

Table 4.2.13 Table of percent Difference between Experimental and CFD Temperature Data at Plane 1 (0.15m (6") from North Wall)

Dist. From Floor (")	Distance From West Wall (")											
	138	132	126	120	114	108	102	96	90	84	78	72
90	11.5	14.1	13.2	11.4	13.7	24.2	15.1	18.2	16.6	26.1	8.7	2.8
84	8.6	15.8	14.2	13.5	14.2	20.0	17.2	18.0	16.9	25.8	9.9	1.2
78	7.1	14.7	15.7	10.6	13.7	19.9	18.1	20.8	22.2	23.9	10.9	1.6
72	7.0	12.8	10.6	8.3	12.4	19.4	15.8	20.7	23.6	14.2	6.2	4.4
66	4.1	10.5	9.7	7.0	10.9	17.4	15.5	19.5	22.2	12.9	8.7	13.4
60	2.4	8.4	8.6	10.8	11.3	18.4	13.8	17.4	19.0	9.9	7.8	3.2
54	2.5	7.2	7.2	8.3	10.2	17.2	8.4	15.9	17.5	9.0	7.1	0.9
48	1.8	7.0	4.5	8.4	9.6	17.4	6.4	15.0	14.2	4.4	8.2	0.5
42	1.4	7.5	4.5	5.4	9.8	17.0	8.4	16.6	15.3	4.2	9.9	0.7
36	1.7	8.4	4.6	7.0	11.9	17.8	6.6	13.7	12.0	4.0	13.1	3.1
30	2.5	8.0	5.8	8.3	12.8	16.0	8.5	14.9	15.0	4.7	12.4	3.6
24	19.2	19.1	23.4	19.0	36.9	29.5	25.5	28.8	29.0	22.2	8.2	12.4
18	21.6	23.6	19.6	19.7	37.0	29.5	20.9	24.8	23.6	22.1	8.8	15.5
12	20.2	26.8	18.4	17.8	36.8	28.8	20.4	25.8	21.8	21.8	10.3	15.2
6	19.8	23.6	18.9	18.6	38.6	30.4	20.5	26.3	22.8	21.5	8.9	15.0

Dist. From Floor (")	Distance From West Wall (")											
	66	60	54	48	42	36	30	24	18	12	6	
90	3.9	3.0	4.3	8.3	8.2	4.5	3.3	4.9	3.9	7.4	2.3	
84	4.1	0.9	5.0	10.3	4.5	4.6	6.4	6.1	6.1	7.7	1.4	
78	0.8	1.4	2.0	7.8	7.2	8.0	6.0	4.4	8.3	6.4	0.2	
72	1.2	0.2	2.3	6.4	8.9	7.4	3.5	5.1	8.3	4.7	0.1	
66	0.5	0.4	3.9	11.6	3.0	7.6	5.7	1.2	8.0	5.8	0.9	
60	1.2	1.0	6.2	14.3	4.2	7.6	5.6	0.8	6.9	4.1	0.9	
54	2.8	1.4	3.1	8.8	11.6	9.4	9.0	6.6	8.8	3.3	2.5	
48	1.5	1.0	2.6	6.2	5.8	4.7	7.4	11.7	9.7	5.8	1.8	
42	1.9	2.8	1.0	6.9	3.6	3.1	6.9	10.6	10.6	7.7	4.0	
36	4.6	6.8	2.5	4.5	6.5	4.1	7.3	7.4	13.9	8.2	5.3	
30	2.5	6.4	3.3	4.2	6.4	7.1	9.1	0.5	15.7	15.8	6.5	
24	9.1	11.9	23.5	20.9	18.2	22.8	22.8	16.0	21.7	22.2	18.8	
18	13.5	11.2	26.9	22.7	15.7	20.1	17.2	17.0	19.0	23.0	18.5	
12	10.2	11.7	26.7	22.1	13.8	18.8	19.2	17.9	17.5	21.6	19.0	
6	11.4	12.7	23.9	28.6	12.4	11.7	14.0	10.1	19.3	23.2	20.4	

Table 4.2.14   Table of percent Difference between Experimental and CFD Temperature data at Plane 8 (1.22m (48") from North Wall)

Dist. From Floor (")	Distance From West Wall (")											
	138	132	126	120	114	108	102	96	90	84	78	72
90	23.7	28.7	18.5	25.2	17.1	22.5	14.7	17.3	19.1	14.2	0.8	2.2
84	26.9	31.4	24.3	41.9	26.9	26.9	18.2	21.8	24.6	19.9	2.6	0.9
78	25.6	26.7	22.6	22.3	25.9	23.1	19.1	23.7	26.6	22.7	0.3	7.2
72	25.4	26.6	22.5	22.5	26.0	23.4	19.4	24.0	27.1	23.2	4.4	11.8
66	20.9	24.8	20.3	20.6	22.0	21.1	20.6	23.0	25.8	20.0	12.5	17.9
60	19.2	24.3	20.7	22.4	26.1	25.0	20.2	27.0	27.5	21.2	11.6	16.0
54	19.6	25.0	19.2	21.9	24.3	23.0	18.1	26.1	27.9	20.7	4.4	8.8
48	18.0	25.5	19.1	18.8	20.7	22.9	19.6	23.5	26.7	26.9	4.6	13.5
42	18.2	25.6	24.0	22.7	25.1	25.6	20.2	25.5	29.9	25.2	0.3	7.3
36	17.8	25.9	24.4	22.4	29.0	27.0	22.4	27.3	28.5	22.0	0.2	7.5
30	19.1	25.5	21.3	22.5	27.9	27.6	23.1	30.5	32.3	25.4	1.2	6.8
24	8.8	13.8	9.9	8.1	22.5	18.4	17.9	15.1	17.6	18.4	15.1	20.9
18	8.0	15.7	8.3	7.6	22.5	19.0	16.2	20.5	24.2	14.7	15.1	23.9
12	8.0	13.5	6.3	7.6	20.8	21.6	17.4	17.5	19.0	11.9	13.6	22.0
6	6.7	6.7	4.4	5.2	19.1	19.7	12.4	16.1	20.5	14.5	16.0	23.5

Dist. From Floor (")	Distance From West Wall (")										
	66	60	54	48	42	36	30	24	18	12	6
90	3.3	2.4	3.2	6.5	4.8	7.9	13.2	18.3	2.1	0.7	1.2
84	0.6	0.8	2.4	5.5	5.0	8.7	12.9	19.5	2.9	0.2	1.1
78	3.5	4.1	5.8	8.4	8.2	11.4	15.5	23.2	3.5	0.4	1.5
72	8.2	9.5	10.9	13.6	12.6	15.5	20.0	27.3	3.5	0.2	1.3
66	16.0	17.5	18.4	20.3	17.7	21.7	24.7	28.8	3.6	0.6	2.3
60	11.7	13.5	13.4	18.1	16.0	20.3	24.7	25.7	4.4	1.5	4.3
54	6.2	7.7	11.3	18.4	15.2	20.5	25.2	27.0	5.5	2.3	5.7
48	4.7	8.8	13.0	20.5	16.6	20.5	24.4	26.3	7.8	5.0	7.3
42	3.3	6.0	13.0	20.2	14.9	19.6	22.3	23.7	9.1	5.8	8.7
36	3.4	5.6	12.4	17.1	11.9	16.1	19.2	20.5	9.6	7.1	7.9
30	2.4	4.1	10.7	15.4	9.3	13.7	16.8	19.2	8.5	7.4	9.5
24	18.4	16.9	21.3	23.8	20.8	20.6	28.4	28.8	24.4	27.1	38.1
18	20.9	14.8	22.8	22.3	17.6	19.9	25.8	25.2	21.9	28.4	27.6
12	15.7	15.6	25.8	22.8	18.9	18.6	23.7	24.5	20.6	21.7	-
6	17.4	15.7	23.8	23.1	19.9	18.7	22.3	24.0	20.2	18.0	28.5
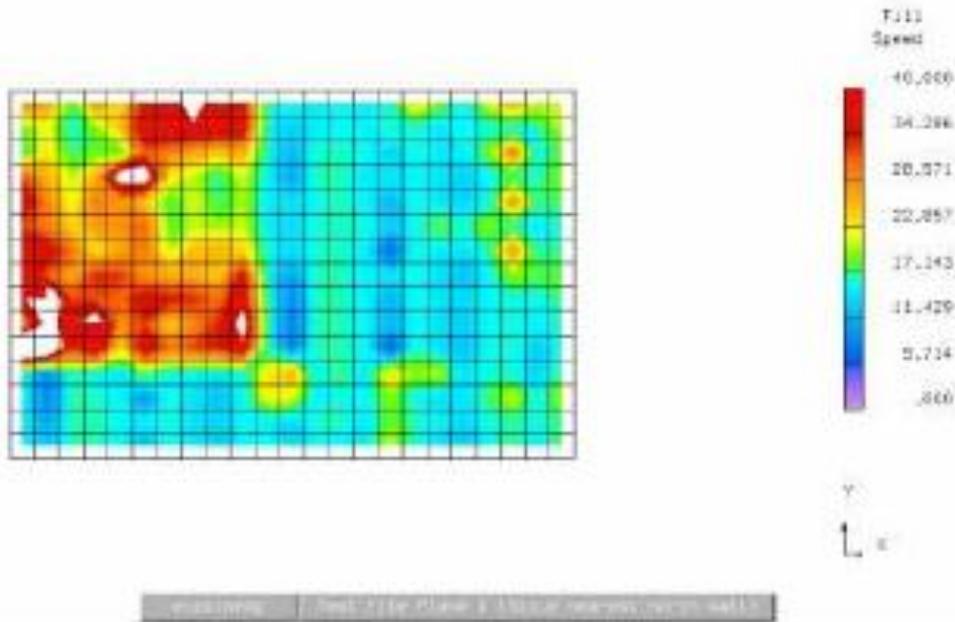
Figure 4.68 *Fill Plot of Speed Field (Experimental) at Plane 1 (Plane (0.15m (6") from North Wall). Empty Room Case.*

Figure 4.69 *Fill Plot of Speed Field (Experimental) at Plane 8 (Plane 1.22m (48") from North Wall). Empty Room Case.*
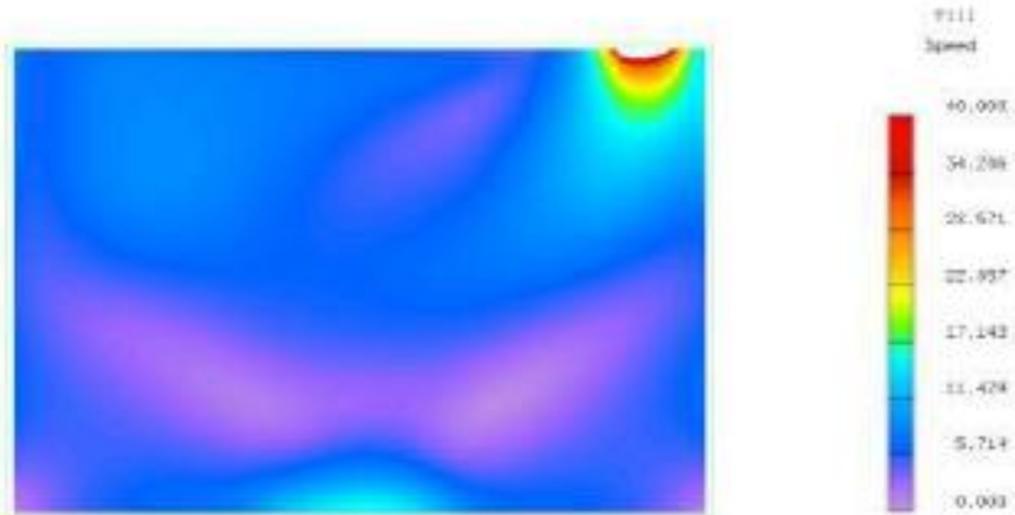
*Figure 4.70   Fill Plot of Speed Field (CFD) at Plane 1 (Plane 0.15m (6") from North Wall).
Empty Room Case.*

*Figure 4.71   Fill Plot of Speed Field (CFD) at Plane 8 (Plane 1.22m (48") from North Wall).
Empty Room Case.*

Figure 4.72   *Fill Plot of Temperature Field (Experimental) at Plane 1 (Plane 0.15m (6") from North Wall). Empty Room Case.*

Figure 4.73   *Fill Plot of Temperature Field (Experimental) at Plane 8 (Plane 1.22m (48") from North Wall). Empty Room Case.*
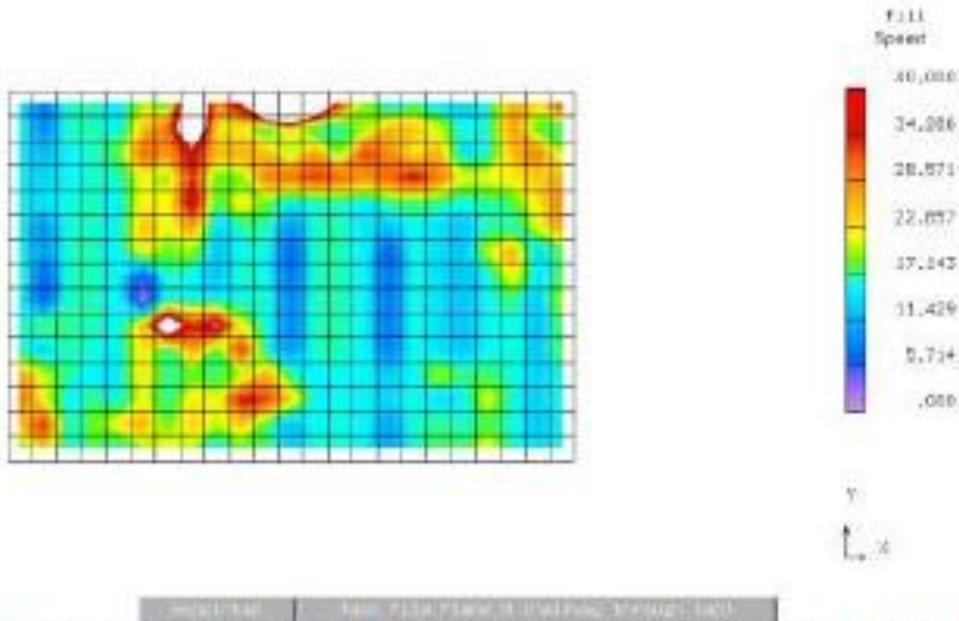
Figure 4.74   Fill Plot of Temperature Field (CFD) at Plane 1 (Plane 0.15m (6") from North Wall). Empty Room Case.

Figure 4.75   Fill Plot of Temperature Field (CFD) at Plane 8 (Plane 1.22m (48") from North Wall). Empty Room Case.
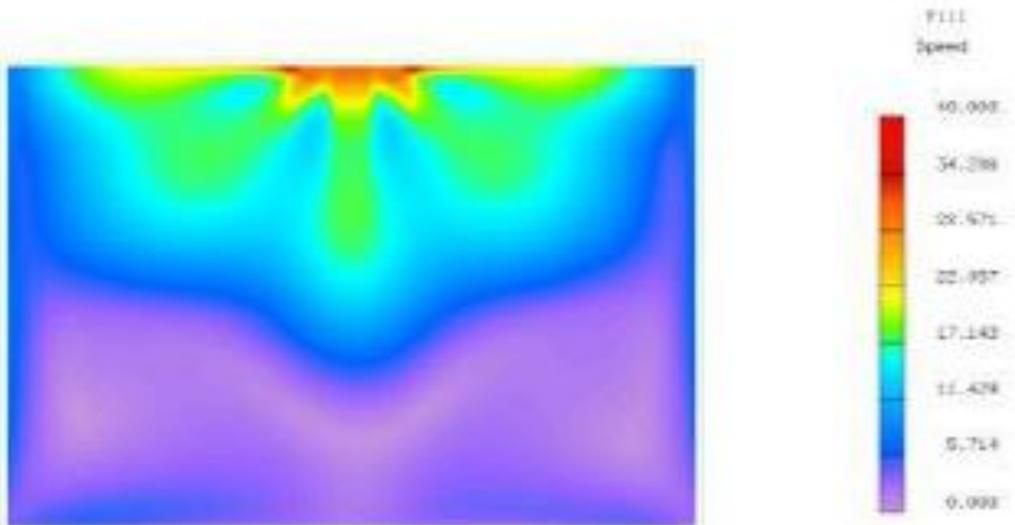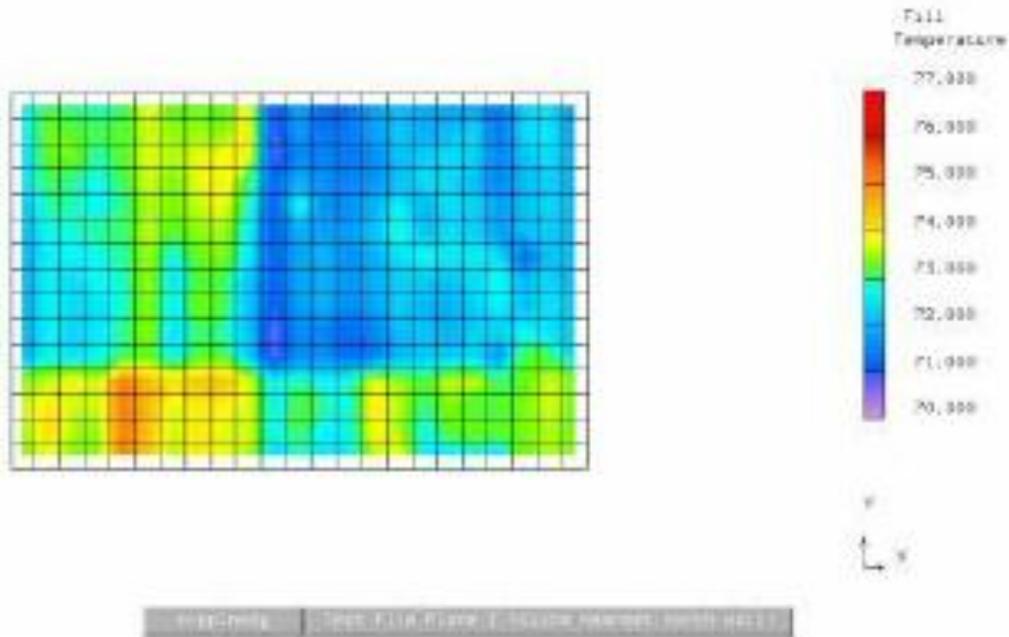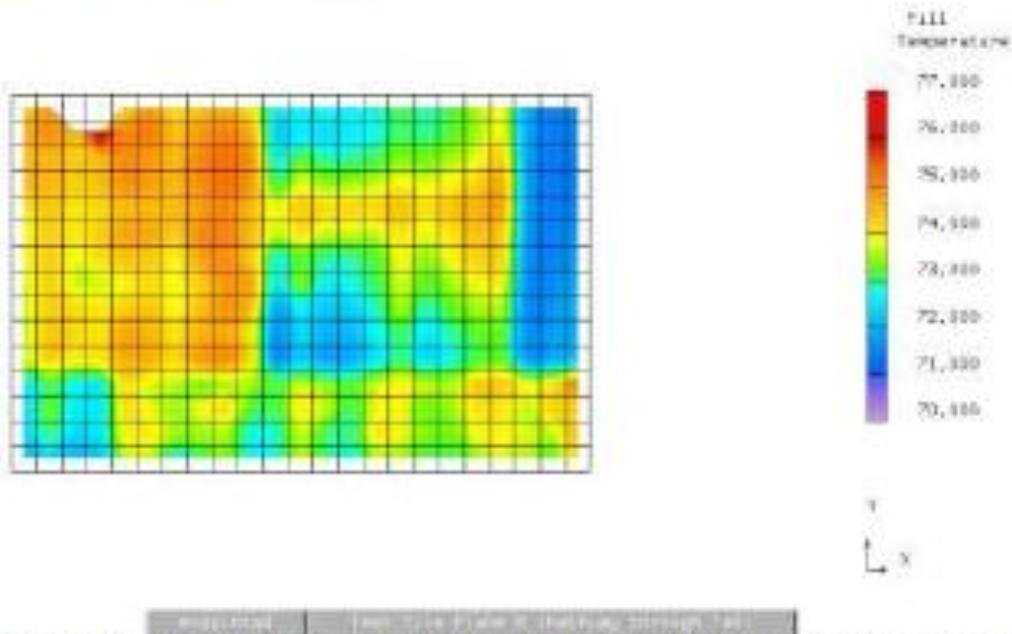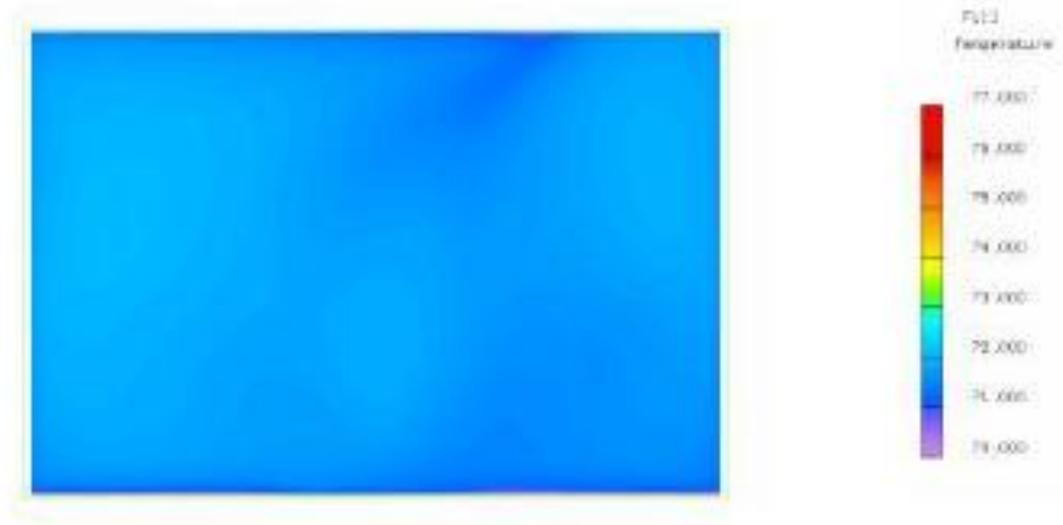
4.2.3.2.2   Populated Room

For ease of comparison here, the experimental data are overlaid on top of the CFD results for this section of work. The experimental data are represented as contour lines, i.e., lines of the same value, while the CFD results are represented as fill plots.

Speed Results

The comparison between the experimental and CFD speed field results at 1.02m (40") from the south wall are shown in figure 4.76. Note that the left side of the plot represents the east wall of the room, and the key range is between 0 and 40 fpm (0.2 m/s). The plot shows that, qualitatively, the CFD simulation predicts the plumes of air resulting from the heaters in the individual cages. However, the experimental data show several spots of high speed in the rest of the plot that cannot readily be explained. Further, the experimental data demonstrate a peak value of 0.86m/s (172 fpm) well away from the cage plumes, and other measurement points where the speed value is above 0.60m/s (120 fpm), whereas the CFD prediction shows more modest peaks. Moving further towards the North Wall, figure 4.77 shows the comparison at the plane 1.93m (76") from the south wall. The experimental data again look a little uncertain. In particular, the high speeds in the lower right and left sides of the plot appear very similar to those in the previous plot. In this physical scenario, the room has very different boundary conditions near the north and south walls, and so these high spots appear unrealistic. Further, the peak experimental speed at this plane is 1.25m/s (250 fpm), with various other places showing values above 1.00m/s (200 fpm). Finally, the experimental data do not show any indication of the effect of the exhaust fan in the corner of the room. This feature is clearly evident in the CFD field.

Temperature Results

The comparisons between the experimental and CFD temperature field data at planes 0.71m, 1.02m, 1.32m, 1.63m, 1.93m and 2.13m (28", 40", 52", 64", 76, and 84") from the South Wall are shown in figures 4.78 to 4.83 respectively. Note that the left side of the plot represents the east wall of the room, and the key range is between 21.1 °C to 25.0 °C (70.0 and 77.0 °F). The planes represent comparisons close to the South Wall cage rack through to the North Wall door. The plots show that there is generally very good agreement between the experimental and CFD results at each of the planes. The CFD also correctly predicts many of the physical features exhibited by the experimental data, for example, the stratification of the air temperature shown most clearly in figure 4.82, and the diffuser airflow shown in figure 4.80.

The percentage differences between the experimental and CFD results confirm the good agreement between the two sets of data, as indicated in Tables 4.2.15 to 4.2.20. In particular, the average difference at the 0.71m (28") plane is 11.9 percent, at the 1.02m (40") plane is 13.0 percent, at the 1.32m (52") plane is 18.7 percent, at the 1.63m (64") plane is 11.9 percent, at the 1.93m (76") plane is 12.1 percent, and at the 2.13m (84") plane is 18.5 percent. These

differences again are within normal values of 20 percent commonly accepted as experimental uncertainty.

Table 4.2.15   Table of percent Difference between Experimental and CFD Temperature Data at Plane 0.71m (28") from South Wall

Dist. from Floor (")	Distance From West Wall (")												
	2	**14**	**26**	**38**	**50**	**62**	**74**	**86**	**98**	**110**	**118**	**130**	**142**
84	15.2	7.1	4.8	3.9	2.2	15.7	6.1	5.7	25.3	15.3	17.2	12.1	7.7
72	14.0	11.3	1.2	5.7	3.8	22.6	0.6	7.3	15.1	22.4	7.2	12.8	9.3
60			14.4	10.8	9.9	23.4	6.4	1.3	15.9	6.1	14.9		
48			22.0	4.4	1.0	19.2	1.1	0.5	2.2	13.4	17.8		
36			27.6	7.8	2.8	8.4	14.3	0.6	2.9	24.3	22.7		
24			22.2	1.0	12.7	6.9	1.0	13.9	27.9	23.6	5.6		
12			3.0	10.4	11.0	7.4	6.3	13.5	37.5	4.0	21.6		

Table 4.2.16   Table of percent Difference between Experimental and CFD Temperature Data at Plane 1.02m (40") from South Wall

Dist. from Floor (")	Distance From West Wall (")												
	2	**14**	**26**	**38**	**50**	**62**	**74**	**86**	**98**	**110**	**118**	**130**	**142**
84	7.6	13.5	6.1	0.6	2.9	13.6	39.9	26.4	17.3	7.3	6.7	3.8	31.8
72	10.3	25.6	19.1	3.0	0.9	12.4	13.1	16.2	0.5	2.7	5.6	1.5	26.6
60			34.0	6.8	2.5	7.3	8.1	5.8	10.0	1.3	23.7		
48			27.2	9.2	2.4	10.1	12.1	16.5	14.7	6.0	20.0		
36			34.0	12.9	4.9	2.3	17.0	13.1	15.9	7.1	29.9		
24			29.8	5.6	14.0	10.6	2.0	9.8	14.1	2.9	6.8		
12			11.9	14.5	9.6	12.3	6.7	12.4	21.4	7.0	9.2		

Table 4.2.17   Table of percent Difference between Experimental and CFD Temperature Data at Plane 1.32m (52") from South Wall

Dist. from Floor (")	Distance From West Wall (")												
	2	**14**	**26**	**38**	**50**	**62**	**74**	**86**	**98**	**110**	**118**	**130**	**142**
84	23.9	3.1	5.5	14.6	29.8	22.6	29.6	36.4	10.6	11.6	13.1	17.2	4.6
72	21.1	4.9	4.5	14.6	21.0	22.6	37.0	25.9	12.7	14.2	3.9	15.4	5.0
60			15.6	11.4	19.5	23.1	32.8	12.5	3.4	20.3	9.9		
48			7.9	21.8	24.1	18.1	34.5	15.6	6.1	33.7	1.2		
36			16.1	18.6	23.0	19.0	26.0	14.9	7.9	31.7	7.6		
24			3.6	11.3	25.3	29.9	25.3	23.3	33.5	21.4	17.1		
12			11.8	4.4	19.1	20.0	3.0	29.3	40.3	7.9	27.3		

Table 4.2.18   Table of percent Difference between Experimental and CFD Temperature Data at Plane 1.63m (64") from South Wall

Dist. from Floor (")	Distance From West Wall (")												
	2	14	26	38	50	62	74	86	98	110	118	130	142
84	0.9	22.5	8.8	2.7	0.3	13.1	7.7	4.7	12.1	11.9	15.1	5.1	7.6
72	6.4	30.6	2.7	11.8	2.2	13.0	11.5	14.2	6.1	2.5	14.2	13.5	5.6
60			28.1	7.3	3.6	7.5	13.0	15.5	1.3	4.8	35.8		
48			26.5	6.4	7.3	7.4	18.5	17.3	0.3	9.6	28.9		
36			33.1	14.4	5.3	7.9	15.1	8.1	4.4	1.9	41.4		
24			27.5	6.6	7.2	4.8	0.9	7.0	17.6	5.8	29.0		
12			7.8	13.9	2.1	0.4	10.9	4.5	15.3	13.2	6.4		

Table 4.2.19   Table of percent Difference between Experimental and CFD Temperature Data at Plane 1.93m (76") from South Wall

Dist. from Floor (")	Distance From West Wall (")												
	2	14	26	38	50	62	74	86	98	110	118	130	142
84	1.6	15.3	4.8	0.5	0.2	12.0	13.0	1.7	0.2	2.4	2.8	1.5	5.3
72	5.6	17.5	4.2	4.2	2.7	13.6	14.6	6.7	3.9	7.7	4.5	15.2	7.4
60			35.0	6.4	2.6	9.2	10.1	16.7	9.1	12.9	8.0		
48			30.0	11.6	1.8	10.3	11.1	13.6	17.4	16.8	14.2		
36			24.0	16.3	4.9	7.0	16.0	22.9	12.6	17.8	9.5		
24			21.7	5.3	18.6	11.1	7.2	14.5	41.3	25.1	13.2		
12			2.7	7.4	18.4	10.1	4.6	14.9	33.8	3.2	19.0		

Table 4.2.20   Table of percent Difference between Experimental and CFD Temperature Data at Plane 2.13m (84") from South Wall

Dist. from Floor (")	Distance From West Wall (")												
	2	14	26	38	50	62	74	86	98	110	118	130	142
84	1.4	2.3	5.8	9.7	14.0	8.3	25.3	13.2	17.4	17.3	13.6	9.2	10.0
72	3.9	18.1	4.5	9.3	12.5	8.9	27.4	16.6	28.6	29.6	22.4	14.9	6.9
60			22.3	9.2	12.0	10.2	28.3	24.2	20.4	29.7	26.7		
48			16.3	14.8	14.3	5.0	24.7	28.6	23.3	32.2	26.1		
36			25.6	19.9	16.5	9.5	24.1	22.0	23.8	33.2	23.8		
24			11.1	14.2	17.2	16.0	12.6	11.4	35.9	28.0	31.6		
12			6.1	1.8	15.4	9.5	10.8	21.7	35.5	9.9	32.5		

Concentration Results

The comparison between the experimental and CFD concentration (CO_2) results at the planes 0.71m, 1.02m, 1.32m, 1.63m, 1.93m, and 2.13m (28", 40", 52", 64", 76" and 84") from the south wall are shown in figures 4.84 to 4.89, respectively. Note that the left side of the plot represents the east wall, and that the key shows a range between 650 and 1200 ppm. The experimental concentration fields appear reasonable except for two large values close to the floor of the room, either side of the central plane: this feature is evident at all experimental planes considered, and is particularly noticeable in figure 4.86. There is no obvious physical reason for these two high spots of concentration, but the fact that they appear at every experimental plane indicates a systematic error at this vertical height. Other than these two locations, the comparison between the experimental and CFD data sets can be seen to be very good.

The percentage differences between the experimental and CFD results confirm the good agreement between the two sets of data, as indicated in Tables 4.2.21 to 4.2.26. In particular, the average difference at the 0.71m (28") plane is 14.9 percent, at the 1.02m (40") plane is 15.2 percent, at the 1.32m (52") plane is 15.2 percent, at the 1.63m (64") plane is 14.2 percent, at the 1.93m (76") plane is 13.7 percent, and at the 2.13 (84") plane is 13.8 percent. It should be noted that these averages would be lower with the elimination of the concentration hot spots.

Table 4.2.21   Table of percent Difference between Experimental and CFD Concentration Data at Plane 0.71m (28") from South Wall

Dist. from Floor (")	Distance From West Wall (")												
	2	14	26	38	50	62	74	86	98	110	118	130	142
84	11.0	2.8	15.7	24.5	11.4	5.9	16.3	14.0	10.5	11.3	12.1	23.3	0.9
72	10.9	5.1	10.3	26.1	14.3	4.9	21.0	20.8	14.1	15.3	9.3	22.4	4.4
60			3.8	23.7	5.5	6.3	18.4	16.8	18.8	15.8	1.8		
48			7.5	24.4	10.3	2.5	19.7	14.8	11.4	17.4	2.3		
36			0.3	29.0	12.6	5.2	16.0	16.9	10.9	18.9	5.1		
24			7.3	16.1	27.9	21.6	11.3	1.7	35.4	17.5	6.1		
12			11.4	22.8	33.2	21.6	11.3	14.7	33.4	15.9	17.1		

Table 4.2.22 Table of percent Difference between Experimental and CFD Concentration Data at Plane 1.02m (40") from South Wall

Dist. from Floor (")	Distance From West Wall (")												
	2	14	26	38	50	62	74	86	98	110	118	130	142
84	11.1	0.5	11.8	23.0	16.8	27.3	35.1	27.2	15.1	9.7	8.7	19.7	3.5
72	6.3	1.3	4.6	23.8	15.3	12.5	23.0	22.7	9.4	14.1	6.4	19.6	2.5
60			7.2	24.6	7.2	7.5	22.6	18.0	5.2	11.6	5.5		
48			8.4	25.1	13.0	3.7	22.5	20.5	1.6	10.8	2.8		
36			9.2	25.1	15.4	10.2	18.3	20.8	4.3	13.1	0.6		
24			2.6	17.1	29.7	22.2	14.5	14.8	29.3	14.8	5.1		
12			12.6	12.9	30.1	22.2	12.0	12.7	30.1	13.1	14.8		

Table 4.2.23 Table of percent Difference between Experimental and CFD Concentration Data at Plane 1.32m (52") from South Wall

Dist. from Floor (")	Distance From West Wall (")												
	2	14	26	38	50	62	74	86	98	110	118	130	142
84	10.0	5.9	6.7	20.7	27.7	23.5	36.3	38.6	13.6	6.5	7.0	17.1	1.3
72	10.3	20.8	8.6	18.7	12.6	2.6	27.5	17.1	3.2	7.1	1.4	18.0	1.6
60			7.3	21.7	10.0	3.1	28.2	12.9	1.5	9.8	8.6		
48			4.8	22.4	18.1	10.0	24.8	17.6	2.7	12.4	8.6		
36			5.5	23.0	15.1	16.9	22.1	21.6	1.1	12.8	12.0		
24			1.9	16.8	23.8	20.3	18.3	16.4	27.8	11.7	8.6		
12			9.7	12.7	27.8	19.5	11.9	10.0	32.4	10.3	18.0		

Table 4.2.24 Table of percent Difference between Experimental and CFD Concentration Data at Plane 1.63m (64") from South Wall

Dist. from Floor (")	Distance From West Wall (")												
	2	14	26	38	50	62	74	86	98	110	118	130	142
84	12.6	0.1	7.3	22.5	6.7	1.5	13.5	17.5	7.4	8.1	5.3	15.4	12.2
72	5.4	9.6	8.7	19.8	3.1	2.7	17.8	25.4	11.4	6.2	5.1	12.4	10.7
60			7.0	23.1	3.9	2.4	17.3	30.3	17.3	9.5	0.1		
48			7.1	24.1	12.9	5.9	19.4	26.9	16.7	12.8	9.9		
36			1.3	21.6	12.5	9.2	16.6	26.5	11.3	13.2	16.0		
24			1.4	16.1	21.4	16.8	15.4	20.0	29.3	17.8	10.2		
12			10.3	22.8	25.1	18.5	7.9	13.4	30.9	10.3	18.5		

Table 4.2.25   Table of percent Difference between Experimental and CFD Concentration Data at Plane 1.93m (76") from South Wall

Dist. from Floor (")	Distance From West Wall (")												
	2	14	26	38	50	62	74	86	98	110	118	130	142
84	8.6	11.2	13.4	22.3	4.2	2.3	9.4	7.9	10.1	5.7	8.0	17.7	4.2
72	2.4	3.8	21.0	19.6	8.0	2.9	20.8	12.4	14.2	6.4	9.5	12.6	1.7
60			10.7	22.0	11.4	8.5	16.2	17.6	11.7	8.3	26.9		
48			10.3	22.7	9.8	3.3	13.6	18.3	13.1	12.3	11.4		
36			4.6	23.4	10.7	7.5	14.3	22.3	9.7	13.1	9.5		
24			4.5	16.3	20.9	16.0	14.1	17.8	26.2	17.5	20.3		
12			11.1	12.7	23.1	18.5	4.1	12.7	30.3	13.0	18.5		

Table 4.2.26   Table of percent Difference between Experimental and CFD Concentration Data at Plane 2.13m (84") from South Wall

Dist. from Floor (")	Distance From West Wall (")												
	2	14	26	38	50	62	74	86	98	110	118	130	142
84	6.8	7.8	25.2	24.9	3.0	3.2	11.4	6.1	8.0	3.9	2.7	13.6	8.0
72	0.3	7.0	18.7	28.9	6.5	7.1	13.6	6.3	10.6	6.1	10.4	11.4	2.0
60			6.9	24.5	9.5	4.0	11.8	14.4	14.5	7.5	3.4		
48			18.8	17.0	8.0	1.9	12.2	15.5	5.1	8.9	10.7		
36			26.4	22.7	6.8	9.9	13.5	16.3	2.5	12.1	9.8		
24			35.2	27.2	20.8	16.0	17.7	15.7	26.5	17.0	20.3		
12			37.3	12.7	23.2	16.0	4.0	11.9	29.6	6.1	20.9		

Discussion and Conclusions

From the above results it can be seen that the CFD simulation for the populated room agrees well with the experimental data for both the temperature and concentration (CO_2) data, but the speed field displays features that cannot be readily explained. This conclusion mirrors that from the empty room validation exercise. The conclusion is that the measured speed data are again the problem, because the comparison for the temperature and concentration data would also be erroneous if the CFD simulation is predicting the physical flow features in the room incorrectly (other than for very localized effects not included in the model). The above data again demonstrate the inherent difficulty in measuring low speed data accurately in a test facility.

Further, especially in the case of the temperature and concentration comparisons, although the experimental data can be used to obtain some feel for the conditions within the room, the CFD results provide a more complete picture of the flow field distributions and physical processes present.
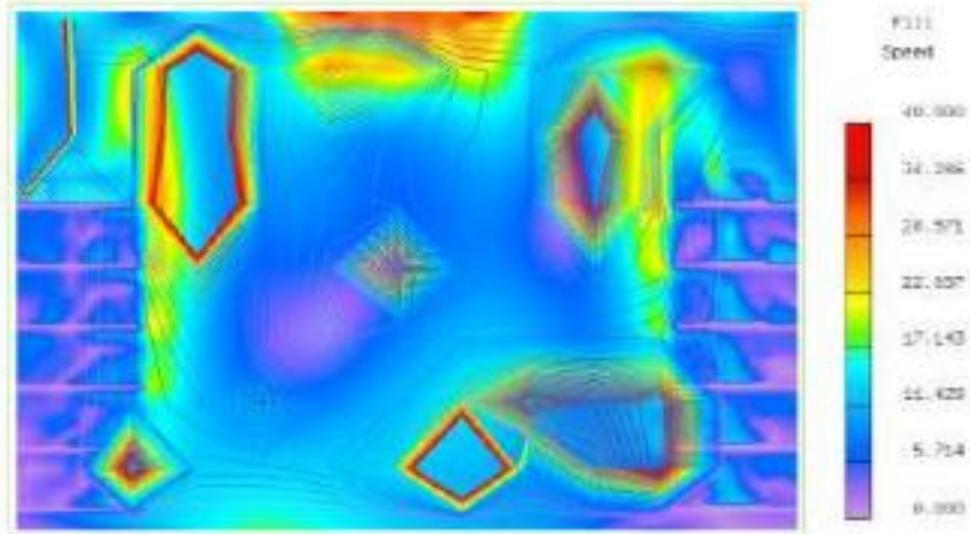
Figure 4.76   Comparison of Experimental and CFD Speed Fields at 1.02m (40") from South Wall.
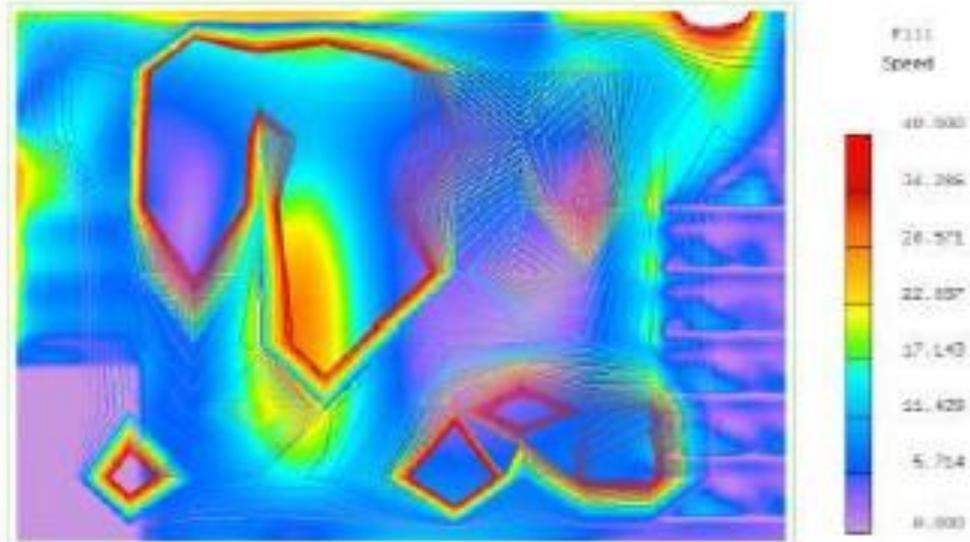

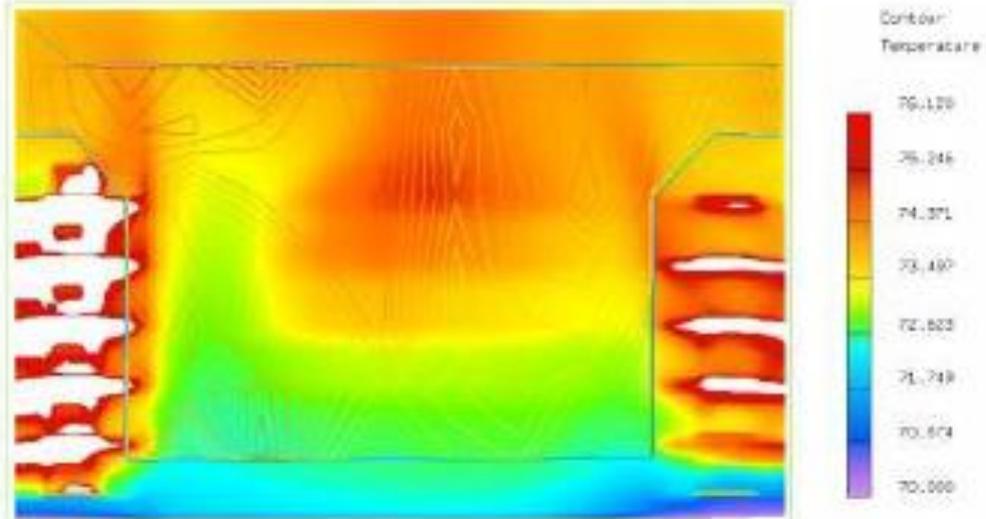**Figure 4.77**   Comparison of Experimental and CFD Speed Fields at 1.93m (76") from South Wall.

Figure 4.78   *Comparison of Experimental and CFD Temperature Fields at 0.71m (28") from South Wall.*
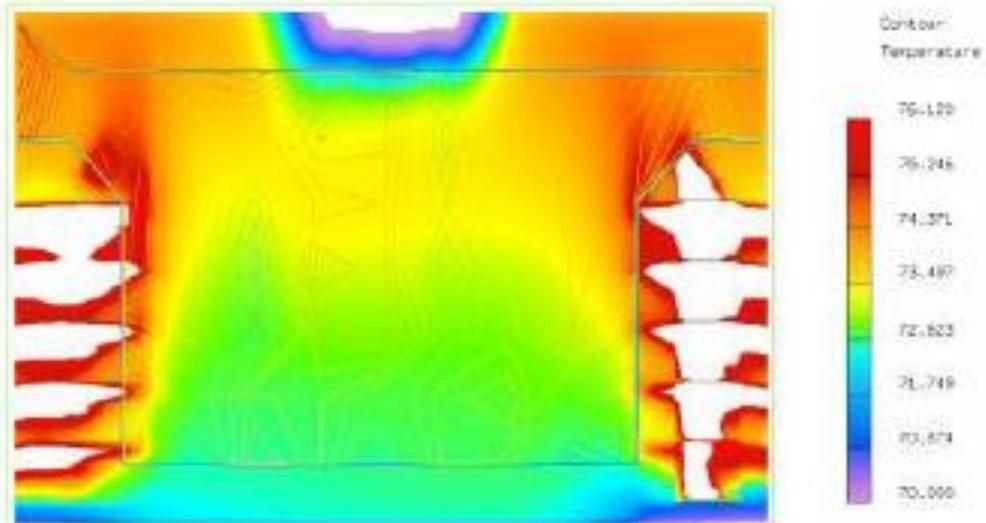

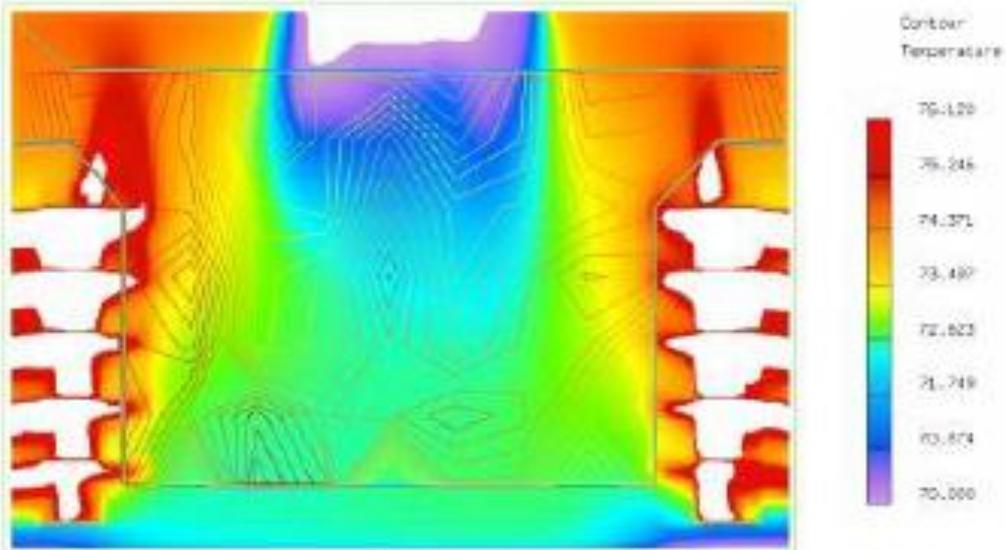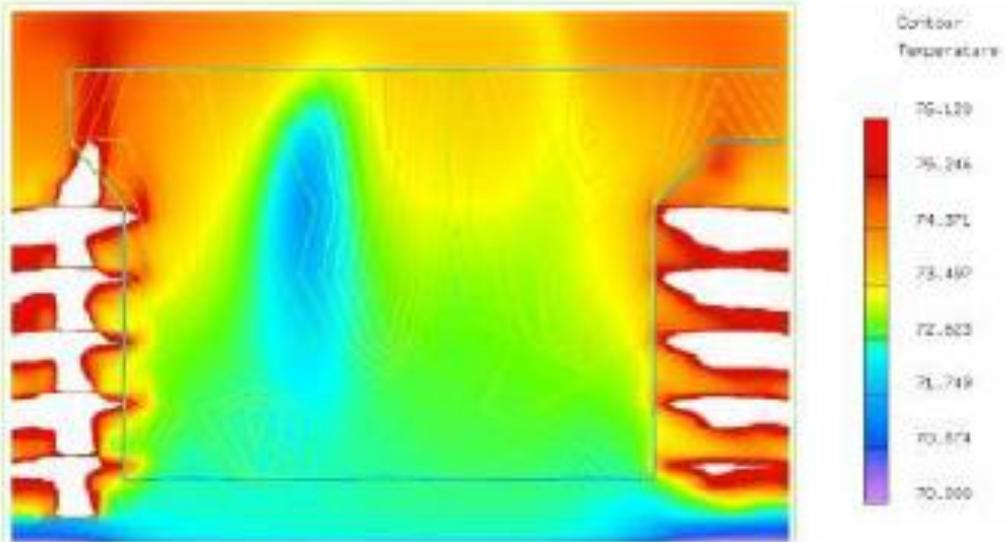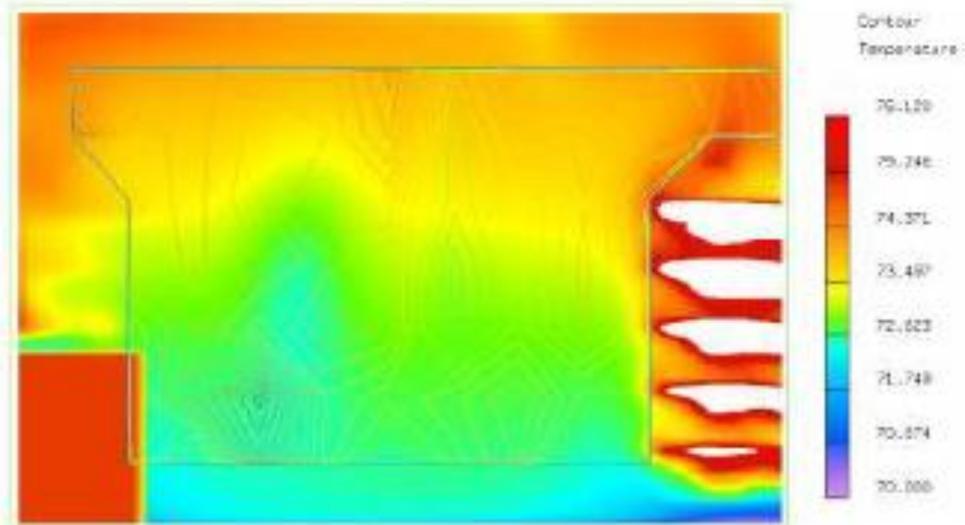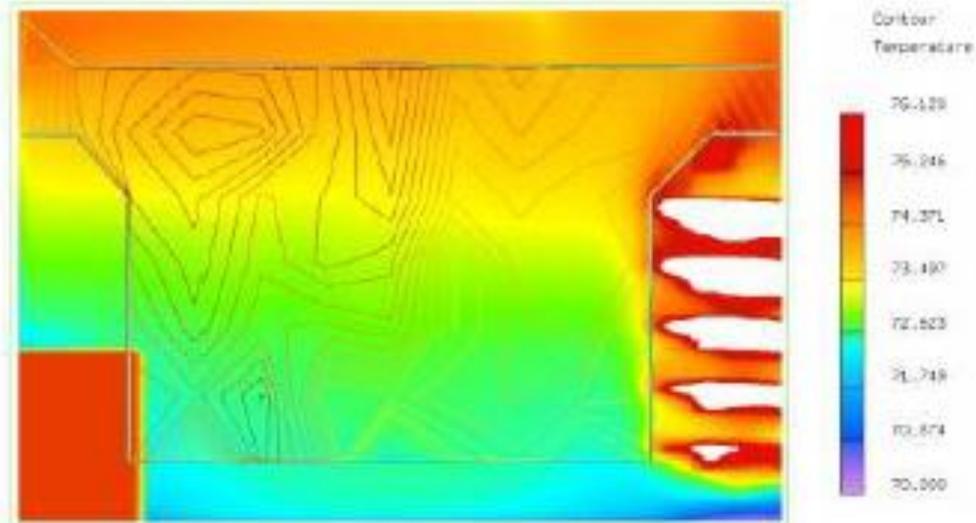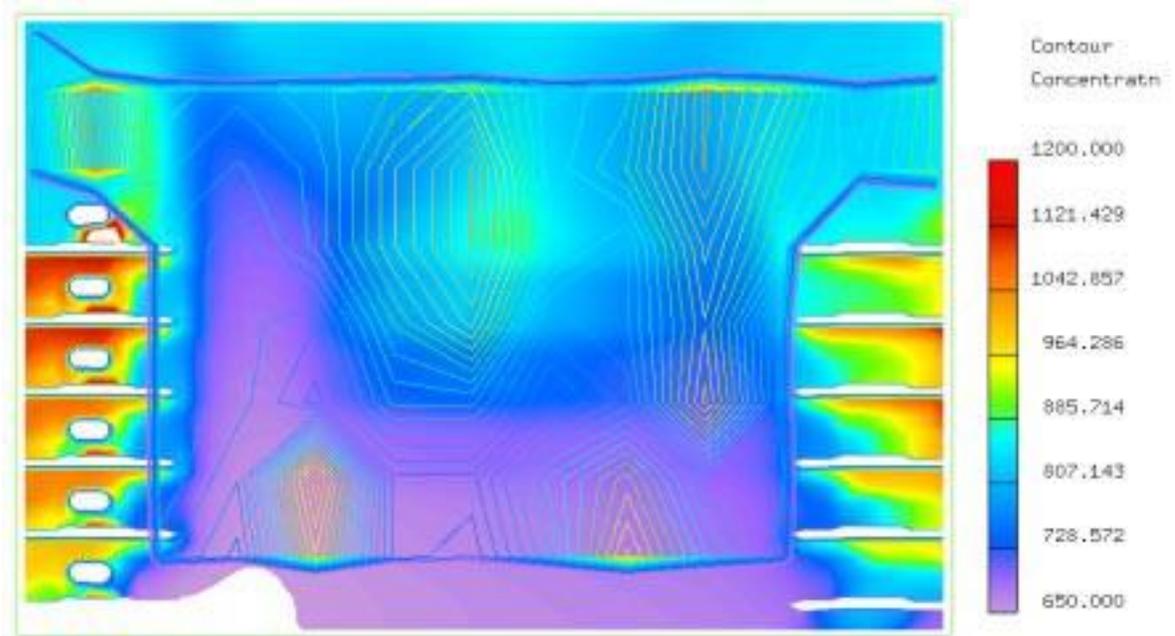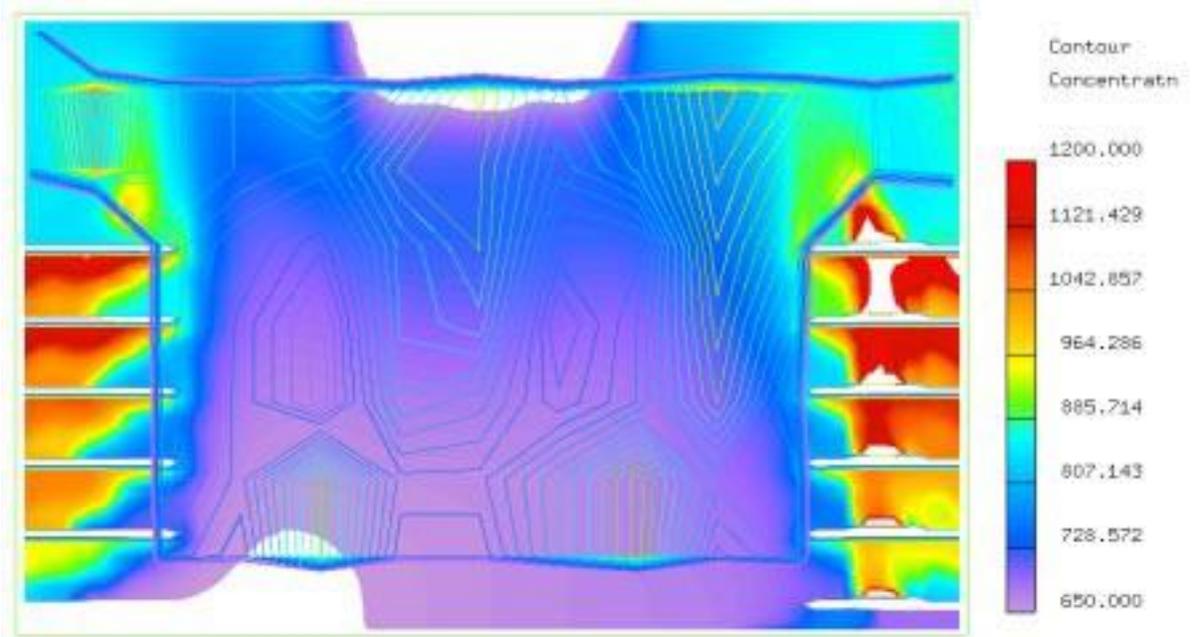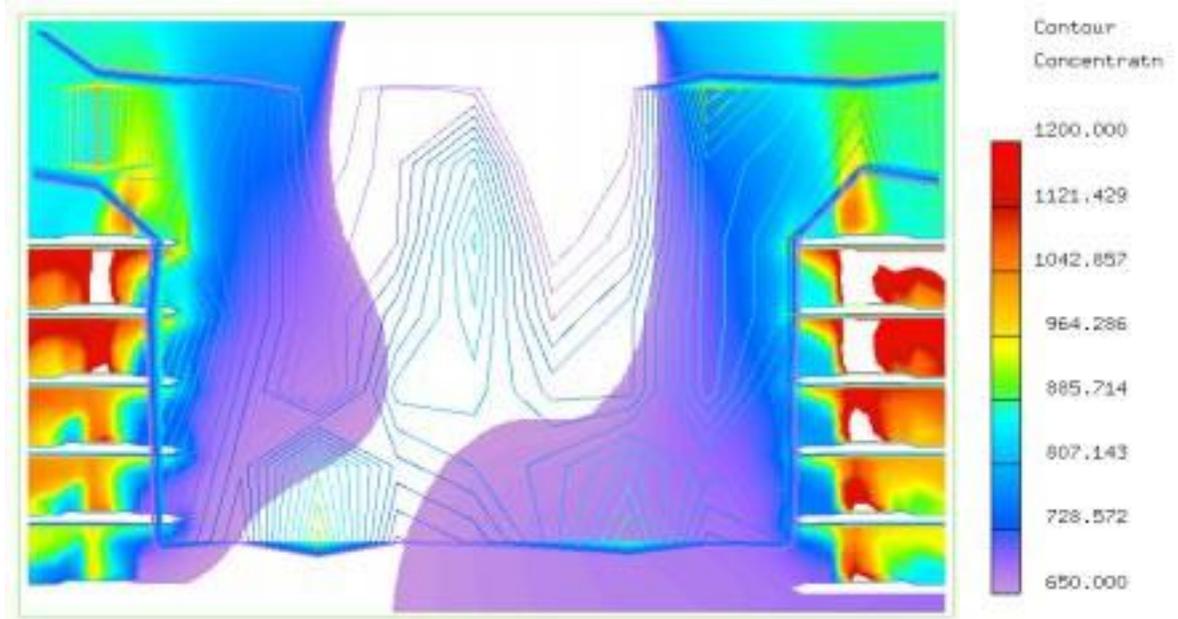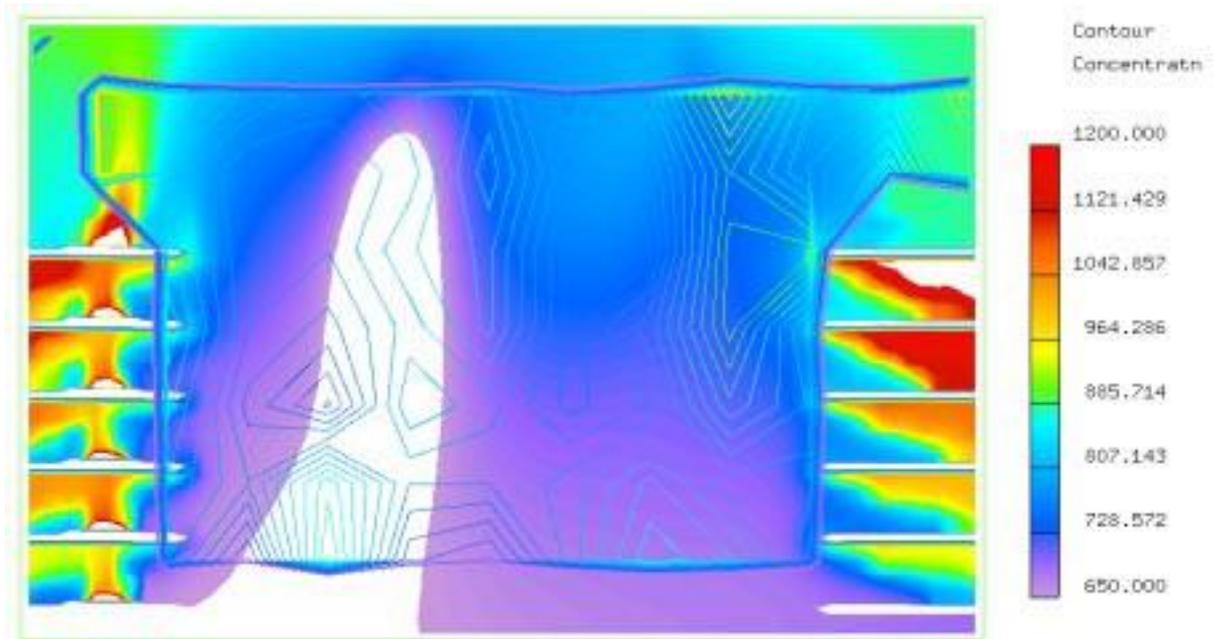*Figure 4.79*   *Comparison of Experimental and CFD Temperature Fields at 1.02m (40") from South Wall.*

Figure 4.80 *Comparison of Experimental and CFD Temperature Fields at 1.32m (52") from South Wall.*

Figure 4.81 *Comparison of Experimental and CFD Temperature Fields at 1.63m (64") from South Wall.*

Figure 4.82   *Comparison of Experimental and CFD Temperature Fields at 1.93m (76") from South Wall.*

Figure 4.83   *Comparison of Experimental and CFD Temperature Fields at 2.13m (84") from South Wall.*

Figure 4.84 *Comparison of Experimental and CFD Concentration Fields at 0.71m (28") from South Wall.*

Figure 4.84 *Comparison of Experimental and CFD Concentration Fields at 1.02m (40") from South Wall.*

Figure 4.85   *Comparison of Experimental and CFD Concentration Fields at 1.32m (52") from South Wall.*

Figure 4.86   *Comparison of Experimental and CFD Concentration Fields at 1.63m (64") from South Wall.*
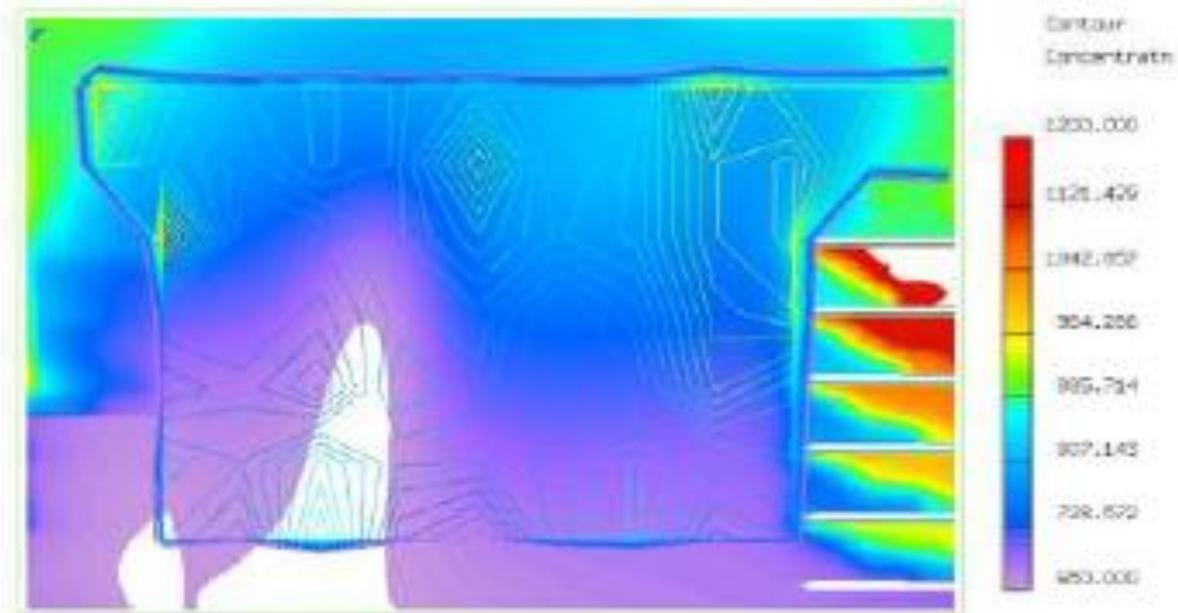
Figure 4.87   Comparison of Experimental and CFD Concentration Fields at 1.93m (76") from South Wall.
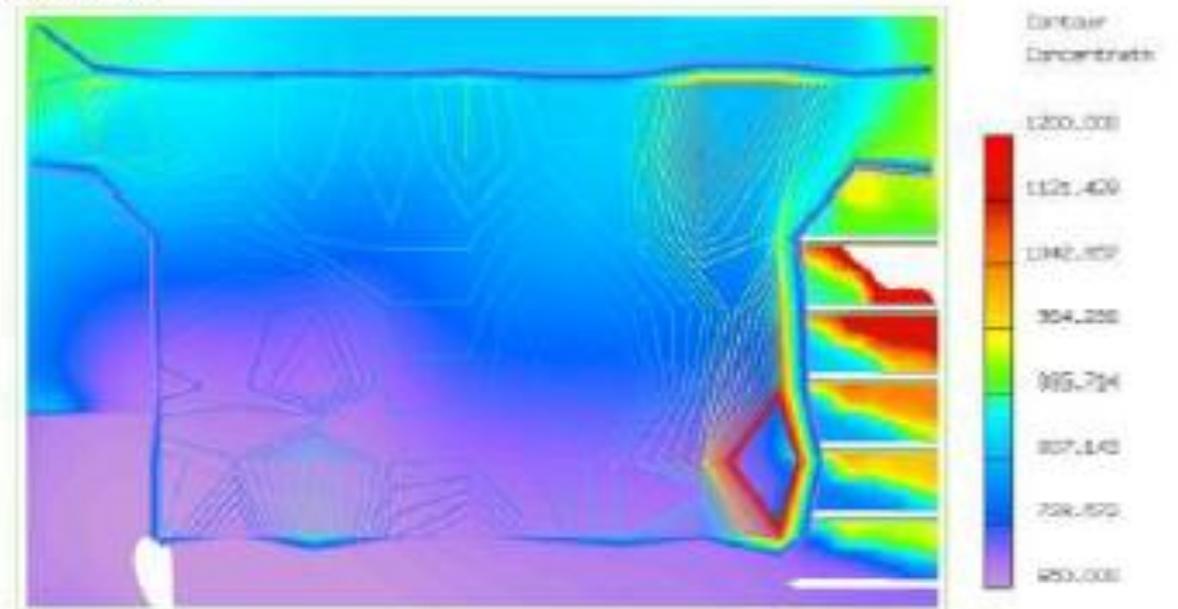

Figure 4.88   Comparison of Experimental and CFD Concentration Fields at 2.13m (84") from South Wall.